Investigating the effect of particle size on the antibacterial activity of gold nanoparticles

UNIVERSITY *of the*
WESTERN CAPE

Retsepile Ephraim Maphasa

A Thesis submitted in partial fulfilment of the requirements for the degree of MSc Nanoscience in the Department of Biotechnology at the University of the Western Cape, Bellville, South Africa.

Supervisor: Prof. A. Dube

Co-Supervisor: Prof. M. Meyer

University general plagarism declaration

Name: ……..

Student number: ……..

1. I hereby declare that I know what plagiarism entails, namely to use another's work and to present it as my own without attributing the sources in the correct way.

2. I know that plagiarism is a punishable offence because it constitutes theft.

3. I understand the plagiarism policy of the Faculty of Natural Science of the University of the Western Cape.

4. I know what the consequences will be if I plagiarize in any of the assignments for my course.

5. I declare therefore that all work presented by me for every aspect of my course, will be my own, and where I have made use of another's work, I will attribute the source in the correct way.

---------- ----------

Signature Date

Acknowledgements

I would like to thank my Supervisor: Dr Admire Dube for his continuous support, patience and assistance throughout this project. I would like to thank my Co-Supervisor: Prof. Mervin Meyer for all his contribution, assistance and for allowing me to use the apoptosis research laboratory facilities during the duration of this project. I would like to thank The Nanomedicine Research Group in the School of Pharmacy and the Apoptosis Research Group and the bioinformatics research group for all the time they selfishly sacrificed to assist me. I would also like to thank the MSc Nanoscience program for all the financial support and the opportunity to undertake my MSc degree. I would like to thank my family for all their support, not just for academic purposes but also for encouraging me to follow my own path in life. To all the people mentioned above, God bless you!

Last but not least, I would like to thank God for blessing me with a very wonderful support structure for both academic and non-academic purposes and for keeping me safe when I travel to university and back.

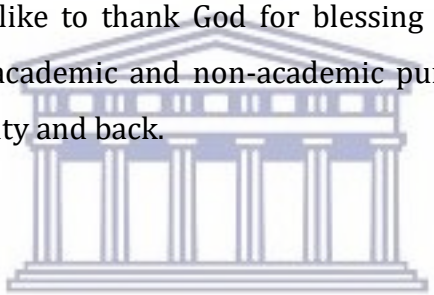

Table of Contents

List of Abbreviations

AFM .....Atomic force microscopy
AgNPs .....Silver nanoparticles
ATCC.....American Type Culture Collection
AuNPs .....Gold nanoparticles
BCG .....Bacillus Calmette-Guérin
CLSI ..... Clinical and Laboratory Standards Institute
CFU .....Colony forming units
DLS .....Dynamic light scattering
E. coli .....Escherichia coli
EDS .....Energy dispersive x-ray
FS..... Fluorescence spectroscopy
HR-TEM ..... High resolution transmission electron microscopy
LB ..... Lysogeny broth
MDR-TB ..... Multi-drug tuberculosis
MIC .....Minimum inhibitory concentration
MRSA .....Methicillin-resistant Staphylococcus aureus
MTT.....Tetrazolium salts, 3-(4, 5- dimethylthiazol-2-yl)-2, 5-diphenyl tetrazolium bromide
NIR .....Near-infrared region
NMR .....Nuclear magnetic resonance
NP ..... Nanoparticle
PPNG.....Penicillin-resistant Neisseria gonorrhoeae
PDI .....Polydispersity index
S. aureus ..... Staphylococcus aureus
sAuNPs ..... Spherical gold nanoparticles
SEM .....Scanning electron microscopy
SPR .....Surface plasmon resonance
SWCNTs ..... Single walled carbon nanotubes
ROS .....Reactive oxygen species
TB ..... Tuberculosis
TEM .....Transmission electron microscopy
TLC .....Thin-layer chromatography

XTT .....2, 3-bis {2-methoxy-4-nitro-5-[(sulfenylamino) carbonyl]-2H- tetrazolium-hydroxide}

XRD ..... X-ray diffraction

ZP ..... Zeta potential

List of Figures

List of Tables

Abstract

Purpose: The increase of antibiotic- and/or multidrug-resistant bacteria has become a major global challenge. Killing of antibiotic-resistant bacteria requires a high dose of multiple, expensive drugs, which possess unfavourable side effects to the infected individuals. As a result, treatment of antibiotic resistant-bacteria is costly and more time is required to complete treatment. Therefore, novel substitutes are required to combat drug resistant infections while preventing further microbial resistance. Spherical gold Nanoparticles (sAuNPs) prepared using the citrate reduction method have been found to exert antibacterial activity against a number of gram positive and gram negative bacteria. However, there is still uncertainty regarding the role of size on the antibacterial activity of sAuNPs. The effect of exposure time on the antibacterial activity of sAuNPs is also still not well understood. In this study, it was hypothesized that AuNPs will show a size- and concentration-dependentantibacterial activity against selected gram positive (+) and gram negative (-) bacteria.

Method: The Turkevich/citrate reduction method was employed to synthesize three sizes of sAuNPs by mixing different ratios of tri-sodium citrate and gold chloride trihydrate. The UV-Vis spectra of each nanoparticle (NP) sample was determined using the POLARstar Omega plate reader. Using the principle of dynamic light scattering (DLS), the hydrodynamic size, polydispersity index (PDI) and zeta potential (ZP) of the NPs were examined using the Malvern Zetasizer Nano-ZS90 instrument. The core-diameter and the morphology of the NPs were determined using HR-TEM. The stability of the NPs in both dH_2O and LB media was also determined over an incubation period of 72 h, at 4˚C and at 37˚C. The bacterial growth inhibiting activity of the NPs was examined using the broth micro-dilution method against *E. coli, S. aureus* and *MRSA,* using Alamar blue as an indicator of bacterial growth.

Results: s AuNPs of core diameters of 50.2 ± 9.4 nm, 27.7 ± 3.5 nm and 14.0 ± 3.3 nm, respectively, were successfully synthesized using the citrate reduction method. All the sAuNPs showed a single λ_{max} absorbance peak near 520 nm, which is distinctive for sAuNPs and the spherical morphology was validated using HR-TEM. The hydrodynamic sizes were found to be 62.7 ± 4.6 nm (AuNP 1), 33.68 ± 1.68 nm (AuNP 2) and 24.49 ± 0.05 nm (AuNP 3), after purification. All the NPs were found to be relatively monodispersed with PDI values of 0.545 ± 0.05 (AuNP 1), 0.398 ± 1.0 (AuNP 2) and 0.259 ± 0.09 (AuNP 3). All the NPs showed sufficient stability in dH_2O, with zeta potential values of -27.0 ± 6.28 mV,-32.7 ± 1.60 mV,-30.7 ± 2.1 mV, for AuNP 1, 2 and 3 respectively. The diameter/size of the AuNPs was found to be inversely proportional to the amount of tri-sodium citrate and directly proportional to the amount gold chloride trihydrate added during the synthesis reaction. The role of size in the antibacterial activity could not be properly examined as the NPs were prone to aggregation when introduced to nutrient media. However, clusters of AuNP 1 showed more activity when compared to clusters of AuNP 2 and AuNP 3. The AuNPs showed a dose- and time-dependent growth inhibiting activity and were more active against gram negative bacteria when compared to gram positive bacteria. In addition, the AuNPs were found to induce inhanced bacterial proliferation at low concentrations.

Conclusion: The sAuNPs were found to be unstable and thus prone to aggregation in LB media. Clusters of AuNP 1, AuNP 2 and AuNP 3 were observed to exert a time-and concentration-dependent growth inhibiting activity and were observed to be more effective at inhibiting the growth of *E. coli* when compared to *S. aureus* and *MRSA*. Therefore, the results indicated that the sAuNP clusters had more growth inhibiting activity against gram negative bacteria when compared to gram positive bacteria. However, due to the aggregation, the role of particle size on the growth inhibiting activity of the AuNPs could not be determined. However, clusters of AuNP 1 were found to be more effective at inhibiting the growth of the selected bacteria when compared to clusters of AuNP 2 and AuNP 3. In addition, the bacteria in this study were found to use Stress proliferation to as a strategy to overcome the stress caused by low concentrations of the AuNPs.

Key Words:

Synthesis of spherical gold nanoparticles

Antibacterial activity of AuNPs

Gram positive and gram negative bacteria

Bacterial growth inhibition

Size and concentration dependent activity of AuNPs

Time dependent activity of AuNPs.

Chapter 1: Introduction

Antimicrobial drugs have long been used to either kill or inhibit the growth of pathogenic microorganisms. However, the efficiency of these drugs has become greatly compromised by the development of microbial resistance in multiple bacteria against a number of antimicrobial drugs; this microbial resistance has become a major challenge for public health (Hajipour *et al.*, 2012). Drug resistance development has a minimum of three steps: (i) Acquisition of resistance genes by microbes, (ii) expression of the resistance genes, and finally (iii) selection for microbes expressing those resistance genes (Hajipour *et al.*, 2012).

In cases of infections, high doses of multiple, expensive drugs are required for killing antibiotic-resistant bacteria, this kind of treatment results in many unfavourable side effects. As a result, treatments are also expensive and require prolonged treatment time (Bbosa *et al.,* 2014). Therefore, novel methods are required to battle drug resistant infections without causing further microbial resistance (Hajipour *et al.*, 2012). Nanotechnology is the field that studies materials with a size range of 1 to 100nm in at least one dimension (Hajipour *et al.*, 2012). Nanoparticles (NPs) can be classified into five groups: semiconductor quantum dots, polymeric particles, carbon-based nanostructures, magnetic NPs and metallic NPs (Huang *et al.,* 2007 and Shah *et al.,* 2014). Metallic NPs, specifically gold nanoparticles (AuNPs), have shown large surface bio-conjugation with a number of molecular probes and possess numerous optical properties. As a result, these particles are frequently used in biotechnology and biomedicine (Khan *et al*., 2014).

Many NPs have been found to exert antimicrobial activity against a number of bacterium and have been effective against several infectious diseases, including antibiotic-resistant ones (Hajipour *et al.*, 2012). Though showing anti-microbial activity, the precise mechanisms involved in the toxicity of NPs against bacteria have not been properly elucidated (Pelgrift and Friedman, 2013). However, it is known that the NPs adhere to bacterial membranes via electrostatic interactions subsequently disrupting the integrity of these membranes (Hajipour *et al.*, 2012).

Spherical gold NPs (sAuNPs) prepared using the citrate reduction method, have been found to show antibacterial activity against a variety of gram positive and gram negative bacteria (Zawrah and El-Moez, 2011). The antibacterial activity of AuNPs is governed by the NP composition, size, shape and the bacterial species being targeted. The susceptibility of bacterial species to the antibacterial activity of NPs is also related to the cell wall structure in case of Gram-positive and Gram-negative bacteria. However, there is still an uncertainty regarding the antibacterial activity of naked AuNPs which are not capped with any antibiotics (Shah *et al.,* 2014).

The effect of size, concentration and exposure time on the antibacterial activity of AuNPs is also still not well understood (Hajipour *et al.*, 2012). It was hypothesized that sAuNPs synthesized using the citrate reduction method would show size- and concentration-dependentgrowth inhibiting activity against bacteria. Therefore, the aim of this study was to determine the effect of size, concentration and exposure time on the growth inhibiting activity of sAuNP against Methicillin-resistant *Staphilococcus aureus (MRSA)*, *Staphylococcus aureus (S. aureus)* and *Escherichia coli (E. coli).*

Chapter 2: Literature Review

2.1. Microbial resistance to antimicrobial drugs

For over 70 years, multiple microbial infections such as bacterial infections and, more recently, viral, fungal and parasitic infections have been controlled or treated using synthetic, semi-synthetic or natural substances known as antimicrobial agents. These agents either kill (microbicidal) or prevent the growth (microbistatic) of microorganisms (Acar *et al*., 2012). However, a large number of studies have revealed that all these microorganisms have a notable ability to evolve and adapt. This ability is used for survival and helps microbes develop resistance against every available therapeutic antimicrobial drug administered (Acar *et al*., 2012).

2.2. Bacterial cell wall and sensitivity to antibacterial agents

Bacteria are commonly classified using the Gram staining reaction into either "gram positive" or "gram negative" bacteria, based on the bacteria's ability to retain the Gram stain (Wiegel, 1981). The cell wall of Gram-positive bacteria consist of a thick layer (i.e., 20–50 nm) of peptidoglycan (PG), which is attached to teichoic acids that are distinct to the Gram-positive cell wall (Scott and Barnett, 2006). On the other hand, cell walls of Gram-negative bacteria are more structurally and chemically intricate and consist of a thin PG layer and an outer membrane, that covers the surface membrane. The outer membrane of Gram-negative bacteria is often resposinble for the resistance to hydrophobic compounds and consists of lipopolysaccharides, which enhance the negative charge of cell membranes and are therefore crucial for the structural integrity and viability of the bacteria (Roberts, 1996). The structure of the cell wall also plays a vital role in the tolerance or susceptibility of bacteria to antibacterial agents (Hajipour *et al.,* 2012).

2.2.1. Antibacterial compounds

Antibacterial drugs are compounds that kill or inhibit the growth of bacteria (Hajipour *et al.*, 2012). Antibiotics/antibacterial drugs are the most frequently used and abused antimicrobial agents globally, to manage bacterial infections (Bbosa *et al.,* 2014). A Majority of currently available antibacterial agents are semi-synthetic compounds, examples include, b-lactams (like penicillin), carbapenems and cephalosporins. Pure natural products, such as amino glycosides, and purely synthetic antibiotics, such as sulphonamides, are also frequently used. Antibacterial agents are classified as either bactericidal, which kill bacteria, or bacteriostatic, which slowing down or prevents bacterial growth. Antibacterial agents are vital in the fight against infectious diseases (Hajipour *et al.*, 2012).

2.2.1.1. Classes of antibiotics and their sites of action on bacteria

Different antibacterial drugs have various targets on the bacteria as shown on **Table 2.1.** These targets include: (i) cell wall and cell membranes, (ii) ribosomes, (iii) nucleic acids, (iv) bacterial cellular metabolism and (v) bacterial cellular enzymes (Bbosa *et al.,* 2014). There are many different mechanisms by which these agents inhibit the multiplication and growth, and the destruction of bacteria. These include: (i) Inhibition of cell wall synthesis such as beta lactams, (ii) Disruption of cell-membrane function, (iii) Inhibition of protein synthesis, (iv) Inhibition of nucleic acid synthesis both the DNA synthesis and RNA synthesis, and (v) function as anti-metabolites (Bbosa *et al.,* 2014).

Table 2.1: Bacterial targets of antimicrobial drugs (Bbosa *et al.,* 2014).

Bacterial target	**Antimicrobial drugs**
Cell wall synthesis	β-Lactam
	Glycopeptides
Protein synthesis	Amino glycosides
	Macrolides
	Lincosamides
	Ketolides
	Streptogramins
	Tetracyclines
	Chloramphenicol
	Oxazolidinones
RNA synthesis	Rifamycins
DNA synthesis	Coumarins
	Naphthyridines
	Quinolones
	2-Pyridones
Intermediary metabolism	Sulfonamides
	Trimethoprim

The differences in the bacteria and mammalian cells especially the structural and metabolic differences enables the antibacterial agents to cause selective toxicity to the bacterial organisms without causing any damage to the host cells (Hajipour *et al.*, 2012). Currently there are a number of classes of antibacterial agents that are commonly used in clinical practice to treat bacterial infections (Bbosa *et al.,* 2014). However, due to the broad use and abuse of these compounds, bacterial resistance to antibacterial drugs has become a common and widespread global problem. Resistance is commonly a result of evolutionary

processes which take place during antibiotic therapy, for example, leading to inheritable resistance (Hajipour *et al.*, 2012).

2.3. Antibacterial Resistance

Antimicrobial drugs have long been used to either kill or inhibit the growth of bacteria and other microbes. However, the effectiveness of these drugs has been greatly reduced by the large scale of microbial resistance that multiple bacteria have developed against a number of these drugs; this microbial resistance remains a growing challenge in public health (Hajipour *et al.*, 2012). The list of known drug-resistant bacteria includes: multidrug-resistant *Mycobacterium tuberculosis, penicillin-resistant Neisseria gonorrhoeae (PPNG), Enterobacter cloacae, E. coli, Klebsiella pneumoniae, Shigella flexneri, Salmonella enterica, Acinetobacter baumannii, Pseudomonas aeruginosa, Vibrio cholerae, and beta-lactamase-expressing Haemophilus influenza*. Methicillin-resistant, sulfonamide-resistant, vancomycin-resistant, and penicillin-resistant *S. aureus,* penicillin-resistant *Streptococcus pneumoniae*, macrolide-resistant *Streptococcus pyogenes*, and vancomycin-resistant *Enterococcus* (Pelgrift and Friedman, 2013).

Drug-resistant bacterial infections result in higher drug doses, use of treatments with higher toxicity, longer hospital stays, and increased amounts of deaths (Pelgrift and Friedman, 2013).Bacterial drug resistance has various negative effects on both medicine and the society at large. (i) Drug-resistant bacterial infections result in higher doses of drugs, (ii) addition of treatments with higher toxicity, (iii) longer hospital stays, and (iv) increased mortality. A good example is *MRSA,* which is associated with more deaths than methicillin-sensitive *S. aureus (MSSA)* (Pelgrift and Friedman, 2013).

2.3.1. Mechanisms of resistance of microbes to antimicrobial drugs.

2.3.1.1. Development of resistance to antimicrobial drugs.

Drug resistance development has at least three steps: (i) Acquisition of resistance genes by microbes, (ii) expression of the resistance genes, and finally (iii) selection for microbes expressing those resistance genes (Hajipour *et al.,* 2012). Bacteria commonly acquire resistance genes through spontaneous mutation of existing genes. Once resistant to a single drug, bacterial cells already containing one type of drug resistance gene can acquires another type of drug resistance gene and become multiple drug resistant (Pelgrift and Friedman, 2013). Microbes express the resistance genes when exposed to the specific antimicrobial drug, and whenever microbes are exposed to the drug but not eradicated, the microbes multiply and the resistance becomes wide spread (Hajipour *et al.*, 2012). This is clearly illustrated on **Figure 2.1** below.

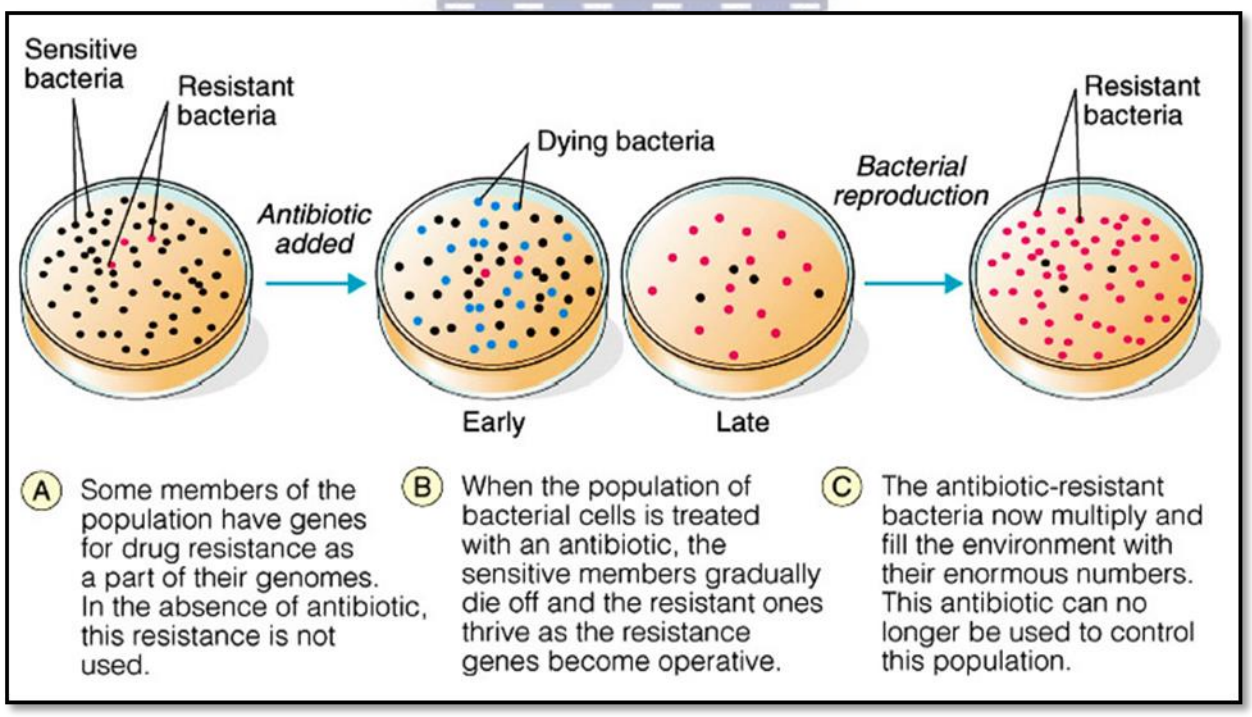

Figure 2.1: The spreading of microbial resistance against a specific antibiotic (Bbosa *et al.,* 2014).

In addition, horizontal gene transfer by means of transformation, transduction and conjugation are also possible ways that may be used by bacteria to build up resistance (see **Figure 2.2** below) (Hajipour *et al.*, 2012). Antibacterial-resistant bacterial strains and species are unofficially referred to as superbugs and are commonly behind the outbreak of various diseases that had been kept under control for many years. A well-known example of such a case is the rise of tuberculosis (TB)-infections caused by TB-causing bacterial strains that are resistant to previously effective antibacterial treatment which has resulted in the occurrence of multi-drug resistant tuberculosis (MDR-TB) (Hajipour *et al.*, 2012).

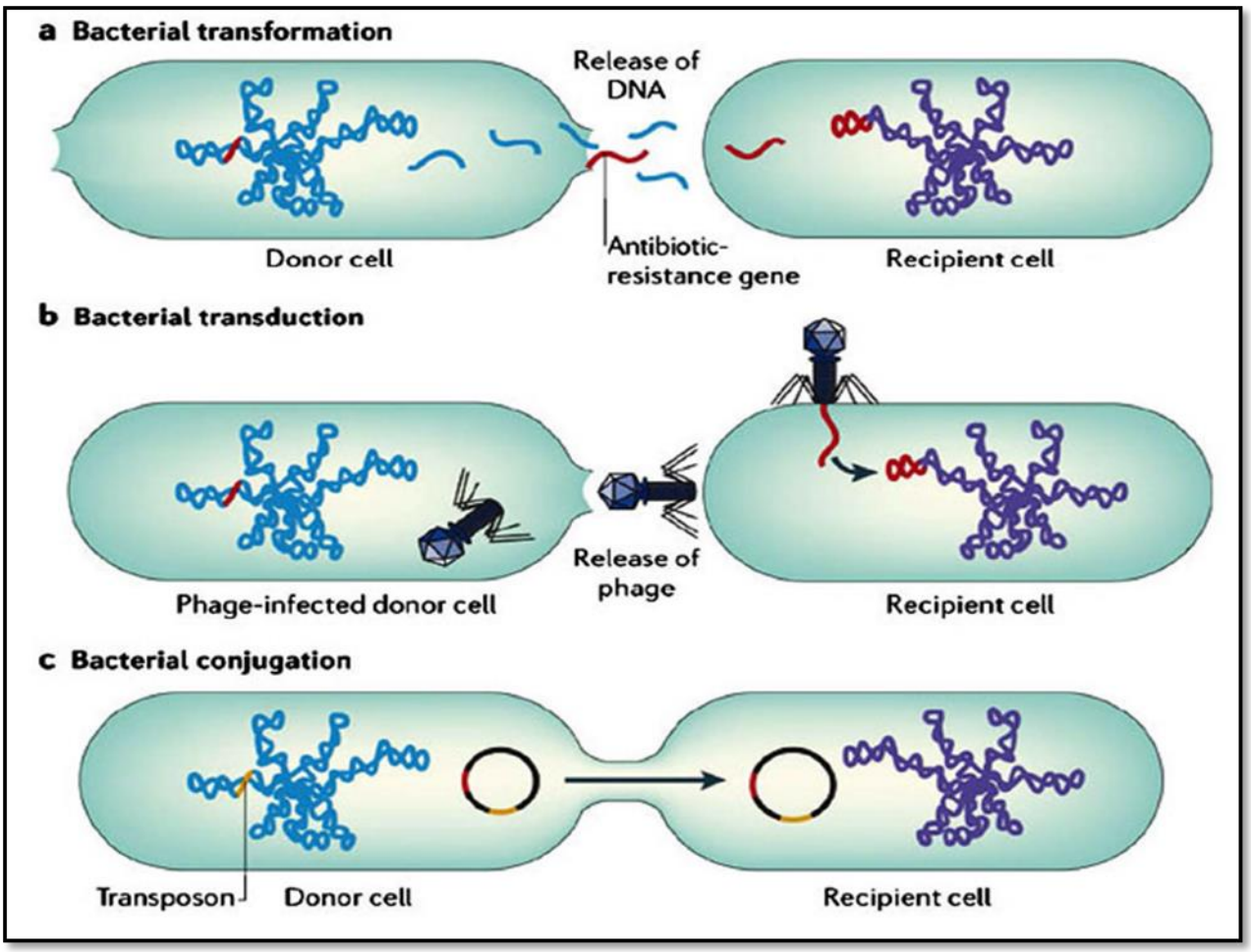

Figure 2.2: Antimicrobial-resistant bacteria can pass the antibiotic resistance gene to non-resistance bacteria using horizontal gene transfer, namely: (a) bacterial transformation, (b) bacterial transduction and (c) bacterial conjugation (Furuya and Lowy, 2006).

The acquired resistance genes grant bacteria various resistance mechanisms to avoid the antibiotics that they are exposed to. There are different mechanisms of antibiotic resistance (as illustrated on **Figure 2.3** below), these include: (i) the presence of an enzyme that inactivates or alters the antibiotic, (ii) metabolic evasion of the targeted pathway or the development of an alternative pathway for the antibiotic inhibited enzyme/s,(iii)mutation of the antimicrobial agent's target, thus reducing the binding of the antimicrobial agent or the sequestering process of the drug via protein binding, (iv) posttranscriptional or post-translational modification of the antimicrobial agent's target, which reduces binding of the antimicrobial agent or modification of targets, (v) reduction of the antimicrobial agent uptake, (vii) active draining of drugs out of the microbe, (viii) overproduction of the antimicrobial agent's target by the microbes (Bbosa *et al.,* 2014).

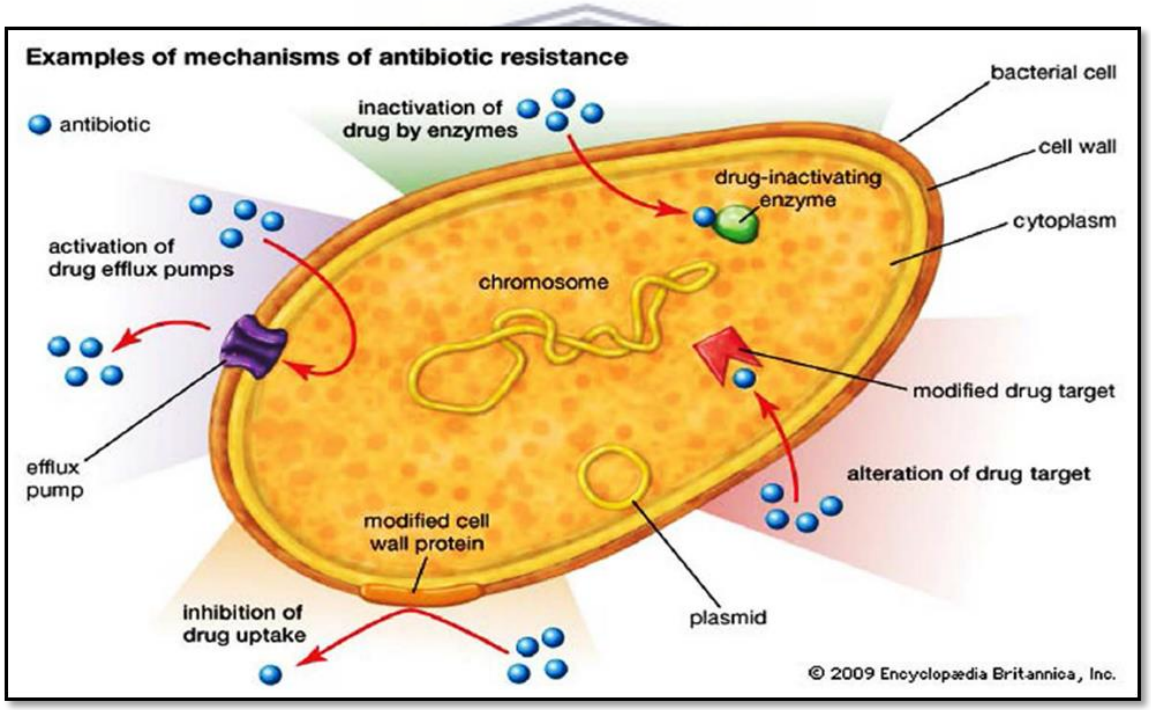

Figure 2.3: Examples of the different mechanisms of antibiotic resistance (Encyclopædia-Britannica, 2013).

Examples of the settings that create selective pressure in favour of drug resistance are poor patient compliance, or the use of a time-dependent antibiotic with long half-life (Bbosa *et al.,* 2014). The chances of developing resistance depend on the duration of use of the antimicrobial drug. Unlike microbicide drugs, microbistatic drugs inhibit but do not kill

microbes and are thus more likely to allow some microbial cells to survive and therefore develop resistance after being exposed to the drug (Levy and Marshall, 2004). Intake of an inadequate amount of doses and missed scheduled doses, cause an increased selective pressure in favour of drug resistance, because the microbes are exposed but notcompletely eradicated by the drug (Cegedim, 2013). This poor patient compliance is mainly a setback for drugs with short elimination half-lives, because these drugs have short dosing intervals, therefore a high number of doses is required for microbial eradication (Levy and Marshall, 2008). However, even when there is good patient compliance, selective pressure in favour of antimicrobial resistance still occurs due to the events that unfold within individual dosing intervals (Bbosa *et al.,* 2014).

In order to assess the efficiency of an antibacterial treatment, three pharmacokinetic and pharmacodynamic indexes (PK/PD) indexes have been defined: the ratio between the area under the curve of dependence between the drug concentration in blood and time within 24 hours to MIC (AUC24/MIC), the time when the concentration of the drug in blood is higher than MIC (T > MIC), and The pharmacological index Cmax/MIC, a variable used to predict the clinical outcomes of concentration-dependent antibiotics (Szalek *et al.,* 2011). Cmax/MIC is defined as the ratio of the maximum drug concentration in the plasma per dosing interval to the minimum inhibitory concentration (MIC). When Cmax/ MIC are above a target threshold value, the antimicrobial activity of these antibiotics reaches a maximum and the probability of antibiotic resistance development is highly reduced. In addition, a *C*max/MIC ratio of >8 is widely associated with an improved clinical outcome (Barger *et al*., 2003). Thus, drug resistance against concentration-dependent antibiotics can develop when the Cmax/MIC is below the target threshold value and the plasma concentrations of the drug are above zero during a given dosing interval (Cegedim, 2013).

2.4. Nanotechnology and nanomedicine

Nanotechnology is the field of developing materials that have a size range of 1 to 100nm in at least one dimension (Hajipour *et al.*, 2012). Interest in nanotechnology was first discussed in a presentation titled “There’s Plenty of Room at the Bottom” by Richard P. Feynman during the 1959 American physical society meeting in California (Feynman,

1960). The presentation described a process by which specific atoms and molecules could be manipulated, and described this as potential tool for future innovation and development (Feynman, 1960). In the Morden time, nanoparticles (NPs) are classified into five different groups. These include: metallic/inorganic NPs, quantum dots, polymeric and lipid NPs, magnetic NPs and carbon-based NPs as illustrated in **Figure 2.4** below (Huang *et al.,* 2007 and Shah *et al.,* 2014).

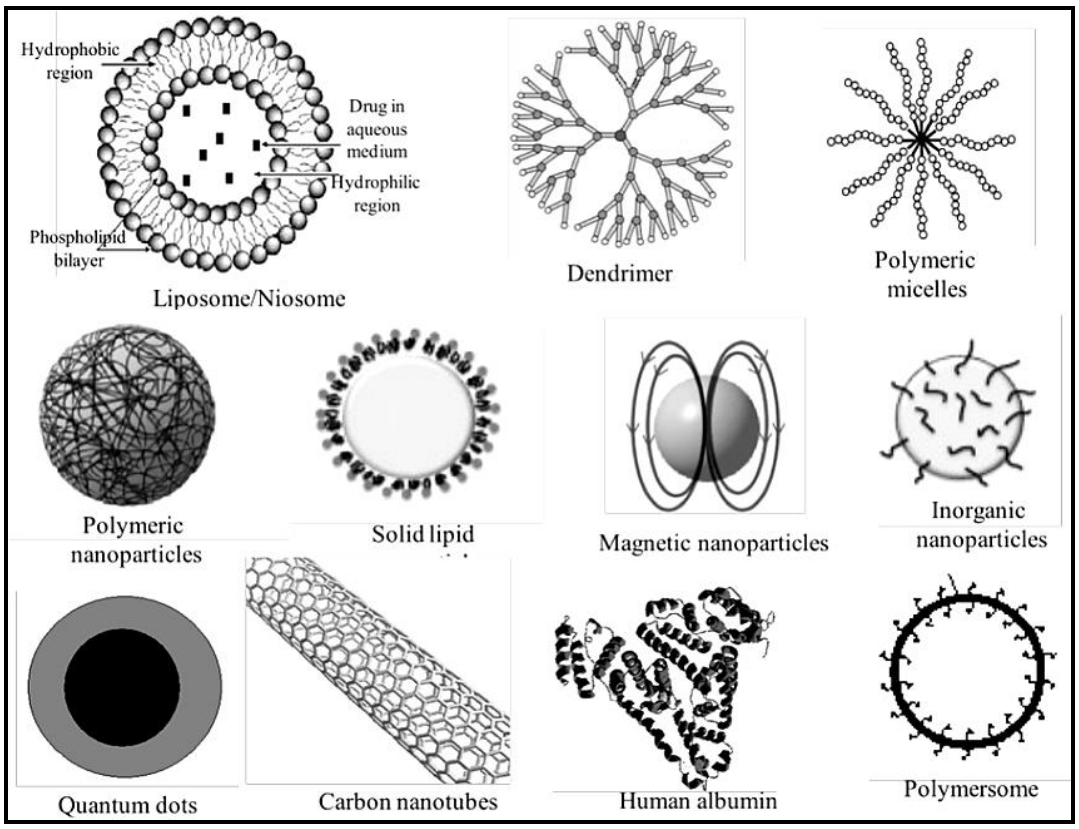

Figure 2.4: Illustration of the different types of NPs (Berciano-Guerrero *et al.,* 2014).

Nanomedicine refers to the applications of nanotechnology towards addressing a number of mankind's healthcare needs (Dube and Ebrahim, 2017). Each of the utilized nanostructures has characteristic properties and applications. For example, semiconductor quantum dots demonstrate fluorescent properties and are therefore useful for biological labelling and imaging (Ruchez *et al.,* 1998), while the magnetic properties of magnetic NPs are very useful for magnetic resonance induction, drug delivery, cell sorting and magnetic hyperthermia therapy (Shah *et al.,* 2014).

Because of their large reactive and exposed surface area and quantum size effect, NPs have unique and improved chemical and physical properties compared to their bulk materials. As a result, these particles are extensively used in various fields including biomedicine, chemistry and electronics (Khan *et al*., 2014). NPs have been proven to be promising multi-functional platforms that can be used for many imaging and therapeutic functions, such particles can be synthesized from organic, inorganic or hybrids of both organic and inorganic materials.

However, NPs synthesized from inorganic materials (such as metals and semiconductors) are of more significant for diagnosis and simultaneous therapy because of their high stability and high drug loading capacity and they can easily be modified (Khan *et al*., 2014). Unlike the other categories, metallic NPs have proven to have a variety of potential applications because they are easy to synthesize and to control their size, shape, composition, structure and assembly. The NPs have also been reported to be easily taken up by cells through endocytosis as illustrated in **Figure 2.5** below (Pan *et al.,* 2007). This therefore allows for fine tunability of their optical properties which are the core for various applications (Shah *et al.,* 2014a). Among all metallic NPs, gold NPs are the most widely used and studied for biological applications (Shah *et al.,* 2014a).

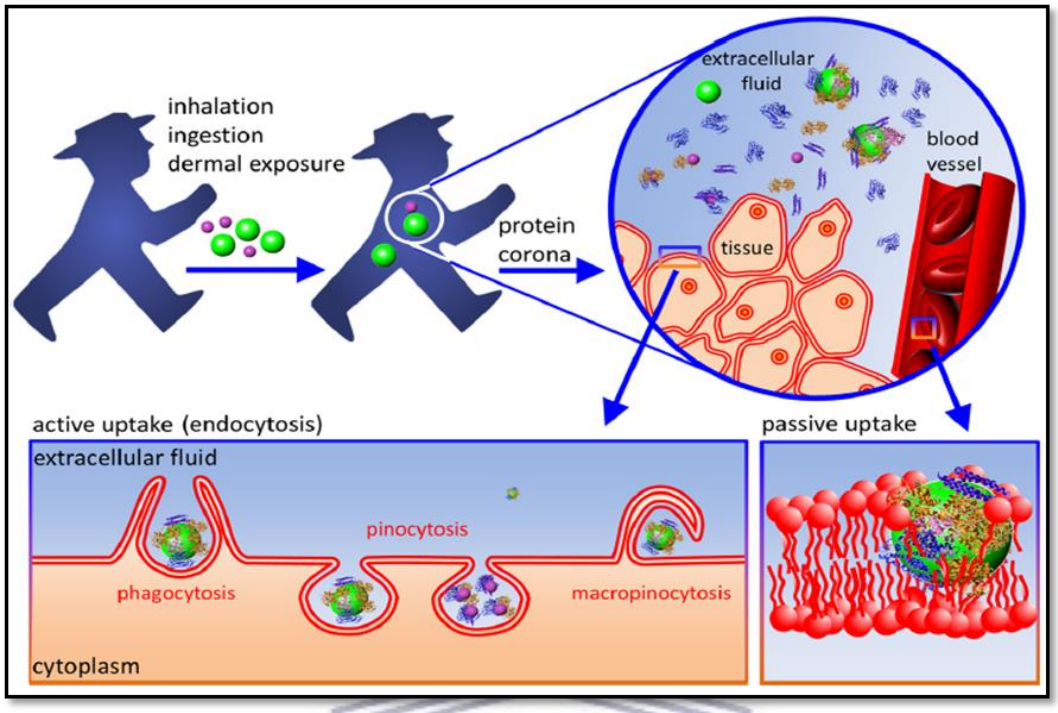

Figure 2.5: NPs can enter the human body through ingestion (oral route), inhalation or via the skin. Upon entering the human body NPs interact with free floating serum proteins forming layers on the surface of the NPs (known as opsonisation) while also facilitating receptor-based uptake of the NPs by cells through endocytosis (Pan *et al.,* 2007).

2.4.1. NPs against bacterial infections and antimicrobial resistance.

A number of metallic NPs have been reported to exert antimicrobial activities against a specific range of bacterium and have been effective against several infectious diseases, including antibiotic-resistant ones (Baek and An, 2011; Devi and Joshi, 2012; Sondi and Salopek-Sondi, 2004). Though NPs such as zinc oxide (ZnO), silver (Ag), copper oxide (CuO) and nickel oxide (NiO) have been found to have anti-microbial properties, the precise mechanisms involved in the toxicity of NPs against bacteria are still partially understood (Pelgrift and Friedman, 2013). However, it is known that NPs adhere to bacterial membranes via electrostatic interactions consequently disrupting the integrity of these membranes (Hajipour *et al.*, 2012).

Increase in reactive oxygen species (ROS) production has also been found to be closely related to metallic NP cytotoxicity against bacteria, The ROS damage the bacterial membrane, DNA, and mitochondria which leads to bacterial death, as illustrated in **Figure 2.6** below (Hajipour *et al.*, 2012; Baekand An, 2011; Devi and Joshi, 2012; Sondi and Salopek-Sondi, 2004).

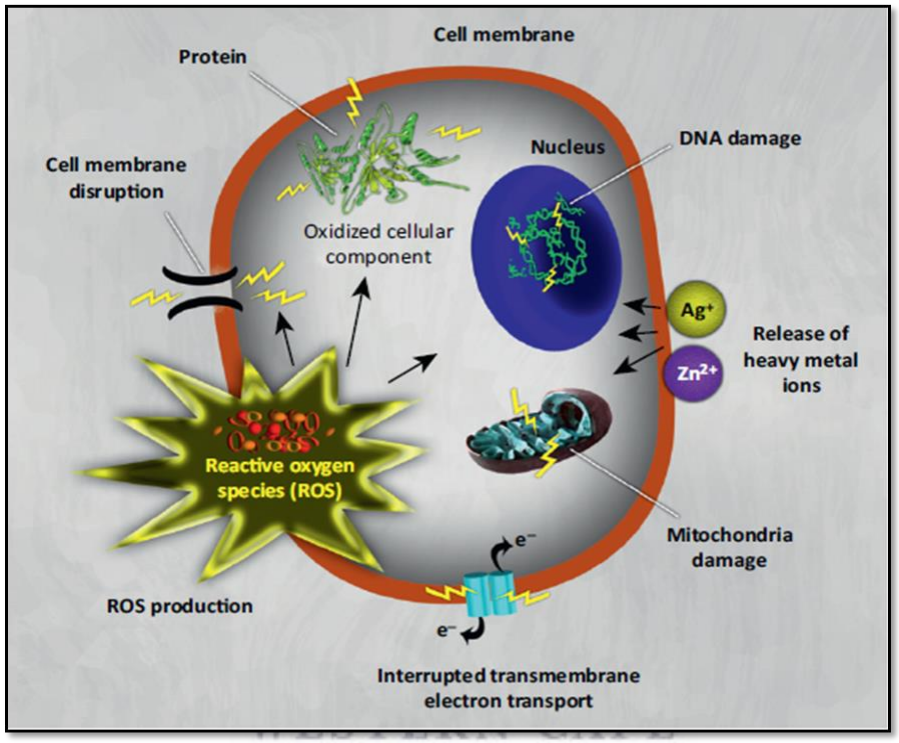

Figure 2.6: NPs and their ions (e.g., silver and zinc) can produce free radicals, resulting in induction of oxidative stress. The produced ROS can irreversibly damage bacteria (e.g., their membrane, DNA, and mitochondria), resulting in bacterial death (Hajipour *et al.,* 2012).

Various metallic NPs use several mechanisms simultaneously to battle microbes. These NPs include metal-containing NPs (MC-NPs) nitric oxide-releasing NPs (NO NPs) and chitosan-containing NPs (CC-NPs). These multiple simultaneous mechanisms of antimicrobial action highly reduce the chance of the development of resistance to these NPs, as multiple simultaneous gene mutations in the same microbial cell would be required for resistance to develop (Huh and Kwon, 2011). NPs can also target and deliver antimicrobial drugs to the site of infection, thus reducing the dose required to treat the infection and potentially overcoming microbial resistance (Hajipour *et al.*, 2012).

2.4.2. AuNPs and their application in antibacterial research

Over the years, gold suspensions have been found useful for treating an assortment of ailments including syphilis, alcoholism, and reducing pain in cancer patients (Shah *et al.,* 2014). AuNPs have large surface bio-conjugation with molecular probes and have many optical properties. As a result, these particles are frequently used in biotechnology and biomedicine (Khan *et al*., 2014). In addition, due to their small size, large surface area and crystallinity, AuNPs are excellent therapeutic agents because they can easily travel into the target cells while carrying high drug loads (Khan *et al*., 2014), and can enter the human body through dermal exposure, inhalation or ingestion (Pan *et al.,* 2007).

The toxicity of AuNPs is a highly debated topic due to the ambiguous results obtained in the studies undertaken to determine their harmful effects. Some studies found them to be non-toxic, while other studies found AuNPs to be toxic to certain human cells (Shah *et al.,* 2014). Toxicological studies suggest that NPs may cause adverse health effects. However, the fundamental relationships between cause and effect are not well defined. Due to this lack of knowledge, studies focused on understanding how AuNPs interact with biological systems such as living cells have taken centre stage in areas of collaborative research between materials science and biology (Pan *et al.,* 2007). AuNPs are very miniscule and can therefore evade natural mechanical barriers, which may possibly lead to unfavourable tissue reactions (Pan *et al.,* 2007).

Presently, AuNPs are broadly used in molecular biology applications such as immunoassays, genomics and clinical chemistry. In medical applications AuNPs are used in the detection and photothermolysis of microorganisms and cancer cells, as well as in targeted delivery of compounds such as peptides or DNA (Shah *et al.,* 2014a). The properties of the nanoparticles and the applications for which the particles are used are primarily governed by the size of the AuNPs. Small size AuNPs (2 nm-15 nm) are commonly used in biomarkers, immunohistochemistry and in microscopy (light and high magnification TEM). Medium size AuNPs (20 nm-60 nm) are generally used in DNA detection, drug delivery, biomarkers as well as in environmental detection and purification,

while large size AuNPs (80 nm-250 nm) are used in forensic science field and in manufacturing electronic device and optical mammography (Shah *et al.,* 2014).

AuNPs have advantages when compared to other inorganic nanoparticles for biomedical applications. These include: facile synthesis, easy bioconjugation with various molecules such as DNA, RNA, polyethylene glycol (PEG), antibodies, peptides, carboxyl groups, amine etc., tunable geometry, excellent biocompatibility with human cells (Lin *et al.,* 2014) and chemical stability (Shah *et al.,* 2014). Many studies have used electrostatic interactions to functionalize gold NPs to a variety of biomolecules including antibodies, peptides and DNA. However, covalent interactions result in a more stable and reproducible molecular functionalization, as a result, many NP-conjugate systems covalently bind therapeutic drugs and biomolecules using bifunctionalized linkers to minimize the chance of unfavourable conformational changes that may arise due to direct NP surface and protein interaction (Papasani *et al.*, 2012). Silver nanoparticles (AgNPs) have been the most widely studies nanoparticles for their antimicrobial properties and have been used mainly as Silver ions (Huang *et al.*, 2011).

AuNPs conjugated with or without antibiotics are currently being used to advance antibiotic delivery, dosage, target specificity and bioavailability among other things. In addition, AuNPs also improve the efficacy of the conjugated antibiotic and have been evaluated by many researchers for antibacterial activity against various bacterial strains. However, these investigations on the antibacterial activity of naked AuNPs have yielded ambiguous results (Lin *et al.,* 2014). However, in a recent study, a group of scientists investigated the effects of spherical AuNPs (sAuNPs) and spherical AgNPs on *E. coli* and *bacillus Calmette-Guérin (BCG),* a bacterium used as a surrogate for TB during the development of anti-TB drugs. The group found that both Au and AgNPs displayed excellent antibacterial potential against the Gram negative bacteria *E. coli* and the Gram positive bacteria *BCG*. The results therefore, suggested that both Ag and AuNPs have potential applications as anti-TB compounds (Zhou *et al.,* 2013).

A study by Misawa and Takahashi investigated the generation of reactive oxygen species induced by AuNPs (diameters: 5, 10, 20, 60 and 250nm) under x-ray and UV Irradiation, the results showed that AuNPs of smaller diameter lead to a greater yield of ROS (Misawa and Takahashi, 2011). It was also found that, electron charge transfer was involved in the generation of superoxide anion (O_2^-) while fluorescent x-rays were involved in the generation of hydroxyl radical (OH), the generation of ROS was also found to be dependent on the AuNP concentration (Misawa and Takahashi, 2011). The activity of AuNPs can be tuned by controlling properties such as their shape and size (Shah *et al.,* 2014). However, research on the role of size and shape on the antimicrobial activity of AuNPs have produced contradicting results (Zhou et al., 2013; Shamaila *et al.,* 2016).

2.4.2.1. Methods for AuNP synthesis

Methods for AuNP synthesis can be grouped into two principles, the "top down" methods or the "bottom up" methods (Shah *et al.,* 2014). Top down methods involve the assembly of atoms (via reduction of ions) into the required nanostructures. These methods include photolithography and electron beam lithography (Sun *et al.,* 2006), and require the deduction of matter from the bulk material to obtain the required nanostructure. Bottom up methods include: nanosphere lithography, chemical, sonochemical, photochemical, templating, electrochemical, and thermal reduction techniques. Both methods can be used to prepare AuNPs of any shape and size, however, each method has its own shortcomings (e.g., poor monodispersity in the bottom up methods, and excessive waste of material in case of top down methods) (Magnusson *et al.,* 1999). Some commonly used "bottom up" methods for the synthesis of AuNPs are discussed below.

2.4.2.1.1. The Turkevich method

The Turkevich method was first discovered in 1951 and has become one of the most commonly used methods for the synthesis of spherical AuNPs in the size range of 10 nm-20 nm (Figure 2.7). The principle of this method is the reduction of gold ions (Au^{3+}) to gold atoms (Au^0) in the presence of reducing agents such as citrate as illustrated in **Figure 2.7** below (Turkevich *et al.,* 1951), ascorbic acid, amino acids or UV light (Niidome *et al.,* 2003). The synthesized AuNPs can be further stabilized using various capping/stabilizing agents. The Turkevich method could initially only be used to generate a narrow size range of

AuNPs. However, the original method has had several modifications which have made it possible for researchers to increase the size range of particles that can be generated through this method (1-100 nm) (Shah *et al.,* 2014). In 1973, Frens found that one can achieve AuNPs of specific size, ranging from 16 nm to 147 nm by varying the ratio of the reducing agent to the stabilizing agent. The roles of temperature, pH and sodium citrate concentration were better understood in the years to follow, making it easier for researchers to generate a particle growth model (Chow and Zukoski, 1994).

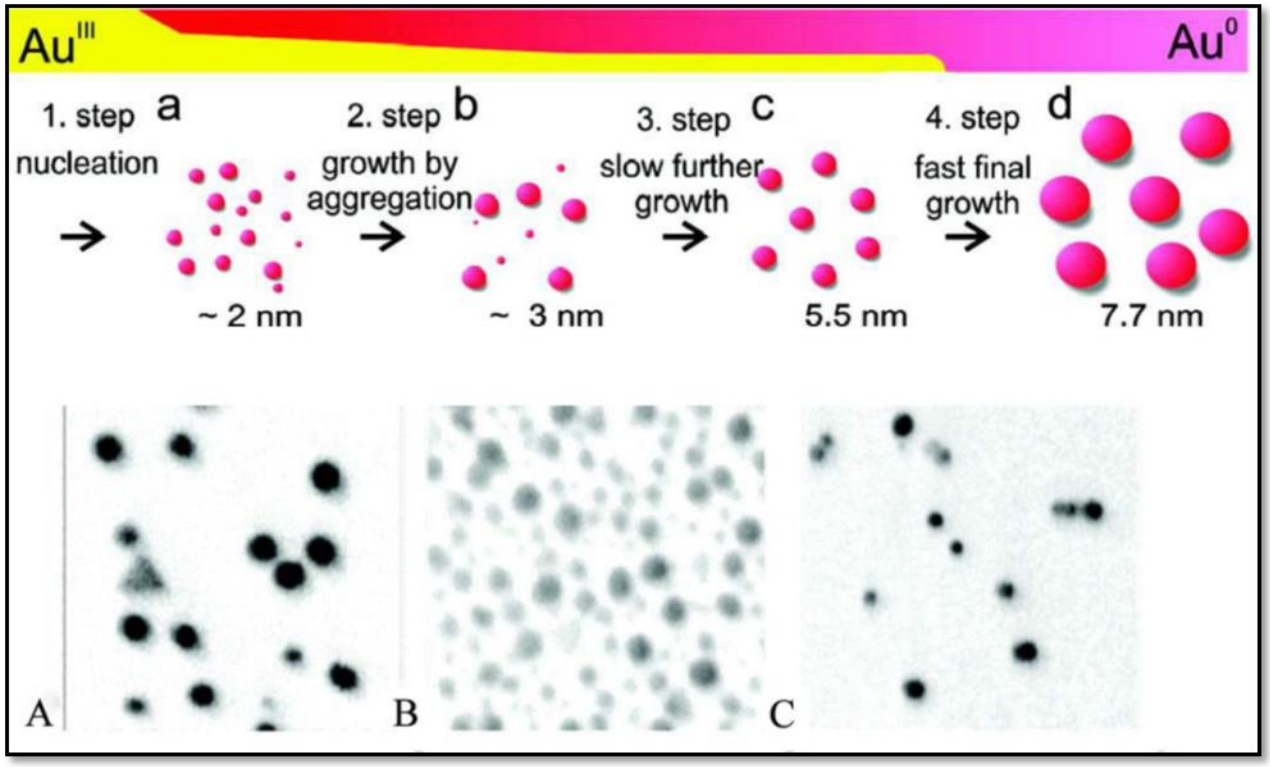

Figure 2.7: Schematic diagram showing the process of synthesizing AuNPs using the Turkevich method. The Upper panel shows an illustration of the system involved in the synthesis of AuNPs using the citrate reduction method. The Lower panel shows SEM images of AuNPs (A-C) synthesized using different chemical reduction methods such as citrate reduction at 100°C, UV irradiation and ascorbic acid reduction respectively (Shah *et al.,* 2014).

2.4.2.1.2. Brust method

The Brust method was first discovered in 1994 (Shah *et al.,* 2014). This method uses organic solvents to synthesize 1.5 nm to 5.2 nm AuNPs in a two phase process by varying the ratio of thiol to Au. The Brust method was adopted from Faraday's two phase system and involves the transfer of gold salt from aqueous solution to an organic solvent such as toluene using a phase transfer agent such as tetraoctylammonium bromide (TOAB). The Au is then reduced using sodium borohydride in presence of an alkanethiol. The alkanethiols are used to stabilize the AuNPs (Giersig and Mulvaney, 1993), the reduction process results in a colour change of the reaction from orange to brown as illustrated in **Figure 2.8** below (Shah *et al.,* 2014).

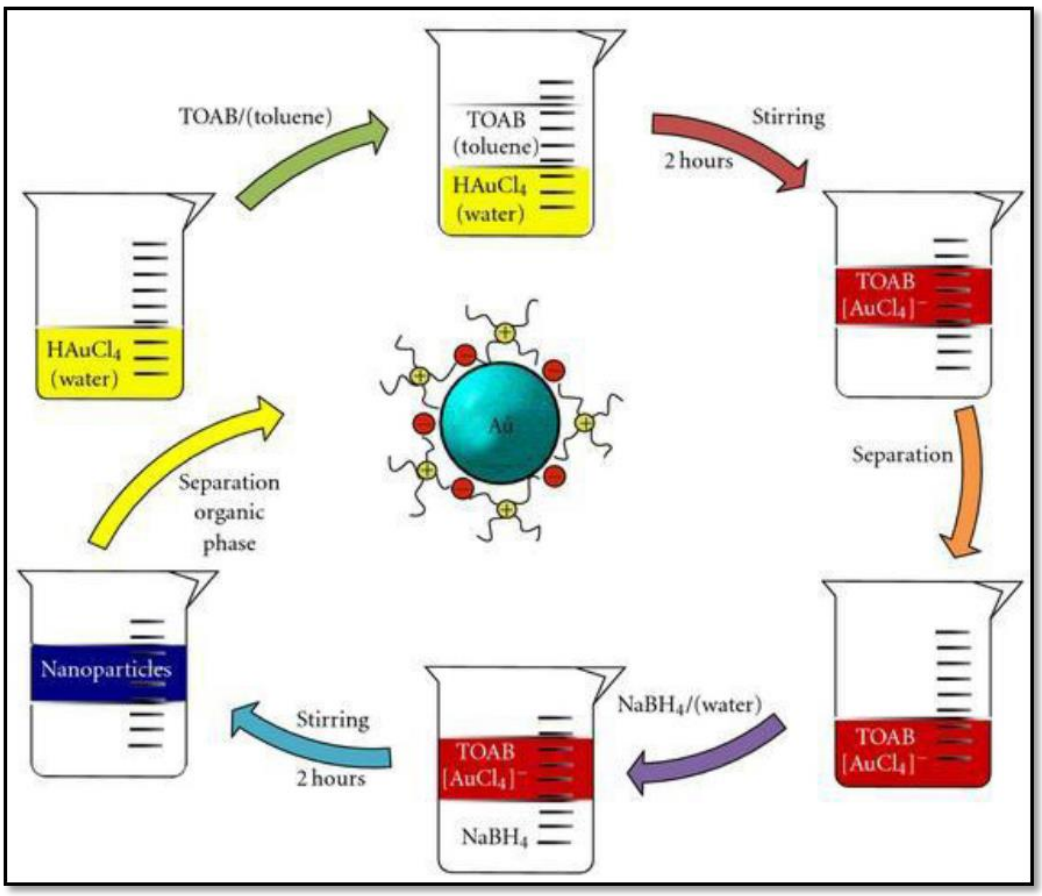

Figure 2.8: A schematic diagram of the steps involved in the synthesis of AuNPs using brust method. In this illustration the gold (Au^{3+}) precursor which is $HAuCl_4$ is moved to an organic phase (toulene) with the help of TOAB where it is reduced to Au0 in presence of NaBH4 to yield 5±1 nm NPs (Shah *et al.,* 2014).

2.4.2.1.3. Seeded growth method

The Turkevich and Brust method are generally used to generate spherical AuNPs, on the other hand, The most widely preferred technique for synthesizing AuNPs in other shapes (common shapes include spherical, rod-shaped and star-shaped AuNPs) is the seed growth method (Zhi-Chuang *et al.,* 2007). As illustrated in **Figure 2.9**, the principle of this method involves first producing seed particles by reducing Au salts with a strong reducing agent such as sodium borohydride. Then silver ions are mixed with a solution of Au salt in the presence of a weak reducing agent (ascorbic acid) and structure directing agent to prevent further nucleation and to accelerate the anisotropic growth of the AuNPs. The geometry of the AuNPs can be controlled by altering the concentration of seeds, structure directing agents, and that of the reducing agents (Shah *et al*., 2014).

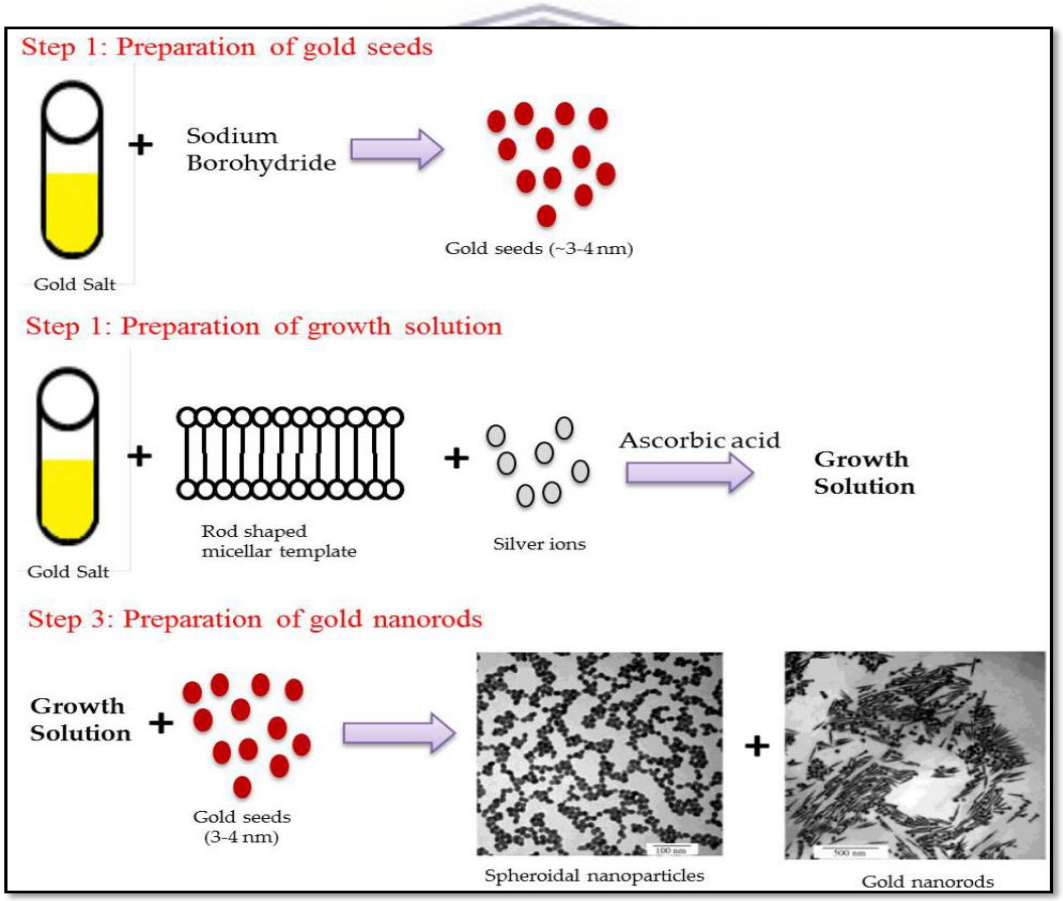

Figure 2.9: A schematic diagram showing the synthesis of Au nanorods and spheroidal NPs using seeding growth method and TEM images of the synthesized NPs. Step 1 involves synthesis of Au seeds which are then mixed with growth solution synthesized in step 2 to yield spherical AuNPs and nanorods (Shah *et al.,* 2014).

2.4.2.1.4. Miscellaneous methods.

The most common method is digestive ripening (Murphy *et al.,* 2005). This method involves generating monodispersed AuNPs from polydisperse NPs by using excessive ligands (also known as digestive ripening agents). A colloidal suspension is heated at high temperatures (~138 ^{0}C) for 2 minutes and then at 110 ^{0}C for 5 hour in presence of alkanethiols. Temperature is used to control the size distribution of the synthesized Au colloids. The various ligands that are used for digestive ripening include: thiols, amines, silanes, phosphines etc. (Lin *et al.,* 2000). In addition, other methods that have been explored for AuNP synthesis include: solvothermal method, ultrasonic waves, laser ablation, microwaves, electrochemical and photochemical reduction (Shah *et al.,* 2014).

2.4.2.1.5. Green synthesis of AuNPs

The methods described above can efficiently generate AuNPs; however, these methods generate toxic by-products that have negative effects to the environment during large scale production (Chen *et al.,* 2009). In addition, these toxic chemicals and solvents may be challenging for downstream biological applications of AuNPs. To overcome these concerns, new strategies to generate AuNPs without toxic chemicals have been developed. Biological synthesis of AuNPs, using natural components like carbohydrates, lipids, nucleic acids or proteins is a fast growing area of research that focuses on synthesizing AuNPs using clean, eco-friendly, non-toxic methods (Shah *et al.,* 2014). These methods not only decrease the toxicity issues associated with AuNPs synthesis, but have additional advantages which include: low cost of production, wide availability, ease of synthesis, and environmentally safe. To date, various studies have been conducted and published where AuNPs of different sizes and shapes where synthesized using the above biological sources. The only disadvantage of the green synthesis method is that the synthesized NPs are coated with the biological reducing agents which may interfere with the activity of the AuNPs. Therefore, green synthesis is not ideal for synthesizing naked uncapped NPs (Shah *et al.,* 2014).

2.4.2.2. Characterization of gold NPs

The applications of AuNPs heavily rely on their size and shape, and where the driving force behind the extensive research to find efficient methods to synthesize AuNPs with specific shapes and sizes (Shah *et al.,* 2014). Nanomaterials have distinct physicochemical properties, such as size, shape, surface properties, molecular weight, stability, purity, zeta potential, and solubility, which are significant to some physiological interactions (Patri *et al.,* 2006). These interactions may grant some benefits in medical applications, such as reduction of side effects, improvements in efficacy, prevention and treatment of diseases (Lin *et al.,* 2014). It is therefore important to understand how the different physicochemical characteristics affect their *in vivo* distribution and behaviour of nanomaterials. This requires the use of reliable and tough techniques (Lin *et al.,* 2014). Some of the physicochemical properties and the techniques used to study them are discussed below.

2.4.2.2.1. Size

Size is a key factor in engineered NPs as it controls penetration of nanomaterials across the physiological drug barrier, controls the navigation and circulation of nanomaterials in the bloodstream, site- and cell-specific localization as well as the induction of cellular responses (Ferrari, 2008). Recent discoveries have showed that activity and toxicity of NPs is correlated to their size (Horváth *et al.,* 2013). Smaller AgNPs have been found to cause more apoptotic effects against some cell lines in comparison to larger AgNPs. In addition, silica NPs of 20 nm in size were found to exhibit more toxicity when compared to 100 nm silica NPs (Kim *et al.,* 2012). The hydrodynamic size of a nanomaterial is the size calculated from the diffusion coefficient using the Stokes–Einstein relationship (Powers *et al.,* 2006).

2.4.2.2.2. Shape

AuNPs can be synthesized to have various sizes, which range from1 nm to 8 μm. As illustrated in **Figure 2.10**, These NPs can also be synthesized in a number of different shapes including nanospheres, nanorods, nanostars and nanotriangles. The shape of nanomaterial can play an important role in drug delivery, degradation, transport, targeting and internalization (Decuzzi *et al.,* 2009).

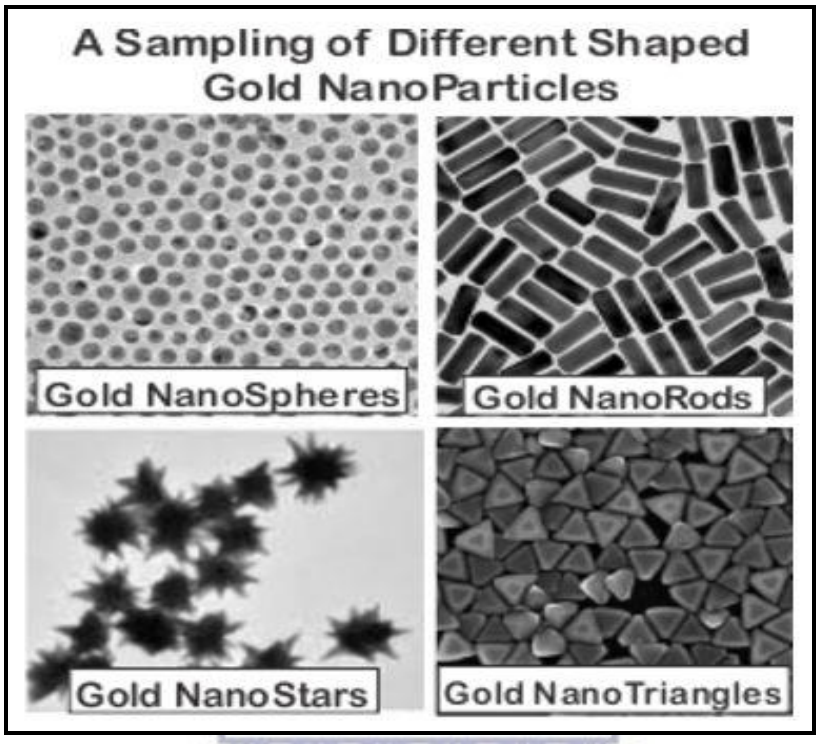

Figure 2.10: HR-TEM images illustrating the four common shapes of AuNPs (Free billion investment guide, 2017).

It has been reported that the efficiency of drug delivery carriers and the phagocytosis of drug delivery carriers through macrophages can be highly influenced by the shape of the carrier (Decuzzi *et al*., 2009). In addition, the shape of AuNPs has been found to play a vital role in the cellular uptake, biocompatibility and in the retention of the NPs in tissues and organs (George *et al*., 2012).

2.4.2.2.3. Stability

Pharmaceutical stability is a term used to describe how long a manufactured pharmaceutical (or nanomedicine) can retain the same properties (Briscoe and Hage, 2009). As it is for single-molecule pharmaceuticals, the stability of nanomedicines/ nanoparticles (such as AuNPs) can be affected by a number of factors, such as pH, temperature, moisture, solvents, particle/molecular size, enzymatic degradation and the presence of other recipients and impurities, as well as exposure to different types of ionizing and non-ionizing radiation, (Patri *et al.,* 2006). One study found that the stability of nanomaterials can have a huge impact on their toxicity (Hardman, 2006).

2.4.2.2.4. Composition and purity

Composition of nanomaterials affects their transport, delivery and biodistribution in biomedical applications. Sometimes there's a need to form an amalgamation of two or more types of nanomaterials to create a more complex material. As a result, the chemical composition analysis of the nanomaterial amalgamations is more complicated than that of individual particles (Patri *et al.,* 2006). Chemical composition is one of the important factors in determining the toxicity of NPs (Buzea *et al.,* 2007).

The presence of pharmaceutical impurities can considerably affect the efficacy of a drug or worse introduce hostile side effects. In general, the purity of nanomaterials can be determined via the analysis of their chemical compositions. To ensure the absence of endotoxin contamination, proper purification measures are necessary for the removal of any residual manufacturing components or side products before finalizing a nanomaterial's formulation and proceeding with the composition analysis (Crist *et al.,* 2013).

2.4.2.2.5. Zeta Potential

Zeta Potential analysis is a technique used to determine the surface charge of NPs in solution (colloids). As illustrated on **Figure 2.11**, NPs have a surface charge that attracts a thin layer of oppositely charged ions from the surrounding solution to the NP surface, resulting in the formation of a double layer of ions around the NPs. This double layer of ions moves with the NPs as they diffuse all over the solution (**Figure 2. 11**). The zeta potential of a NP is the electric potential at the boundary of the double layer and has values that range between +100 mV to -100 mV (Sosenkova and Egorova, 2011).

The zeta potential can be used to predict the colloidal stability of NPs, NPs with Zeta Potential values greater than +25 mV or less than -25 mV are considered to be typically very stable, on the other-hand NPs with zeta potential values less than + 25 mV or higher than – 25 mV can be predicted to be less stable and more prone to eventually aggregate due to Van Der Waal inter-particle attractions (Nanocomposix, 2012). These physicochemical properties can be examined using a variety of techniques as summarized in **Table 2.2 and Table 2.3** below.

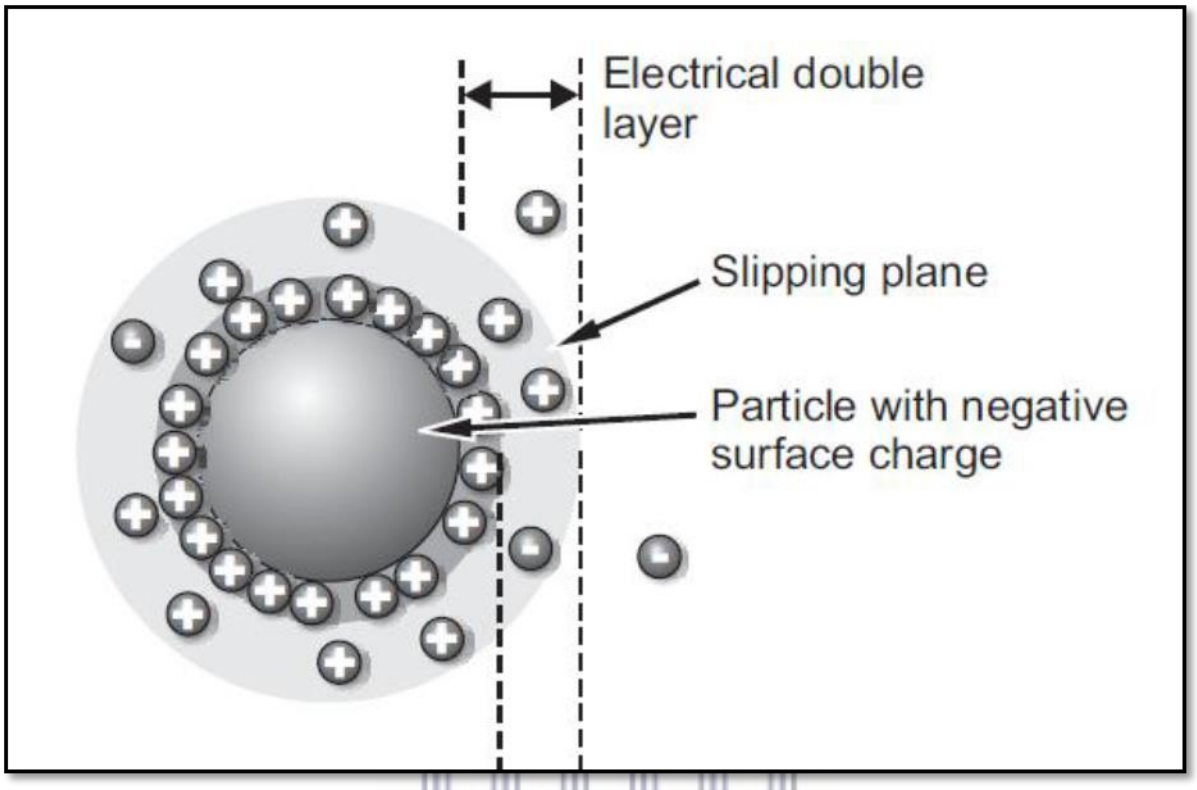

Figure 2.11: Electrical/ionic double layer surrounding NPs in suspension (Nanocomposix, 2012).

Table 2.2: Techniques used to characterize the physicochemical properties of nanomaterial.

Name of technique	**Physicochemical properties characterized**
Scanning electron microscopy (SEM)	Electron microscopy (EM) uses beams of accelerated electrons and electrostatic or electromagnetic lenses to generate images of high resolution, based on the much shorter wavelengths of electrons than visible light photons. SEM is a surface imaging method in which the incident electron beam scans across the sample surface and interacts with the sample to generate signals reflecting the atomic composition and topographic detail of the specimen surface (Johal, 2011).
Transmission electron microscopy (TEM)	TEM provides direct images and chemical information of nanomaterials at a spatial resolution down to the level of atomic dimensions (< 1 nm); in addition to the high spatial resolution of TEM that enhances the morphological and structural analyses of nanomaterials (Williams and Carter, 2009).
Atomic force microscopy (AFM)	Analyzes the size, shape, structure, sorption, dispersion and aggregation of nanomaterials. Is also capable of characterizing dynamics between nanomaterials in biological situations, such as observing the interaction of nanomaterials with supported lipid bilayers in real time, which is not achievable with other EM techniques (Patri *et al.,* 2006).

Table 2.3: Techniques used to characterize the physicochemical properties of nanomaterial.

Name of technique	**Physicochemical properties characterized**
Dynamic light scattering (DLS)	Explores several physicochemical characteristics of nanomaterials including hydrodynamic size, shape, structure, aggregation state, and biomolecular conformation using radiation scattering techniques (Patri *et al.,* 2006).
Infrared (IR) spectroscopy	Commonly employed to express the characteristic spectral bands to reveal nanomaterial–biomolecule conjugation, *e.g.* proteins bound to NP surfaces, and to illustrate the conformational states of the bound proteins (Johal, 2011).
Nuclear magnetic resonance (NMR)	Resolves the structures of amorphous materials, polymers and biomolecules that lack long-range order, also evaluates the compositions of the species and provides tools to investigate dynamic interactions of the species in different conditions (Wang *et al.,* 2001).
X-ray diffraction (XRD)	Crystalline size, shape and lattice distortion by long-range order, but is limited to disordered materials (Chapman *et al.,* 2011).
UV–visible absorbance and Fluorescence spectroscopy (FS),	Size, concentration, aggregation state and even bio-conjugation when the absorption profiles of nanomaterials are distinct (Biju *et al.,* 2010).

2.5. Methods for screening antimicrobial activity

Numerous laboratory methods are available that be used to assess or screen pure compounds or an extract for any *in vitro* antimicrobial activity. Two of the most commonly known and used methods are the agar dilution and the disk diffusion methods. However, flow cytofluorometric and the time-kill test methods are recommended for a further in depth study of the antimicrobial effect of an agent, as the two methods provide precise information on the nature of the inhibitory effect (bactericidal or bacteriostatic)(time-dependent or concentration-dependent) and the type of damage inflicted to the target microorganism.

2.5.1. Agar disk-diffusion methods

Agar disk-diffusion testing was first developed in 1940 and is the most commonly used method in many clinical microbiology laboratories for regular antimicrobial susceptibility testing (Baoum *et al.,* 2010). However, not all fastidious bacteria can be tested accurately using this method, therefore new standards have been made to test certain fastidious bacterial pathogens such as *Haemophilus influenzae, Neisseria meningitides, Neisseria gonorrhoeae, Haemophilus parainfluenzae* and *streptococci,* using specified culture media, various incubation conditions and interpretive criteria for inhibition zones (Balouiri *et al*., 2015). The Clinical and Laboratory Standards Institute (CLSI) has published many accepted and approved standards for bacteria and yeasts testing as summarized on **Table 2.4** below (Balouiri *et al*., 2015).

In this procedure, standardized inoculums of the test microorganism are inoculated onto agar plates. Then, filter paper discs of about 6mm in diameter, dipped in the test compound at a desired concentration, are placed on the agar surface. The Petri dishes are then incubated under appropriate conditions. Normally, antimicrobial agents diffuse into the agar and inhibit the growth and germination of the tested microorganism and then the diameters of inhibition growth zones are measured and compared. An antibiogram categorizes bacteria as either susceptible, intermediate or resistant (Jorgensen *et al*., 2009). However, this method cannot distinguish between bactericidal and bacteriostatic effects. therefore, agar disk-diffusion is not an appropriate method for determining the minimum inhibitory concentration (MIC) of an agent, as it is

impossible to quantify the amount of the antimicrobial agent diffused into the agar medium(Nijs *et al*., 2003). Nonetheless, the disk-diffusion assay still offers many advantages over other methods such as low-cost, simplicity, the ability to test enormous numbers of microorganisms and antimicrobial agents, and the ease to interpret results provided (Balouiri *et al*., 2015).

2.5.2. Thin-layer chromatography (TLC) bio-autography

This technique is a combination of TLC with both biological and chemical detection methods. TLC bio-autography has been commonly used to screen organic extracts, mainly plant extracts, for antibacterial and antifungal activity (Balouiri *et al*., 2015). Three bio-autographic techniques are regularly employed for investigating antimicrobial drugs, these are; agar diffusion, direct bio-autography and agar – overlay assay (Balouiri *et al*., 2015).

2.5.3. Dilution methods

Dilution methods are regarded as the best methods for determining MIC values of antibacterial and antifungal agents, because they allow for the estimation of the concentration of the tested antimicrobial agent in the agar (agar dilution) or broth medium (macro dilution or micro dilution). Both broth and agar dilution methods can be used to quantitatively measure the *in vitro* antimicrobial activity against bacteria and fungi. An MIC value is defined as the lowest concentration of an antimicrobial agent that can inhibit the visible growth of the tested microorganism; the value is usually expressed in mg/ml or in mg/l (Balouiri *et al*., 2015). Many approved guidelines have been published for dilution antimicrobial susceptibility testing of fastidious or non-fastidious bacteria, yeast and filamentous fungi. These guidelines provide a tested and practical blueprint to performing most clinical microbiology laboratories. The Clinical & Laboratory Standards Institute (CLSI) and the European Committee on Antimicrobial Susceptibility Testing (EUCAST) are the most recognized standards (Pfaller *et al.,* 2004).

Table 2.4: Culture media, microbial inoculums size and incubation conditions for antimicrobial susceptibility testing methods as recommended by CLSI (Balouiri *et al*., 2015).

Methods	Microorganism	Growth medium	Final inoculums size	Incubation temperature (°C)	Incubation time (h)
Disk-diffusion	Bacteria	MHA	(0.5McFarland)(1–2)x10^8 CFU/ml	35±2	16 – 18
	Yeast	MHA + GMB	(0.5McFarland)(1–5)x 10^6 CFU/ml	35±2	20 – 24
	Mold	Non-supplemented MHA	(0.4–5)x10^6 CFU/ml	-	-
Broth microdilution	Bacteria	MHB	5 x 10^5x CFU/ml	35±2	20
	Yeast	RPMI 1640	(0.5–2.5) x 10^3 CFU/ml	35	24 – 48
	Mold	RPMI 1640	(0.4–5) x 10^4 CFU/ml	35	48 for most fungi
Broth macrodilution	Bacteria	MHB	5 x 10^5 CFU/ml	35±2	20
	Yeast	RPMI 1640	(0.5–2.5) x 10^3 CFU/ml	35	46 – 50
	Molds	RPMI 1640	(0.4–5) x 10^4 CFU/ml	35	48 for most fungi
Agar dilution	Bacteria	MHA	10^4 CFU/spot	35±2	16 - 20
Time-kill test	Bacteria	MHB	5 x 10^5 CFU/ml	35±2	0, 4, 18, and 24

2.5.4. Time-kill test (time-kill curve)

Time-kill test is regarded as the most suitable method for determining the bactericidal or fungicidal effect. The method is well-suited for obtaining information about the dynamic interaction between the antimicrobial agent and the microbial strain. The time-kill test can be used to obtain time-dependent or concentration-dependent antimicrobial effects of an antimicrobial agent (Pfaller *et al.,* 2004).The test is performed in broth culture medium using three tubes which each contain a bacterial suspension of 5 x 10^5 CFU/ml. The first and the second tubes contain the antimicrobial agent usually at final concentrations of 0.25 x MIC and 1 x MIC, and the third tube is used as the growth control. The incubation is done under suitable conditions for varied time intervals (e. g. 0, 4, 6, 8, 10, 12 and 24 h) (Konaté *et al.,* 2014).

The percentage of dead cells is calculated relatively to the growth control by determining the number of living cells (CFU/ml) in each tube using the agar plate count method. The bactericidal effect is usually obtained with a lethality percentage of 90% for 6 h, which is equivalent to 99.9% of lethality for 24 h (Konaté *et at.,* 2014). This method can also be used to determine synergy or antagonism between two or more drugs in combinations (Pfaller *et al.,* 2004).

Chapter 3: Problem statement, aims and objectives, hypothesis

3.1. Problem statement

The emergence of antibiotic- and/or multidrug-resistant bacteria has become a major global challenge for public health. The killing of antibiotic-resistant bacteria requires a high dose of multiple, expensive drugs, which possess unfavourable side effects. These treatments require longer time to clear the infection and as a result are more costly (Leid *et al*., 2012). Due to this antibiotic/ multidrug resistance, novel strategies are required to combat drug resistant infections and to prevent further microbial resistance (Hajipour *et al.*, 2012). AuNPs in solution, prepared using the citrate reduction method, have been found to be photo-mutagenic against *Salmonella Typhimurium (–)* strain TA102. The antibacterial activity of AuNPs commonly involves the formation of free radicals, mainly ROS, which induce oxidative stress after the administration of the NPs (Hajipour *et al.*, 2012).

The antibacterial activity of NPs depends on the nanoparticle composition, surface modification, intrinsic properties, and the bacterial species being targeted. The susceptibility of bacterial species to the antibacterial activity of NPs is also related to the cell wall structure i.e. whether the bacterium is Gram-positive or Gram-negative. However, the effect of AuNP size, concentration and exposure time on bacterial growth is still not well understood (Shamaila *et al.,* 2016; Zawrah and El-Moez, 2011). In Zawrah and El-Moez (2011), AuNP were found to have antibacterial activity. However, the effect of size and exposure time was not fully investigated (only studies for 24 hours) and the results were all based on visual inspection. In Shamaila *et al.,* (2016), the effect of concentration and size were investigated. However, exposure time was short (only 24 hours), and the absorbance interference of the AuNPs was not taken into account when conducting the spectrophotometry of the MIC experiments. Therefore, the correlation of concentration with size still needs to be properly elucidated as well as the influence of exposure time.

3.2. Detailed Research Plan

3.2.1. Aim

The aim of this study was to examine the effect of size, concentration and exposure time on the bacterial growth inhibition activity of spherical gold nanoparticles (sAuNPs).

3.2.2. Objectives

- Synthesis of three different sizes of sAuNPs.
- Characterize the physicochemical properties of the three AuNPs.
- Determine the effect of size, concentration and exposure time on the bacterial growth inhibition activity of sAuNPs.

3.2.3. Hypothesis

It was hypothesized that the antibabacterial activity of AuNPs depends on the size and on the concentration of the AuNPs.

Chapter 4: Synthesis and Characterization of sAuNPs

4.1. Introduction

Citrate capped sAuNPs can be synthesized using the Turkevich method (also known as the citrate reduction method), where gold ions (Au^{3+}) are reduced to gold atoms (Au^{0}) in the presence of citrate as a reducing agent (Turkevich *et al.,* 1951). The method is popular and opportune; however the stability and dispersity of the resulting NPs are frequently limited. In recent years however, this method has been modified to improve the monodispersity and to get an improved control of the size (nm) of the synthesized NPs by adjusting the reaction conditions (Jingyue and Bernd, 2015). Through these investigations, it has been discovered that solutions used in the process of the Turkevich method are sensitive to the alteration of the ionic strength of the medium, pH and the presence of other organic materials (Jingyue and Bernd, 2015). This information has been used in a variety of studies which have discovered that the Turkevich method can be controlled to achieve defined size distribution requirements. Due to the low-cost reducing agents, non-toxic water solvent, and the minimal pollution caused by reaction, the Turkevich method is considered to be a suitable route for producing quality sAuNPs of distinct sizes (Jingyue and Bernd, 2015).

The potential of AuNPs for biomedical applications can be accredited to their surface plasmon properties (Dykman and Khlebtsov, 2012). Surface plasmon resonance (SPR) is a unique phenomenon witnessed in AuNPs when the frequency of oscillating electrons in the conduction band of the Au resonates with the frequency of the incoming light radiation thus resulting in a plasmon band that can be determined using an absorbance spectrophotometer (Mie, 1908). In AuNPs, the resonance properties are marked by a drastic colour change from a golden colour in its bulk form to a variety of colours when reduced to its nano-structures (Dykman and Khlebtsov, 2012). In colloidal solutions, small (1-50 nm) sAuNPs display a wine red colour with a λ_{max} at generally 520 nm which can be visualized easily without any further development process. However, due to aggregation the size of the NPs can increase resulting in a colour change from red to purple (≤ 60 nm), to blue (≤ 90 nm) and almost black (≤ 150 nm), depending on the size of the NPs as illustrated in **Figure 4.1** (Agnihotri *et al.,* 2009; Lata *et al.,* 2014).

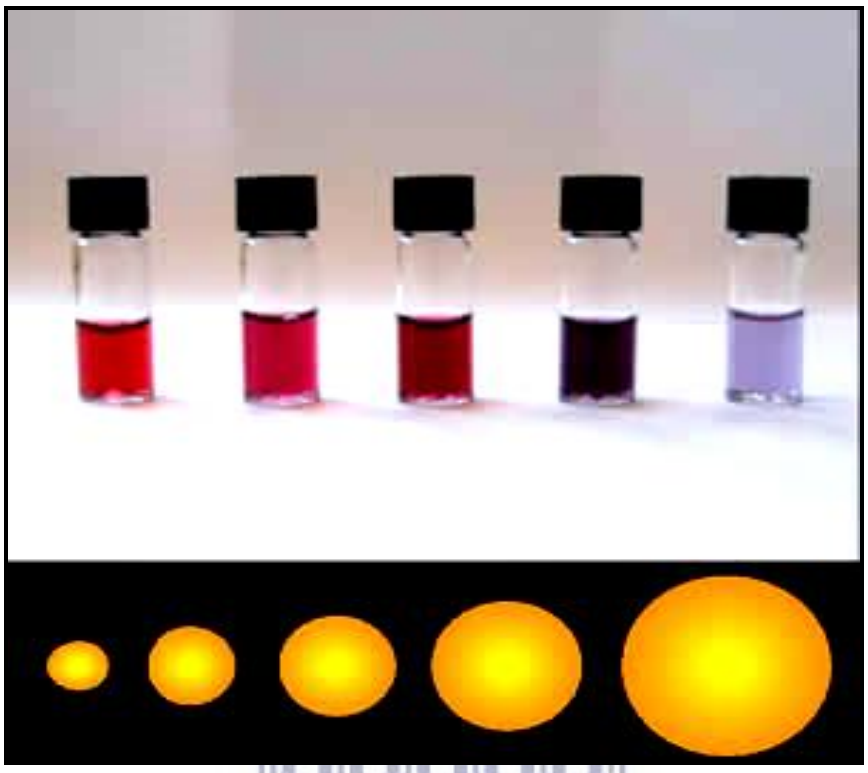

Figure 4.1: An illustration of the colour change associated with different sizes of sAuNPs (Agnihotri *et al.,* 2009).

The narrow frequency range of light radiation responsible for achieving SPR in AuNPs generally falls in the visible and near-infrared region (NIR). A single plasmon band is normally observed for sAuNPs at approximately 520 nm, the Plasmon band of different sizes of sAuNPs are well defined and have been listed on **Table 4.1** below (Shah *et al*., 2014a). For anisotropic NPs like nanorods, two plasmon bands are observed due to the electron oscillation along two axis viz. longitudinal (long) and transverse (short) respectively. The transverse plasmon band occurs at ~ 520 nm whereas the longitudinal plasmon band appears at a longer wavelength depending upon the aspect ratio of nanorod (ratio of length/width) (Huang *et al.,* 2007).

Table 4.1 : Size dependent change in peak SPR wavelength of spherical AuNPs Source (Shah *et al.,* 2014).

Size of sAuNP	**Peak SPR wavelength**
5 nm	515-520 nm
10 nm	515-520 nm
20 nm	524 nm
30 nm	526 nm
40 nm	530 nm
50 nm	535 nm
60 nm	540 nm
80 nm	553 nm
100 nm	572 nm

SPR is a vital tool for analysing the morphological properties of AuNPs (Shah *et al.,* 2014). The SPR band intensity and peak depends on factors which mainly influences the electron charge density of the particle surface such as particle size, type of metal, structure, shape, composition and the dielectric constant of the surrounding medium (Huang *et al.,* 2007). These properties may play a vital role in biological applications, it is therefore important to understand the different physicochemical characteristics before using the produced NPs (Lin *et al.,* 2014).

The physicochemical properties of NPs in a given suspension are commonly analyzed using a DLS technique and the DLS results are commonly expressed in terms of z-average (Lim *et al.,* 2013). However, the use of z-average to provide the characteristic hydrodynamic size of NPs is only accurate or recommended if the suspension is spherical, monomodal (only one peak), and monodisperse. Therefore, the z-average of a NP mixture with obvious size differences (bimodal distribution), is less accurate at predicting the true average hydrodynamic size of an AuNP sample (Lim *et al.,* 2013).

The application of nanomaterials in biological environments and bio-materials may compel the NPs to a state of aggregation, coagulation and/or non-specific absorption. This can be as a result of a variety of intermolecular interactions that may occur between the interfaces of the nanomaterials with the bio-molecules and the interaction-mediating fluids (Nel *et al*., 2009). The surface properties of nanomaterials in a specified medium are generally characterized by their physicochemical properties, such as shape, surface geometry and crystallinity, chemical composition, porosity, heterogeneity and hydrolytic stability. However, other properties, such as surface charge, size distribution, dissolution, dispersion stability and aggregation, are mainly regulated by the ionic strength, pH and temperature (Nel *et al*., 2009).

Pharmaceutical stability refers to the time period a given pharmaceutical agent can retain its properties after the manufacturing process. The stability of nanomaterials can be affected by a variety of factors, including particle size, type of solvent, pH, exposure to different types of ionizing and non-ionizing radiation, enzymatic degradation, moisture, temperature and the presence of impurities (Briscoe and Hage, 2009; Patri *et al.,* 2006). Therefore, when NPs are introduced into biological environments/ media, many unfavourable effects such as non-specific absorption, coagulation and aggregation are likely to occur. This may be due to a range of intermolecular interactions taking place at the interfaces of NPs and interaction-mediating fluids (Nel *et al.,* 2009).

In a given medium, the surface properties of a nanomaterial are governed by their physicochemical properties, which include shape, porosity, chemical composition, crystallinity, surface geometry, heterogeneity and hydrolytic stability. On the other hand other properties, such as hydrodynamic size distribution, surface charge, hydration, dissolution, dispersion stability, agglomeration and aggregation of nanomaterial, are mainly governed by their ionic strength, temperature, pH and the presence of biological or organic macromolecules in the specific medium (Lin *et al.,* 2014). The stability of nanomaterials may have a vital contribution on their corresponding efficacy, thus it is important to investigate the stability of NPs in different biological media before conducting any vital experiments (Lin *et al.,* 2014).

4.2. Objectives of this chapter

The objective of the work described in this chapter was to synthesize sAuNPs of three different sizes using the Turkevich method and to characterize the produced NPs by analyzing their different physicochemical properties in distilled water (dH_20) using appropriate techniques. A further objective was to determine the stability of each AuNP sample in dH_20 and Lysogeny broth (LB) at 4 °C and at 37°C.

4.3. Materials & methods

4.3.1. Reagents and materials

Gold (III) chloride trihydrate (HAuCl4•3H2O) ACS, (99.9 %) was obtained from Sigma Aldrich (St. Louis, USA), tri-Sodium Citrate ($Na_3\ C_6H_5O_7.\ 2H_2O$) and Lysogeny Broth (LB) were obtained from Merck Laboratory Supplies (Darmstadt, Germany). All glass ware was washed with anti-bacterial liquid hand soap purchased from KIMIX (Cape Town, South Africa) Ultra-purified distilled water (18.2 MΩ cm, Millipore) was used in all experiments.

4.3.2. Instrumentation

The AuNPs were synthesized on a Stuart Hot Plate Stirrer (Stuart equipment, UK). The UV-Visible spectra were determined using a POLARstar Omega plate reader (BMG LABTECH, Germany). The hydrodynamic size, poly-dispersity index (PDI) and the zeta-potential of the NPs was determined using The Malvern Zetasizer Nano-ZS90 (Malvern, UK). Transmission Electron Microscope (TEM) images and the elemental analysis of the AuNPs were obtained using a Field Emission TEM (Tecnai F20) (FEI Company, USA).

4.4. Methods

4.4.1. Synthesis of AuNPs

The NPs were synthesized using a modified approach of the Turkevich method as described by Jingyue and Bernd (2015). All glassware was cleaned with anti-bacterial liquid hand soap and rinsed three times with dH_20 and allowed to dry. For each size a specific concentration of tri-sodium citrate in an Erlenmeyer flask sealed with aluminum foil was boiled at 100°C. The temperature was measured using a rod thermometer. Thereafter, a gold chloride trihydrate solution of a specific concentration (**Table 4.2**.) was rapidly added to the boiling tri-sodium citrate while stirring at 200 revolutions per minute (RPM) using a 3cm magnetic stirrer bar. The setup of the experiments can be seen on **Figure 4.2**.

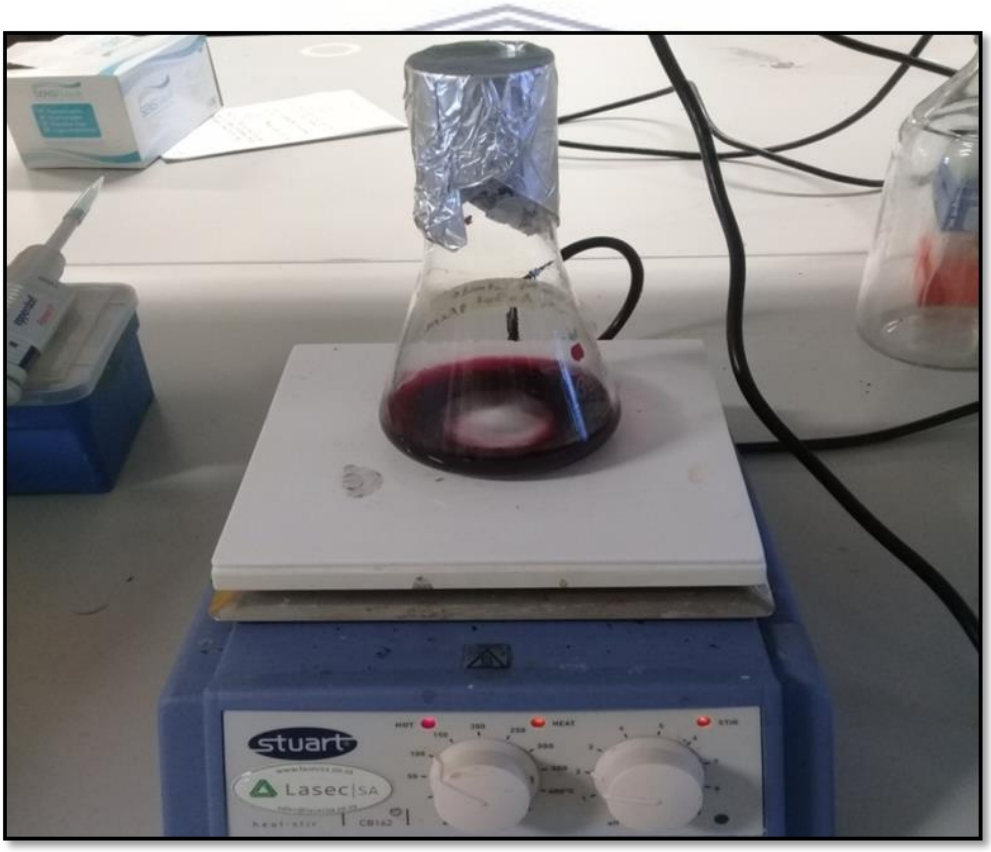

Figure 4.2: General setup for the citrate reduction synthesis of spherical AuNPs at 100 °C.

The reaction was allowed to take place for 5 minutes until a colour change from yellow to ruby-red was observed; the Erlenmeyer flask was then removed from the hot plate and placed on ice to stop the reaction. The synthesized NPs were then stored at 4 °C for further use. The synthesis of each AuNP size was repeated three times. The precise volumes and concentrations used in the synthesis of each AuNP are given in (**Table 4.2**) below. To separate the AuNPs from excess gold chloride trihydrate and tri-sodium citrate, 1- 2 ml of each AuNP size was centrifuged at a specific relative centrifugal force (RCF)/ G-force (given on **Table 4.2** below) and the NP pellets were subsequently resuspended in dH_20.

Table 4.2: Parameters used for the synthesis and purification of the citrate capped AuNPs (Jingyue and Bernd, 2015)

AuNPs	**Target Size**	**Concentration and volume of Gold Chloride Trihydrate**	**Concentration and volume of Tri-Sodium Citrate concentration**	**Mass Ratio**	**Centrifuge speed**
AuNP 1	50 nm	19.4 mM (0.9 ml)	0.15 mM (100 ml)	1: 1.16	700 RCF
AuNP 2	30 nm	2 mM (20 ml)	8.5 mM (10 ml)	1: 1.39	1200 RCF
AuNP 3	10 nm	51 mM (1 ml)	2 mM (100 ml)	1:2.56	2500 RCF

4.4.2. AuNP characterization

4.4.2.1. Absorbance spectrometry

UV-visible spectrophotometry is an important technique for the characterization of AuNPs, this method determines the absorbance of a nanomaterial at a specific wavelength (λ) and can also generate the entire absorption spectra of the nanomaterial (Biju *et al.,* 2010). The absorbance spectra of the AuNPs were generated using a POLARstar Omega microplate reader. The instrument combines an ultra-fast UV/vis full spectrum absorbance spectrometer, and an extremely sensitive filter based detection incorporating advanced optics and photomultiplier tubes to provide good sensitivity. An increase in particle size causes a shift in the absorption peak towards longer wavelengths and the width of the absorption spectra is related to the size distribution range, with narrow absorption spectra generally indicating a narrow size distribution range (Biju *et al.,* 2010, Verma *et al.,* 2014).

Generally, sAuNPs display a single absorption peak in the visible range between 510-550 nm, because of SPR and show intense absorption of visible light at 520 nm. This gives sAuNP an intense red colour, which varies according to the size of the AuNP (Verma *et al.,* 2014; Lata *et al*., 2014). To measure the absorbance spectra, three replicates of 100 µl of each AuNP sample were measured in a flat bottom Greiner 96 well plate and the readings were measured using a POLARstar Omega microplate reader set to a wavelength (λ) range of 350 to 650 nm.

4.4.2.2. Hydrodynamic size, PDI and zeta potential measurements

The hydrodynamic size, PDI and zeta potential of a solution of each NP (before and after purification) was analyzed using a Malvern Zetasizer Nano-ZS90 instrument. To determine the hydrodynamic size and PDI, 1ml of each AuNP was placed into a disposable cuvette cell (DTS0012), the cell was wiped clean of any fingerprints or dust using a paper towel and the content was analyzed at 25 °C, using the automatic mode settings. The zeta-potential of each AuNP sample was determined by pipetting 0.8 ml of each sample (AuNP 1, 2 and 3) into a disposable folded capillary cell (DTS1070). The cell was wiped clean with paper towel and the contents of each suspension were analyzed using the Zetasizer Nano-ZS90 instrument at 25 °C using the automatic mode settings. The data analysis was performed by analyzing three independently prepared samples of each AuNP, the measured hydrodynamic size, PDI and zeta potential results were presented as average values of 30 run triplicates.

4.4.2.3. High Resolution TEM

High resolution TEM (HRTEM) micrographs were obtained using a TECNAI F20 TEM microscope instrument. One drop of the AuNPs in dH_20 was placed onto a Nickel/copper (Ni/Cu) grid, supported by a thin film of amorphous carbon and dried using UV-Light before analyzing using the HRTEM microscope. This technique uses electrons that are shot through the sample at a high acceleration voltage. The interaction between the sample and the electron beam causes a scattering discharge which causes changes in the electron beam. This interaction between the electrons and the sample causes a difference in contrast between the sample and the background Cu grid; this produces images that provide direct information about the morphology of the NPs (Rao and Biswas, 2009). The core-diameter of the NPs was measured from from the HR-TEM images using the Image J software (https://imagej.net).

4.4.2.4. Energy dispersive x-ray spectroscopy

The energy dispersive x-ray (EDS) spectra of each AuNP sample were obtained using a field emission TEC NAI F20 TEM microscope (the same samples from Section **4.4.2.3** were used). EDS is a technique used to obtain the elemental and chemical composition of a NP (Rao and Biswas, 2009). EDS relies on the unique atomic structure of each element. Therefore, the x-ray spectrum emitted by different atomic structures is clearly distinct between different elements. The spectrum is created by the excitation of electrons in the inner shell (lower energies) of NPs. When the NP is probe by/exposed to an energy source, the low energy electrons in the inner shell of the NP become excited. The excited electrons move to a higher energy state (outer shell), therefore leaving unoccupied shells in the electronic structure of the probed atoms. As a result, electrons from the outer shells (higher energies) fill the unoccupied shells; and the difference in energy between the higher and lower energy shells is emitted in the form of x-rays. The emitted x-rays are then measured by an energy dispersive spectrometer (Rao and Biswas, 2009 & Russ, 1984).

4.4.2.5. Sterilization of AuNPs using short wave UV light exposure

Fresh samples of AuNPs were synthesized using the modified Turkevich approach (**Figure 4.1**) and centrifuged at rcf speeds specified on **Table 4.2**. The obtained pellets were re-suspended in dH_2O and the concentration for each AuNP size was calculated using the Beer lambert formula ($c = A_{450}/\varepsilon_{450}$), using the absorbance of the AuNPs at 450 nm and experimentally validated Molar decadic extinction coefficient (ε) values of spherical AuNPs at λ = 450 nm (Haiss *et al.,* 2007). The AuNPs were then exposed to short wave UV light (254 nm) for 10, 15, 20, and 30 minutes using a UV light chamber. The effect of the UV light exposure on the hydrodynamic size of the AuNPs was assessed using the Malvern zetasizer ZS90 instrument. To validate that the sterilization process was successful, a solution of the UV-treated AuNP samples was streaked on LB agar plates and incubating for 24 hours at 37 °C to determine if any bacterial growth was obtained.

4.4.2.6. The stability of AuNPs in LB at different temperatures

AuNPs were freshly synthesized and characterized, aliquot of the prepared AuNPs were centrifuged at specific G-force speeds (**Table 4.2**) and pelleted AuNPs were suspended in LB and the colour of each suspension was analyzed visually. To determine the stability of the AuNPs in LB, each AuNP suspension (in both LB and dH_20) was incubated at 4 °C and at 37 °C for 72 hours. The hydrodynamic size and Zeta potential of each suspension was analyzed after 0, 24, 48 and 72 hours using the Malvern Zetasizer ZS90 instrument.

4.5. Results and Discussion

4.5.1. Synthesis of AuNPs

In this study, the effects of gold chloride trihydrate and tri-sodium citrate concentrations on synthesizing sAuNPs of three different sizes (i. e. AuNP 1, AuNP 2 and AuNP 3) were investigated, while temperature was used as a catalyst. The sizes of the NPs were controlled by varying the concentration of both citrate and Au chloride solutions (the optimized concentrations are listed in **table 4.2** above). After adding Au chloride trihydrate to the boiling solution of tri-sodium citrate, a colour changed from a yellowish colour to a clear water-like colour, to grey, black, blue, purple-pink and with the smaller NPs whine-red or a ruby-red colour was clearly visible in less than 5 minutes after adding the Au chloride trihydrate as illustrated on **Figure 4.3**.

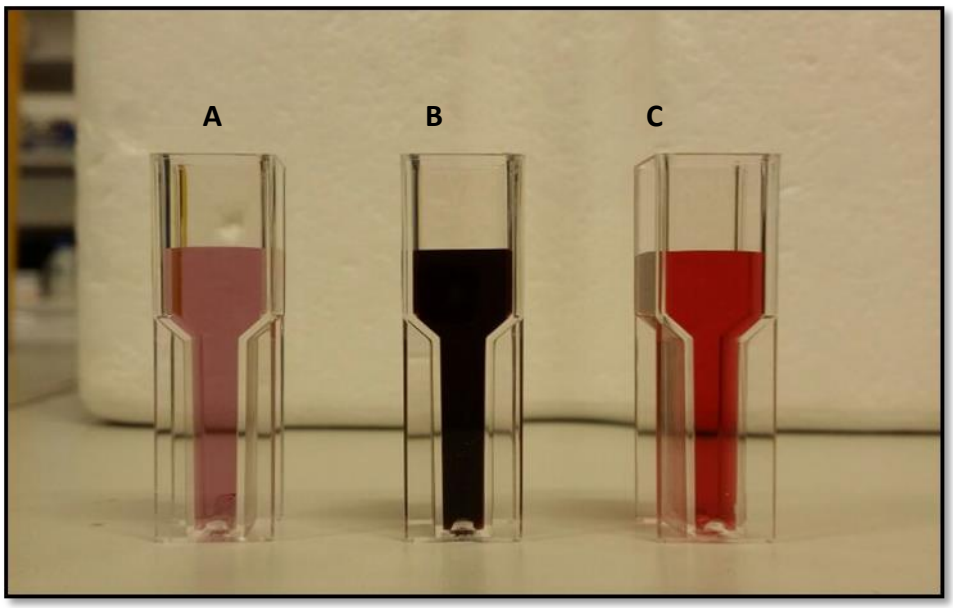

Figure 4.3: Spherical AuNPs with different colours caused by their different SPR bands. (A) AuNP 1 had a light pink-red colour; (B) AuNP 2 had a dark wine-red colour, while (C) AuNP 3 had a ruby-red colour.

4.5.2. Absorbance spectrometry

The absorption spectrum of each AuNP was measured using a POLARstar Omega microplate reader at an absorption range of 350-650 nm, and the absorption maximum (λ max) was noted at different wavelengths. All the synthesized gold colloids showed a single absorption peak near 520 nm (**Figure 4.4**), which indicated that all the synthesized AuNPs had a spherical morphology. The λ_{max} was 528 for AuNP 1 and AuNP 2, respectively, and 518 nm for AuNP 3. Therefore, AuNP 1 and AuNP 2 to had the same $\lambda_{max.}$ A possible reason for this phenomenon could be that the accuracy of the λ_{max} prediction decreases as the PDI of AuNP samples increases, therefore meaning that the λ_{max} of a given AuNP solution can only be predicted with complete accuracy if that sample is monomodal with a maximum PDI of 0. 2. Therefore, since both AuNP 1 and AuNP 2 have PDI values above 0.2 their λ_{max} may have been incorrectly predicted. In addition, When observing Table 4.1, the λ_{max} of the two size ranges are very close to each other, therefore any overlapping between the two size ranges can result in the the two samples having the same λ_{max} value. However, though not always the case due to a lack of correlation between AuNP size and λ_{max}, differences in λ_{max} between AuNPs generally indicate that the AuNPs have different sizes with larger AuNPs having λ_{max} at longer wavelengths (Lata *et al*., 2014).

The observed results, thus suggested that AuNP 3 had the smallest size, as the λ_{max} of AuNP 3 occurred further away from longer wavelengths when compared to the λ_{max} of AuNP 1 and AuNP 2 which had λ_{max} at longer wavelengths. The width of the absorption spectra of AuNP 1 was found to be wider compared to that of AuNP 2 and AuNP3. According to Lata *et al*., (2014) and Verma *et al.,* (2014), a wide width of the absorption spectra suggests that a AuNP sample has a wider size distribution and is therefore more polydisperse. AuNPs with a low concentration have a dampened SPR peak (Shamaila *et al*., 2016), as can be seen with AuNP 1 on **Figure 4.4.**

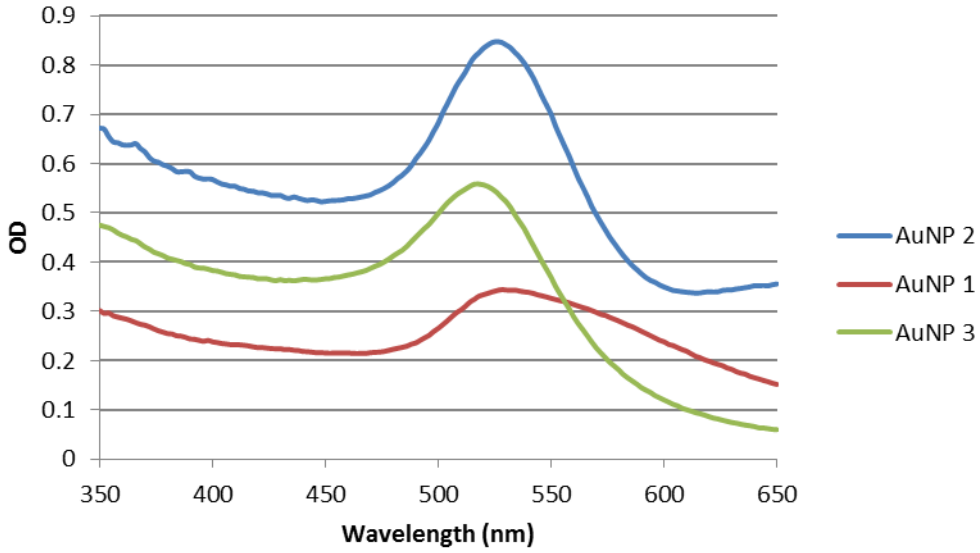

Figure 4.4: The superimposed Ultra violet (UV)-visible spectrum of AuNP 1, 2 and 3 synthesized using the citrate reduction method.

4.5.3. AuNP size determination using dynamic light scattering.

The synthesized AuNPs were purified by centrifuging the NP samples at different speeds (rcf) for 30 min. The hydrodynamic diameter and zeta potential of each AuNP were measured before and after purification and the results are presented in **Table 4.3** and **Table 4.4**. The peak mean gives the mean diameter of each particle while the peak area gives the percentage of the mean diameter according to intensity. For the DLS study, three independently prepared samples were read using the Malvern Zetasizer Nano ZS90. Three cycles of different counts were run analysing both diameter and zeta potential analysis and the average of the counts was taken.

Table 4.3: The hydrodynamic size, PDI and zeta potential of AuNPs 1, 2 and 3 before purification. The peak area refers to a percentage (%) of AuNPs with a given hydrodynamic size.

	AuNP 1	**AuNP 2**	**AuNP 3**
Z-average size (nm)	13.3 ± 1.11	18.2 ± 1.0	17.06 ± 0.80
PDI	0.544 ± 0.05	0.273 ± 0.93	0.152 ± 0.09
Peak 1 average size (nm)(Peak Area)	49.3 ± 8.07 (68.87 ± 1.50 %)	31.10 ± 2.10 (94.1 ± 0.60 %)	18.87 ± 0.99 (99.47± 0.61 %)
Peak 2 average size (nm)(Peak Area)	4.299 ± 0.55 (31.13 ± 1.50 %)	1.068 ± 0.90 (5.9 ± 0.60 %)	4101 ± 2362.2 (0.53 ± 0.61 %)
Zeta-potential (mV)	-28.47 ± 2.80	-34.8 ± 8.20	-32.27 ± 5.05 mV

Table 4.4: The hydrodynamic size, PDI and zeta potential of AuNPs 1, 2 and 3 after purification.

	AuNP 1	**AuNP 2**	**AuNP 3**
Z-average size (nm)	17.26 ± 1.11	22.87 ± 1.0	20.07 ± 2.73
PDI	0.545 ± 0.05	0.398 ± 1.0	0.259 ± 0.09
Peak 1 average size (nm)(Peak Area)	62.7 ± 4.6 (68.6 ± 4.16 %)	33.68 ± 1.68 (91.63 ± 2.16 %)	24.49 ± 0.05 (96.7± 1.56 %)
Peak 2 average size (nm)(Peak Area)	4.516 ± 0.4 (31.4 ± 4.16 %)	1.068 ± 0.1 (8.37 ± 2.16 %)	4101 ± 2362.2 (3.3 ± 1.56 %)
Zeta-potential (mV)	-27.0 ± 6.28	-32.7 ± 1.60	-30.7 ± 2.1

The data revealed that before purification **(Table 4.3)**, AuNP 1 possessed a hydrodynamic diameter of 49.3 ± 8.1 nm, while AuNP 2 and AuNP 3 were found to have a hydrodynamic size of 31.1 ± 2.1 nm and 18.87 ± 0.99 nm, respectively. The difference in mean size between AuNP 1 and AuNP 2 was statistically significant (p-value = 0.0023), while the difference in mean size between AuNP 2 and AuNP 3 was not statistically significant (p-value = 0.0507). When comparing the Hydrodynamic size of the AuNPs with the mass ratios used in the synthesis process, the results suggested that hydrodynamic size of the AuNPs was inversely proportional to the amount of tri-sodium citrate and directly proportional to the amount of gold chloride trihydrate. Therefore,

the hydrodynamic size of the AuNPs increased with increase in the amount of tri-sodium citrate added.

After purification **(Table 4.4)** the hydrodynamic size of AuNP 1 in dH_2O was found to have increased from 49.3 ± 8.07nm to 62.7 ± 4.6 nm (p-value = 0.0279).The hydrodynamic size of AuNP 2 and AuNP 3 showed no statistically significant increase in size, with p-values of 0.9999 and > 0.9999, respectively. After purification AuNP 1 was found to be larger than AuNP 2 (p-value < 0.0001), and AuNP 2 was found to be larger than AuNP 3 (p-value = 0.0088). No significant changes were observed on the PDI of AuNP 1 (p-value> 0.9999), AuNP 2 (p-value > 0.9999) and of AuNP 3 (p-value = 0.7210). In addition, no significant changes were observed in the zeta potential of AuNP 1 (p-value> 0.9999), AuNP 2 (p-value> 0.9999) and AuNP 3 (p-value > 0.9999) as well.

4.5.4. AuNP morphology and size distribution determined using HR-TEM

The HR-TEM micrographs of each AuNP sample are shown on **Figure 4.5–4.7**. The micrographs show that the AuNPs were approximately spherical in shape and relatively monodispersed with good lattice fringes. The core diameter of the AuNPs **(Table 4.5)** was calculated by measuring the circumference of 20 individual particles of the HR-TEM images of AuNP 1, AuNP 2 and AuNP 3 using the Image J software. The core diameters of AuNPs were found to be 50.2 ± 9.4 nm, 27.7 ± 3.5 nm and 14.0 ± 3.3 nm, for AuNP 1, AuNP 2 and AuNP 3, respectively. When compared to the mass ratios used in the synthesis procedure, these results were found to be parallel with the results of the hydrodynamic size futher supporting the observation that size or diameter of the AuNPs were inversely proportional to the amount of tri-sodium citrate and directly propotional to the amount of gold chloride trihydrate.

Table 4.5: Nanoparticle average sizes measured by analyzing images obtained from HRTEM.

	AuNP 1	**AuNP 2**	**AuNP 3**
Average size (nm)	50.2	27.7	14.0
Standard diviation	9.4	3.5	3.3

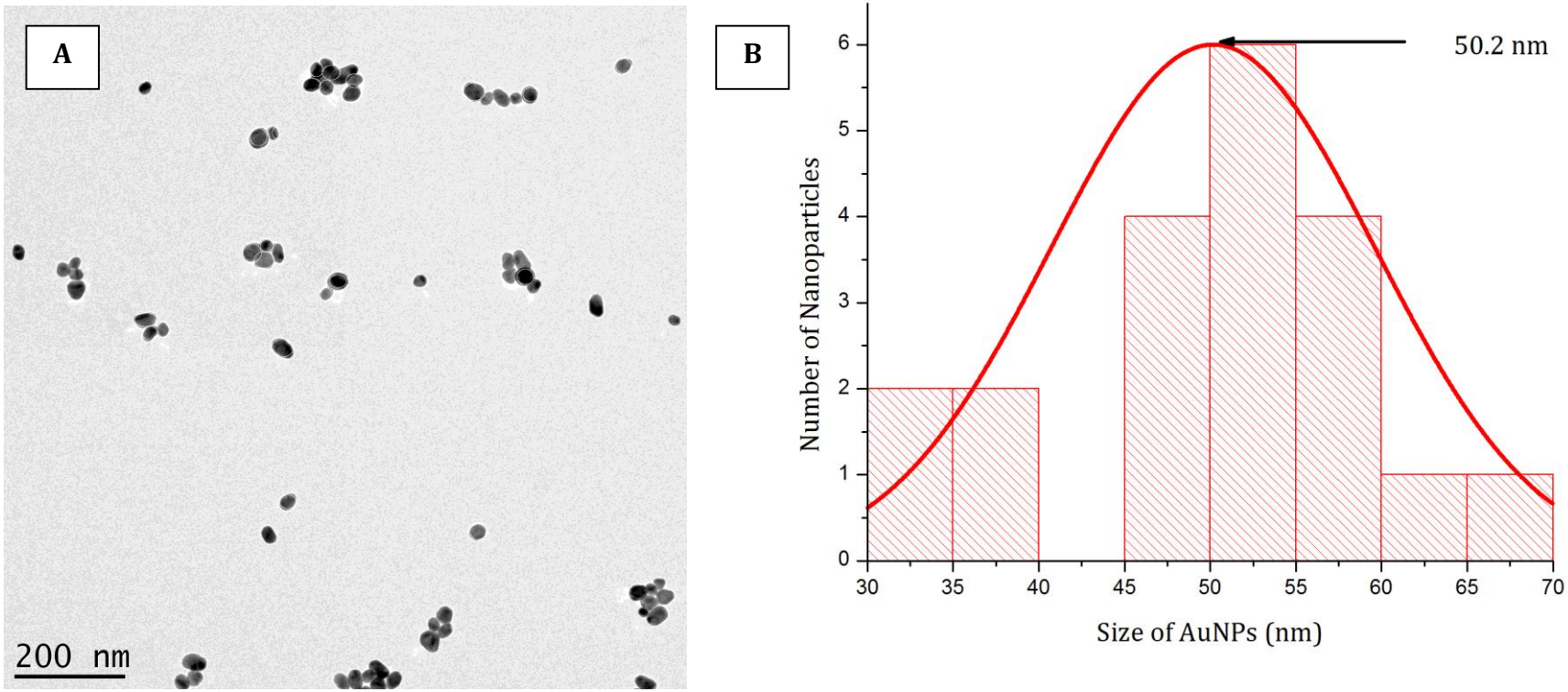

Figure 4.5: The morphology and average core diameter of AuNP 1. (A) HR-TEM images of AuNP 1 at 200 nm resolution scale, (B) the number size distribution of AuNP 1 as measured using the Image J Software.

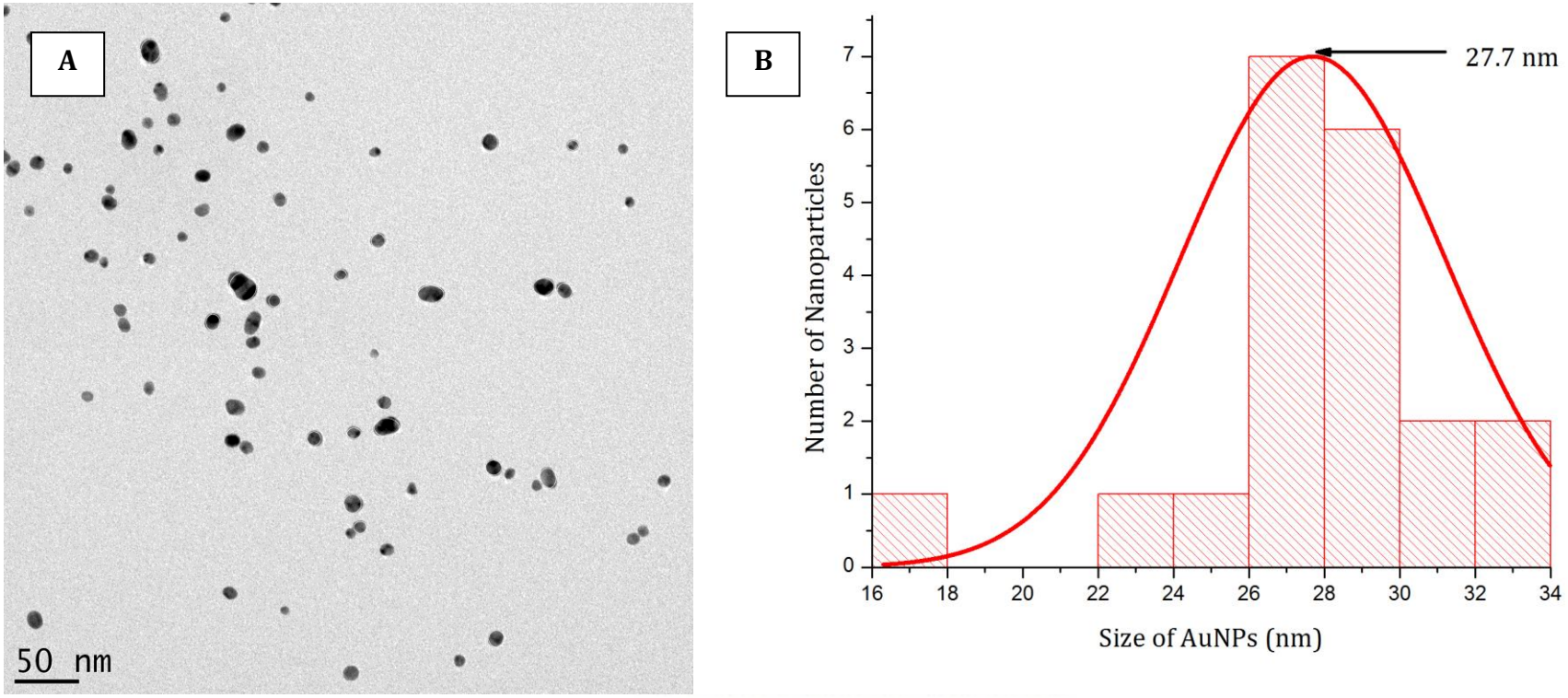

Figure 4.6: The morphology and average core diameter of AuNP 2. (A)HR-TEM images of AuNP 2 at 50 nm resolution scale, (B) the number size distribution of AuNP 2 as measured using the Image J Software.

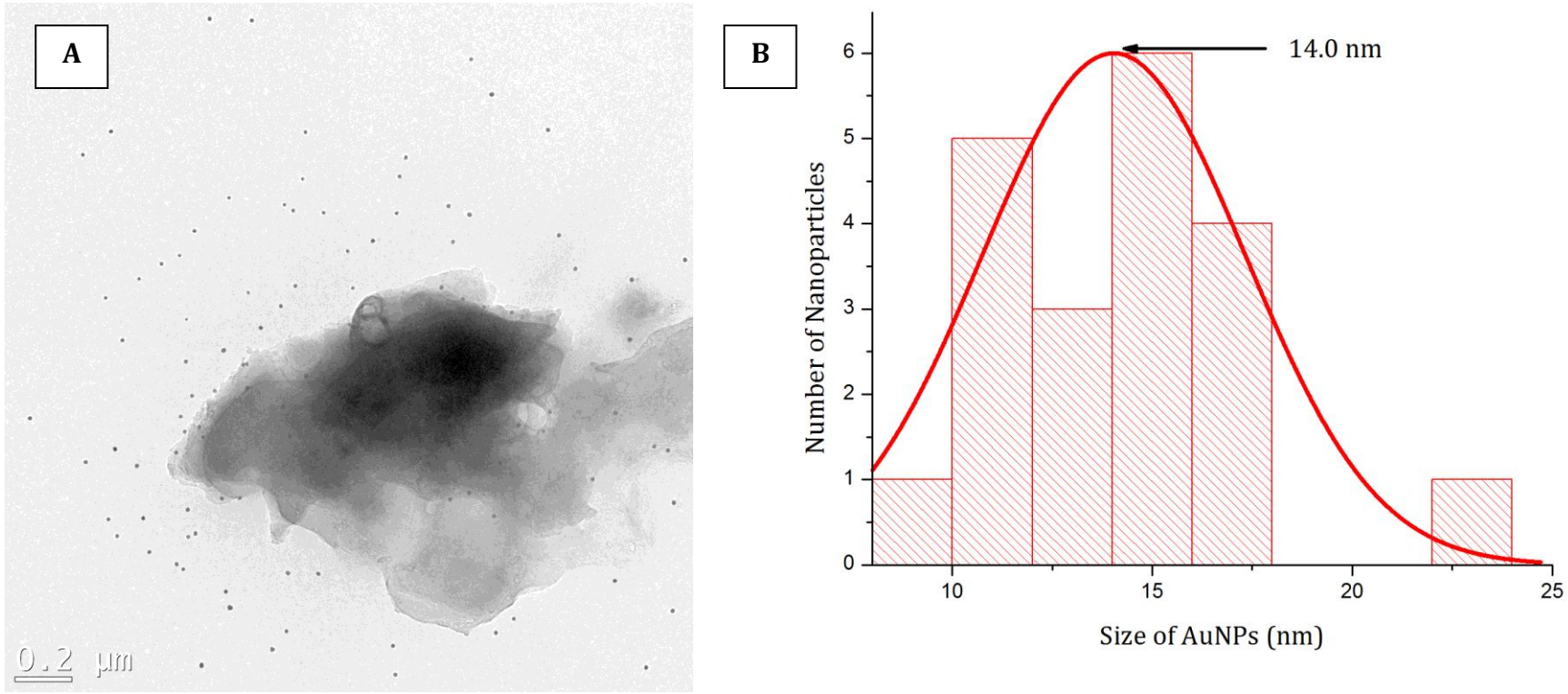

Figure 4.7: The morphology and average core diameter of AuNP 3. (A) HR-TEM images of AuNP 3 at 0.2 µm resolution scale, (B) the number size distribution of AuNP 3 as measured using the Image J Software.

The results revealed that the peak numbers of the DLS results were more comparable to the core diameter and therefore a more reliable measure for predicting the hydrodynamic diameter/size of both bimodal and monomodal AuNPs. On the other hand, the accuracy of using the Z-average to predict the hydrodynamic diameter was found to be reliant on the size distribution/PDI of the NP sample being studied. The relationship between peak number and Z-average revealed that the Z-average of AuNP 1 was found to be very small compared to the peak number (p-value < 0.0001) with a PDI of 0. 544 ± 0.05, the Z-average of AuNP 2 was also found to be smaller than the core diameter (p-value = 0.0407) with a PDI of 0.273 ± 0.93. However, no significant difference was found between the Z-average and the peak number of AuNP 3 (p-value = 0. 8989) with a PDI of 0.152 ± 0. 09.

These results therefore indicate that the Z-average size of a given NP sample can be only be considered as an accurate prediction of the hydrodynamic size of a AuNP sample if there is no significant difference between the peak number and the Z-average of the NP sample being studied, such a NP sample can be considered monomodal/monodispersed. The results also aligned with the absorbance spectrometry results **(Figure 4.4)**. However, the results still supported the theory that the differences in λ_{max} between the AuNP solutions was due to the AuNPs having different sizes, with larger AuNPs having λ_{max} at longer wavelengths. The results also supported the theory that NPs with a wider width of absorption spectra have a larger hydrodynamic size distribution/PDI as was seen with AuNP 1.

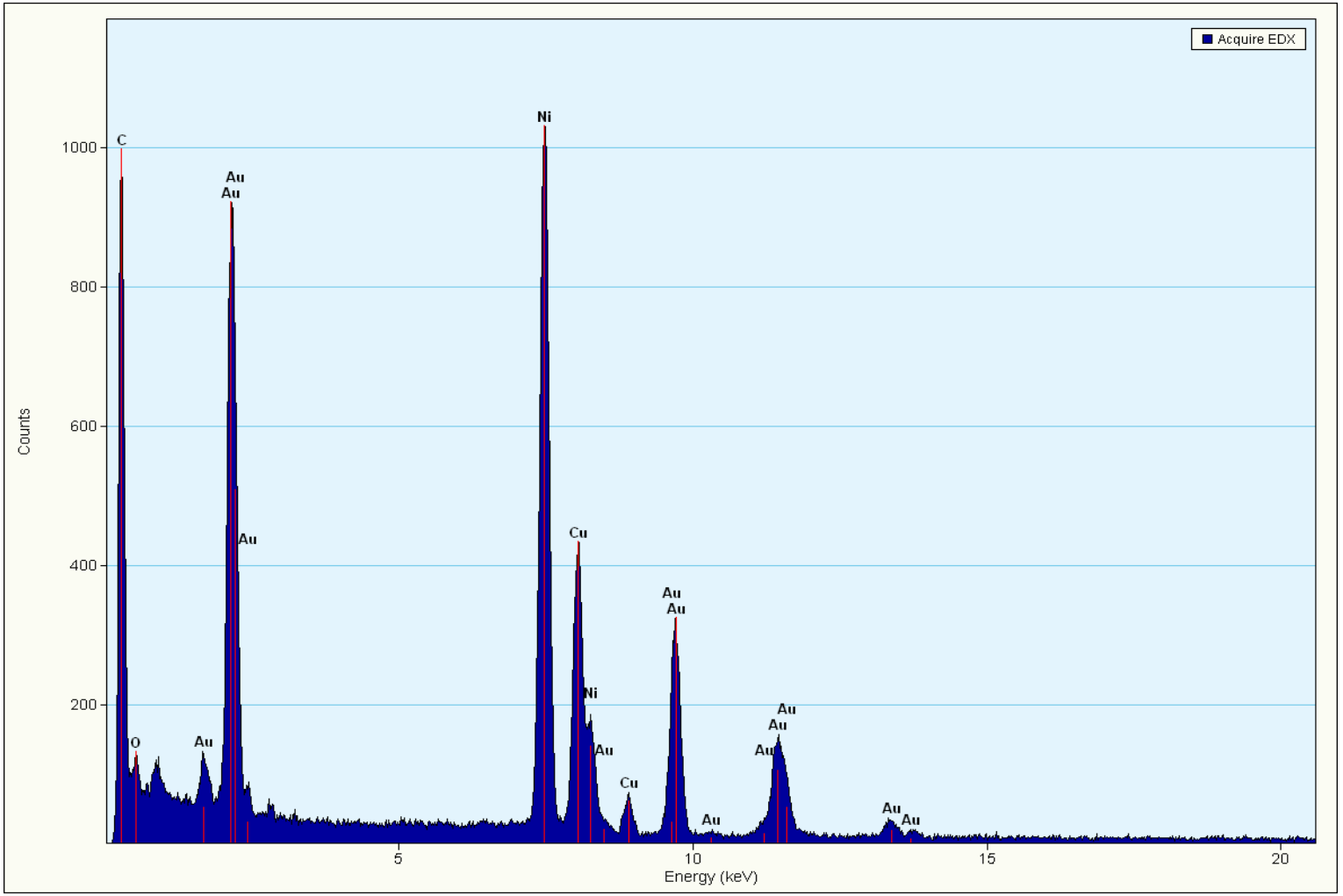

Figure 4.8: The chemical composition/EDS Spectrum of the prepared AuNP 1.

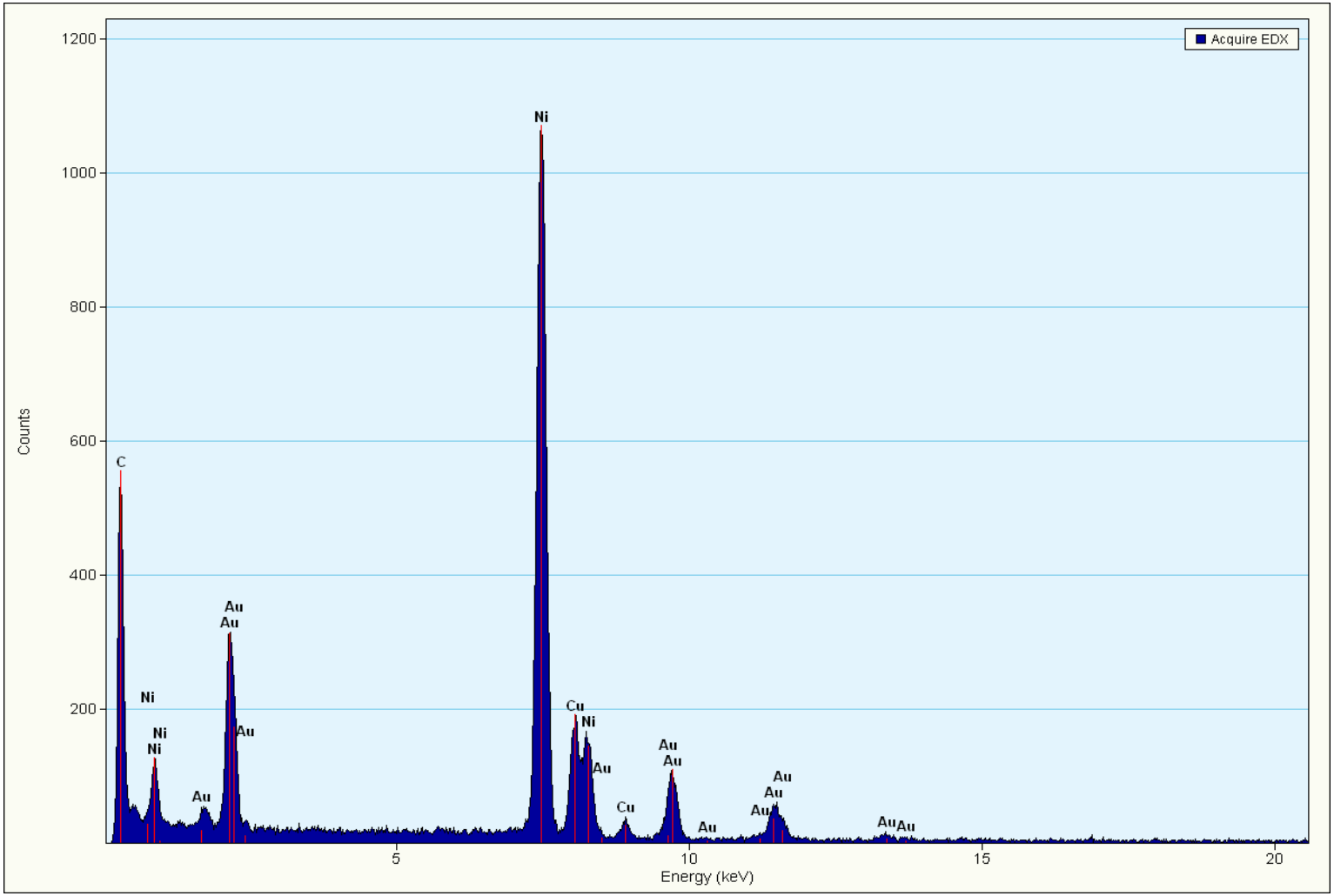

Figure 4.9: The chemical composition/EDS Spectrum of the prepared AuNP 2.

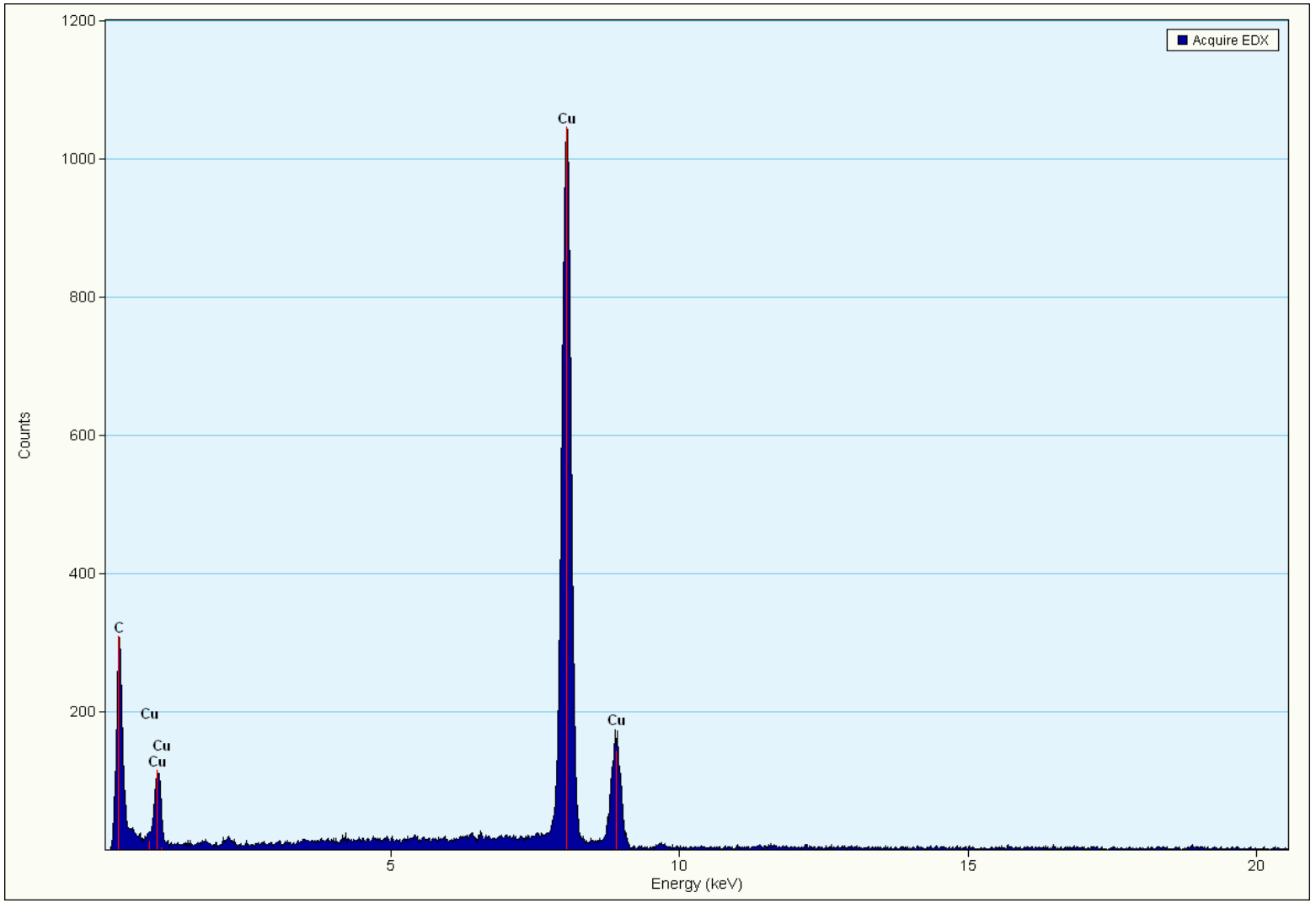

Figure 4.10: The chemical composition/ EDS Spectrum of the prepared AuNP 3.

4.5.5. Energy dispersive x-ray spectroscopy

The elemental composition of each AuNP was carried out using a field emission (TEC NAI F20 TEM microscope). The EDS spectrum of AuNP 1 (**Figure 4.8)** and AuNP 2 (**Figure 4.9)** showed the presence of Nickel (Ni), Copper (Cu) and gold (Au). The presence of Ni and Cu are due to the Ni/Cu grid that the AuNPs were placed on during the analysis. However, the EDS of AuNP 3 (**Figure 4.10)** only showed the presence of Ni, C, and Cu without Au. The absence of Au in the EDS was likely due to the AuNPs being deposited too close to edge of the Ni/Cu grid; as a result only elements of the grid were detected. However, the presence of AuNP 3 was detected using HR-TEM and the image of AuNP 3 can be seen above on **Figure 4.7**.

4.5.6. Sterilization of AuNPs using short wavelength UV light exposure

The effectiveness of using short wavelength (254 nm) UV light to sterilize spherical AuNPs of different sizes and the effect that the UV exposure had on the physicochemical properties of the AuNPs was investigated. The effect of exposing AuNPs to the UV light on the hydrodynamic size and PDI was analyzed using the Malvern zetasizer ZS90.

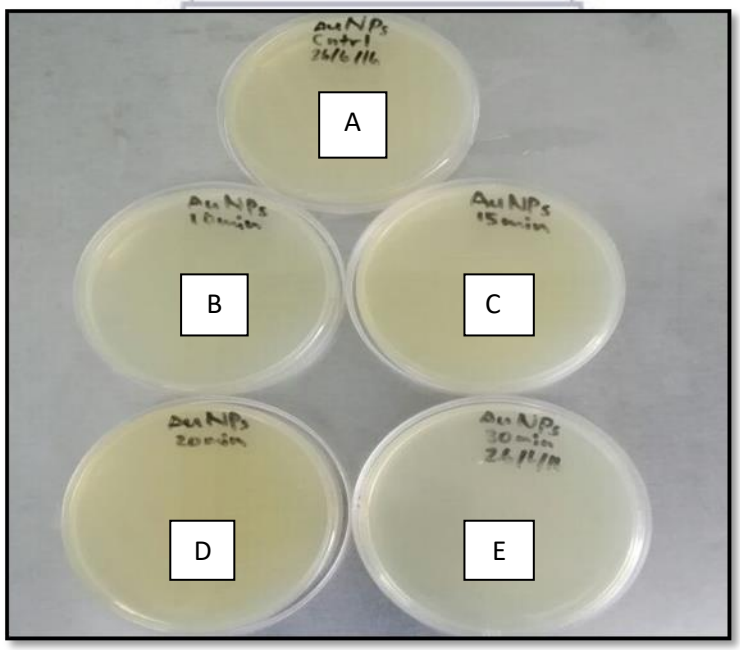

Figure 4.11: Confirmation of sterilization after exposing AuNP 1 to (A) no UV light, (B) 10 minutes, (C) 15 minutes, (D) 20 minutes and (E) 30 minutes of short wavelength UV light (254 nm) using the streak plating method.

The LB agar plate results (**Figure 4.11**) indicated that exposure to short wavelength UV light was successful in sterilizing the AuNP samples. No bacterial growth was observed after streaking the AuNP samples exposed to short wave UV light (254 nm) for 10, 15, 20 and 30 minutes on LB agar plates. However, even the unexposed AuNPs showed no bacterial growth after being streaked on LB agar plates. Therefore, to investigate if the LB agar was incorrectly prepared, 0.5 McFarland standards of *S. Aureus* and *E. coli* were grown using the same LB agar **(Figure 1 on the Appendix)**.

4.5.7. The effect of UV light exposure on the Hydrodynamic size of the AuNPs

The effects of exposing AuNPs to short wavelength UV light (254 nm) on the hydrodynamic size and PDI of the AuNPs were examined using the Malvern zetasizer ZS90. The obtained results (**Figure 4.13**) showed a minimal decrease in the hydrodynamic size of AuNP 1 from 62.7 ± 4.6 nm to 55.21 ± 0.73 nm (p-value = 0.0163) after 10 minutes of exposure to short wavelength of UV light. However, no significant changes in the hydrodynamic size were observed for the remainder of the exposure time (p-value> 0.9999). A minor decrease in PDI from 0.545 ± 0.05 to 0.450 ± 0.00 (p-value =0.0022) was found after 10 minutes of UV light exposure. However, no significant changes after 15 minutes (p-value = 0.9986), 20 minutes (p-value> 0.9999) and after 30 minutes (p-value> 0.9999) of UV light exposure were observed. The results therefore showed that the short wavelength UV light had no negative effects on the stability, hydrodynamic size and size distribution, as shown by the lack of colour change/aggregation and no significant changes in the PDI of AuNP 1.

The results (**Figure 4.13**) also showed no significant changes in the hydrodynamic size of AuNP 2 from 33.68 ± 1.68 nm after 10 minutes (p-value = 0.3682), 15 minutes (p-value> 0.9999), 20 minutes (p-value> 0.9999) and after 30 minutes (p-value =0.9849) of exposure to short wavelength of UV light. The PDI results also showed no significant changes from 0.398 ± 1.0 after 10 minutes (p-value> 0.9999), 15 minutes (p-value > 0.9999), 20 minutes (p-value = 0.9823) and after 30 minutes (p-value> 0.9999).The results therefore signified that the short wavelength UV light had no negative effects on the stability, hydrodynamic size and size distribution, as shown by the lack of colour change/aggregation and no significant changes in the PDI of AuNP 2.

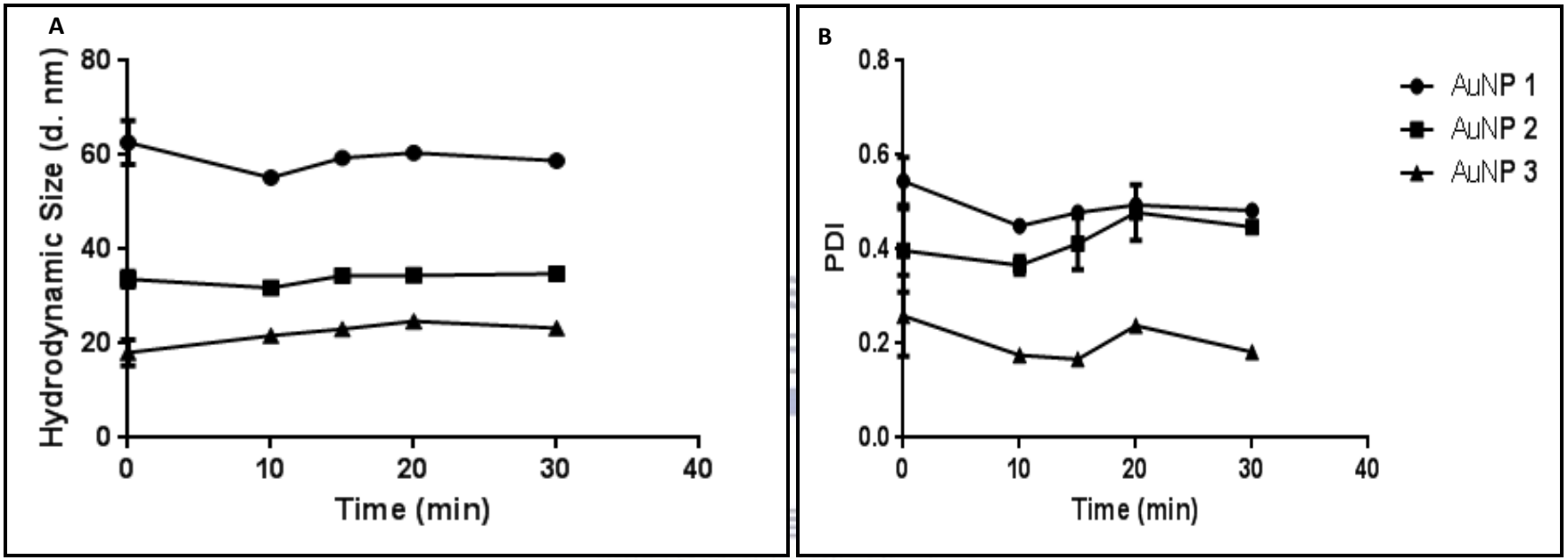

Figure 4.12: The effect of short UV light on the (A) hydrodynamic size and (B) the PDI of the AuNP 1, 2 and 3 after 30 minutes of exposure to short wave UV light.

No significant changes in the hydrodynamic size of AuNP 3 (**Figure 4.13**) were observed from 24.49 ± 0.05nm after 10 minutes (p-value = 0.0887), however, a slight size increase was observed from 24.49 ± 0.05nm to 23.11 ± 0.21 nm after 15 minutes (p-value= 0.9999) of UV exposure. No significant changes were observed from 23.11 ± 0.21 nm after 20 minutes (p-value= 0.9956) and after 30 minutes (p-value =0.9993) of exposure to short waves of UV light. The PDI results also showed no significant changes from 0.259 ± 0.09 after 10 minutes (p-value= 0.1467), 15 minutes (p-value = 0.0867), 20 minutes (p-value = 0.9995) and after 30 minutes (p-value> 0.2303).The results therefore indicated that the short wave UV light had no negative effects on the stability, hydrodynamic size and size distribution of AuNP 3, as shown by the lack of aggregation and no significant change in the PDI.

4.5.8. The stability of UV sterilized AuNPs in dH2O and LB at different temperatures.

The use of nanomaterials for biomedical applications such as imaging, diagnostics, and drug delivery has become widespread. However, when introduced to complex biological media containing proteins, lipids, electrolytes, etc., NPs become subjected to a variety of forces which influence their behaviour in this environment. One aspect of NP behaviour in biological systems that is frequently overlooked is aggregation. NP aggregation significantly modifies the *in vitro* behaviour (e.g. toxicity, efficacy, cellular uptake), as well as *in vivo* fate (pharmacokinetics, biodistribution) of NPs (Moore *et al.,* 2015). To investigate the stability of AuNPs 1, 2 and 3 in LB, the AuNPs were incubated in dH_2O and in LB at 4 °C and at 37 °C and the hydrodynamic size; PDI and Zeta Potential of each AuNP sample were measured after 24, 48, and 72 h of incubation.

The AuNPs were found to change colour from red-pink to a dark blue colour after introducing the AuNPs to LB for approximately 5 minutes, and to a light blue colour over-time **(Figure 4.13)**. The observation indicates a rapid increase in the size of the AuNPs, this size increase coul be an indication that the AuNPs lack stability in LB and are therefore prone to server aggregation when introduced to LB without any capping agents.

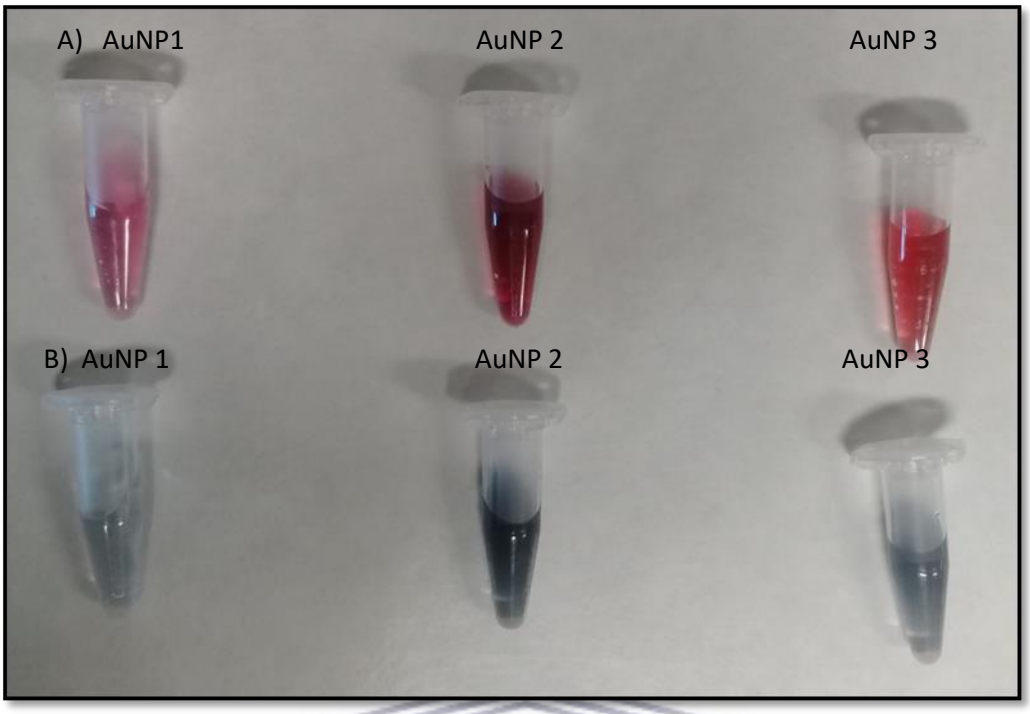

Figure 4.13: (A) The Colour of AuNPs in dH2O and (B) the colour of AuNPs in LB after 24 hours of incubation.

4.5.8.1. The Stability of AuNP 1 in dH_2O at 4 °C and at 37 °C

The hydrodynamic size (peak 1) of the UV treated AuNP 1 in dH_2O was measured and found to be 55.21 ± 0.73 nm with a PDI of 0.450 ± 0.00 and a zeta potential of -26.3 ± 1.2 mV. The hydrodynamic size of AuNP 1 was then measured again after 24, 48 and 72 h of incubation at 4 ° C (**Figure 4.15**). No significant difference was found in the size of AuNP 1 after 24, 48 and 72 h of incubation (p-values >0.9999). No significant difference was found in the PDI of AuNP 1 after 24 h (p-value = 0.8695), 48 h (p-value = 0.8514) and 72 hours (p-value = 0.8717) of incubation. However, the zeta potential of AuNP 1 showed a significant reduction from -26.3 ± 1.2 mV to -34.6 ± 0.4 M after 24 h, to -34.5 ±1.6 mV after 48 h and to -33.1 after 72 h (p-values < 0.0001) of incubation, when compared to the negative control. The hydrodynamic size of freshly synthesized AuNP 1 in dH_2O was measured at 37 °C (**Figure 4.15**).

No significant difference in the hydrodynamic size of AuNP 1 was found after 24h (p-value = 0.3491), 48h (p-value = 0.1864) and 72 h (p-value > 0.9999). The PDI results showed fluctuating results, the PDI was found to have changed from 0.545 ± 0.05 to 0.776 ± 0.06 after 24 h (p-value = 0.211), to 0.495 ± 0.08 after 48 h (p-value = 0.0034) to 1.0 ± 0.0 after 72 h (p-value <0.0001). The zeta potential was found to have increased from -26.3 ± 1.19 mV to -16.0 ± 1.18 mV after 24h (p-value <0.0001), to -17.9 ± 0.71 mV after 48 h (p-value <0.0001) and to -34.0 ± 0.26 after 72h (p-value <0.0001) of incubation, when compared to the negative control. After 72 h of incubation, both the PDI and zeta-potential of the NPs were found to have significantly increased, this increase in PDI and zeta-potential could have been an indication of loss of stability. When compared to the AuNP 1 at 4 °C, the results suggested that an increase in temperature results in a time-dependent loss of stability in AuNP1 suspensions.

4.5.8.2. The Stability of AuNP 1 in LB at 4 °C and at 37 °C

Firstly, within 5 min, the hydrodynamic size was found to significantly increase from 62.7 ± 4.6 nm to 282.6 ± 5.6 nm (p-value <0.0001) after the AuNPs were suspended in LB, this hydrodynamic size of the 0 min incubation time. This drastic size increase was accompanied by a colour change from a pink/red colour to a navy blue colour **(Figure 4.13)** and a significant decrease in PDI from 0.545 ± 0.1 to 0.254 ± 0.02 (p-value < 0.0001) which suggested that the NPs were aggregating. The aggregation was validated by HR-TEM images (**Figure 4.14).**

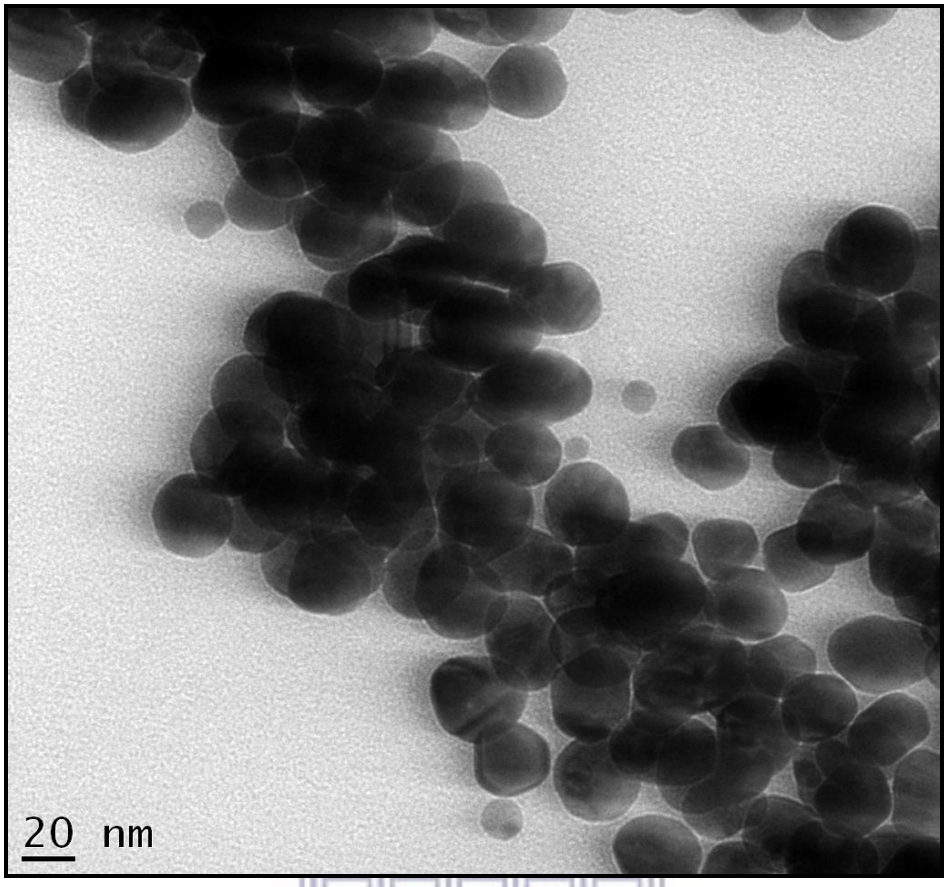

Figure 4.14: HR-TEM image at a 20 nm scale showing a cluster of AuNP 1 as a result of aggregation after re-suspending the NPs in LB for 5 minutes.

The size, PDI and Zeta Potential of AuNP 1 in LB at was then measured at 4 °C and at 37 °C for 24, 48 and 72 h. At 4 °C, no significant change in the hydrodynamic size of AuNP 1 was observed after 24 h (p-value = 0.2724), 48 h (p-value = 0.2655) and 72 h (p-value = 0.5639). However, the PDI was found to have significantly increased to 0.877 ± 0.1 (p-value <0.0001) after 24 h and to 0.694 ± 0.3 after 48 h (p-value <0.0001). The the PDI was then found to have decrease but after 72 hours of incubation the PDI significantly decreased to 0.453 ± 0.04 after 72 h (p-values = 0.0554) of incubation, when compared to the negative control. The zeta potential was found showed a time-dependent increase from -26.5 ± 2.6 mV to -16.0 ± 1.0 mV after 24 h (p-value <0.0001), to -15.1±1.3 mV after 48 h (p-value <0.0001) and to -14.0 ±0.8 mV after 72 h (p-value <0.0001) of incubation, when compared to the negative control.

After incubation at 37 °C, the results showed a significant time-dependent size increase from 282.6 ± 5.6 nm to 468.6 ±138.4 nm after 24 h (p-value = 0.2297), to 753.8 ± 6.8 nm after 48 h (p-value = 0.0002) and 1248 ± 242.0 nm after 72 h (p-value <0.0001) of incubation. The size increase was accompanied by a significant increase in PDI from 0.254 ± 0.02 to 0.909 ± 0.08 after 24 h, to 0.546 ± 0.12 after 48 h (p-value = 0.0001) and to 0.279 ± 0.02 after 72 h (p-value = 0.0057). The zeta potential was found to have also significantly increase after -26.5 ± 2.6 mV to -17.7 ± 1.04 mV after 24 h (p-value <0.0001), to -16.03 ± 2.24 mV after 48 h (p-value <0.0001) and to -22.5 ± 0.40 mV after 72 h (p-value <0.0075) when compared to the negative control.

The results suggested that the AuNPs in LB were susceptible to time-dependent aggregation and stability loss at 37 °C. Therefore, the results suggested that the stability of AuNP 1 was affected by both temperature (37 ° C) and by LB. these two conditions promoted time-dependent aggregation and deterioration of the quality of AuNP 1. However, the NPs were found to be less stable in LB as the aggregation began within 5 min after suspending the AuNPs in LB, before the incubation at both 4 °C and 37 °C began. The AuNPs were also found to be more stable in dH_2O.

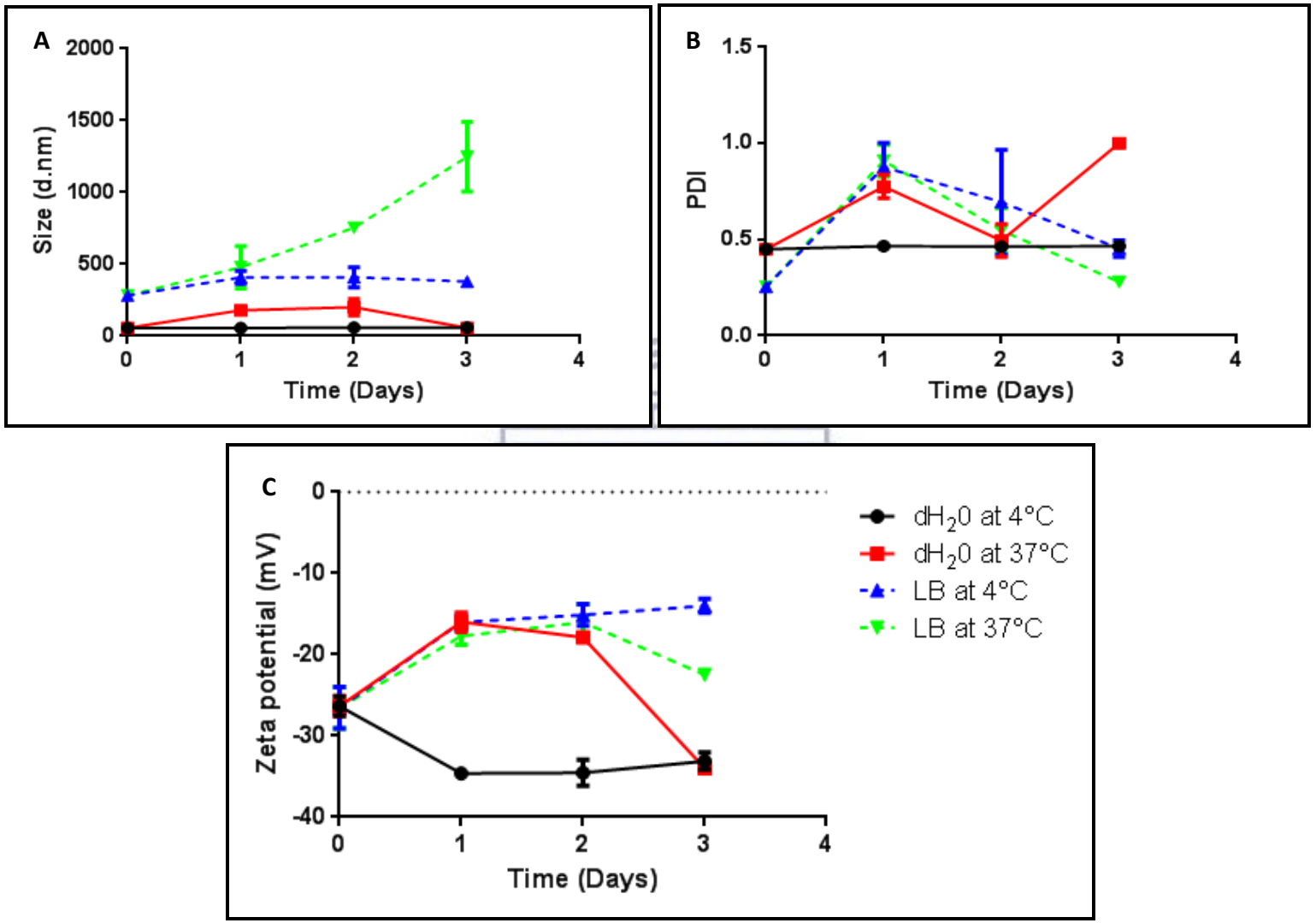

Figure 4.15: The stability of the of AuNP 1 in dH20 at 4 °C (-λ-) and 37 °C (-ν-) over 72 h of incubation, and the stability of AuNP 1 in lysogeny broth at 4 °C (-σ-)and at 37 °C (-τ-) over 72 h of incubation. Data is expressed in mean ± SD (n=3). (A) The hydrodynamic size, (B) PDI and (c) zeta potential of the AuNP.

4.5.8.3. The Stability of AuNP 2 in dH_2O at 4 °C and at 37 °C

The hydrodynamic size of UV treated AuNP 2 in dH_2O was measured and found to be 31.82 ± 0.18 nm with a PDI of 0.366 ± 0.02 and a zeta potential of -32.67 ± 1.60mV. The hydrodynamic size of AuNP 2 was then measured again after 24, 48 and 72 h of incubation at 4 ° C and at 37 ° C, at 4 °C (**Figure 4.17**), and no significant difference was found in the size of AuNP 2 after 24, 48 and 72 hours of incubation (p-values>0.9999). This stability in hydrodynamic size was accompanied by a stable PDI, where no significant difference was found in the PDI of AuNP 2 after 24 h (p-value = 0.8524), 48 h (p-value = 0.4944) and 72 h (p-values = 0.7583). The zetapotential of AuNP 2 was also measured and no significant changes in the zeta potential of were found after 24 h (p-value = 0.9725), 48 h (p-value = 0.8069) and 72 h (p-value = 0.4305), when compared to the negative control. The results suggest that AuNP 2 was stable for 72 hours in dH2O with no significant changes in the hydrodynamic size, PDI or zeta potential.

The hydrodynamic size of UV treated AuNP 2 in dH_2O at 37 °C (**Figure 4.17**), also showed no significant difference in the hydrodynamic size of AuNP 2 after 24, 48 and 72 h (p-value >0.9999) of incubation when compared to the negative control. The PDI results also showed no significant changes after 24 h (p-value =0.6446), 48 h (p-value = > 0.9999) and 72 h (p-value > 0. 9999) of incubation. No changes were observed in the zeta Potential after 24 h and after 48 h (p-values > 0.9999). However, a slight increase in the zeta potential occurred after 72 h of incubation (p-value = 0.0099). The stable hydrodynamic size, PDI and Zeta potential suggests that AuNP 2 was stable in dH2O at 37 °C after the 72 h period of incubation.

4.5.8.4. The Stability of AuNP 2 in LB at 4 °C and at 37 °C

The hydrodynamic size of AuNP 2 was found to significantly increase from 31.82 ± 0.18 nm to 658.5 ± 9.5 nm (p-value <0.0001) after 5 min of introducing the AuNPs to LB at room temperature. The drastic size increase was accompanied by a colour change from a dark wine-red colour to a navy blue colour **(Figure 4.13),** which indicates that the NPs were aggregating. The aggregation led to a significant decrease in PDI from 0.366 ± 0.02 to 0.206 ± 0.04 (p-value = 0.0056) and an increase in zeta potential from -32.67 ± 1.6mV to -28.43 ± 1.8 mV (p-value = 0.0323), indicating the loss of NP stability. The NP aggregation was subsequently validated using HR-TEM (**Figure 4.16**) analysis.

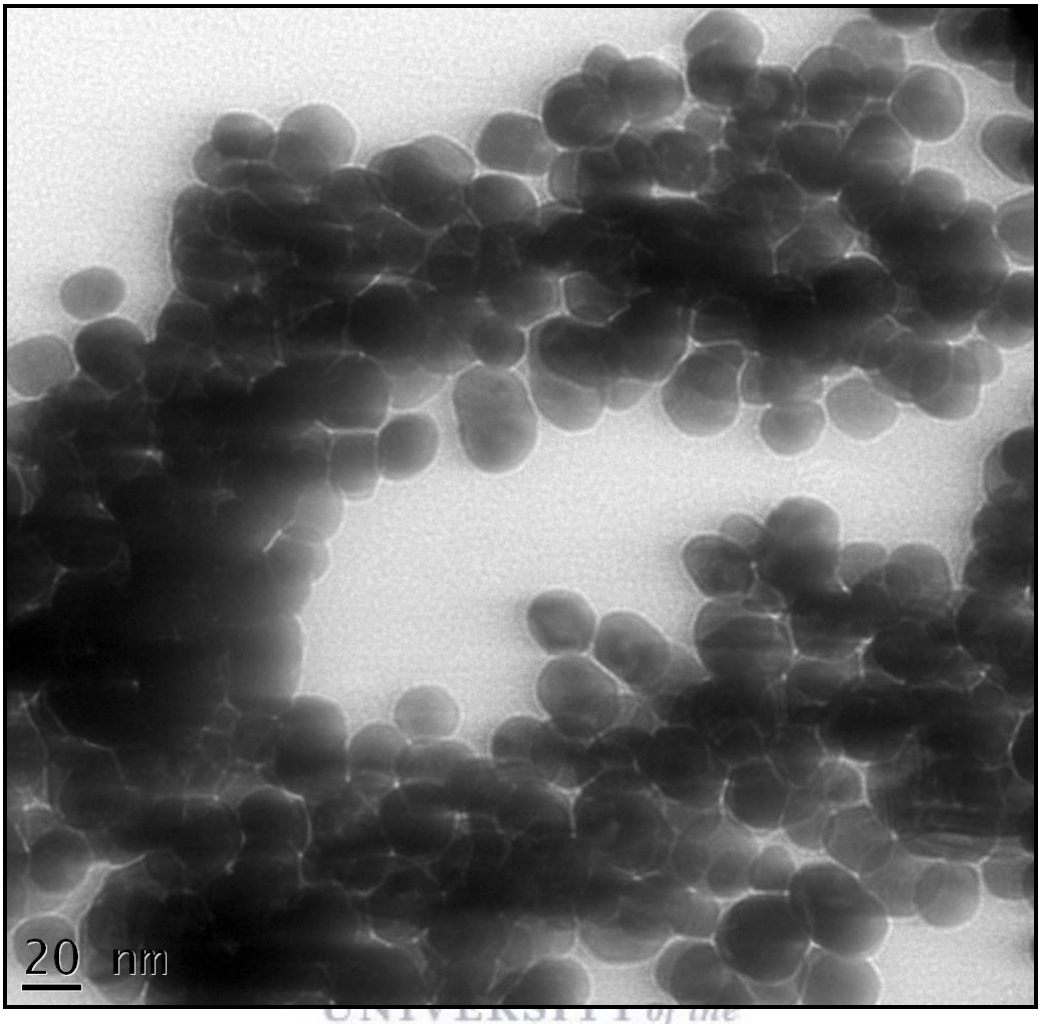

Figure 4.16: HR-TEM image at a 20 nm scale showing a cluster of AuNP 2 as a result of aggregation after re-suspending the NPs in LB for 5 minutes.

The hydrodynamic size, PDI and zeta Potential of AuNP 2 in LB was then monitored at 4 °C and at 37 °C for 24 h, 48 h and 72 h. At 4 °C, no significant change in the hydrodynamic size of AuNP 2 was observed after 24 h (p-value>0.9999) and after 48 h (p-value = 0.9407). However, the hydrodynamic size reduced to 527.87 ± 52.08 nm after 72 h (p-value = 0.0045) of incubation. The PDI was found to increase from 0.206 ± 0.04 to 0.515 ± 0.12 after 24 h (p-value <0.0001). The PDI reduced to 0.296 ± 0.05 after 48 h (p-value = 0.0053) and to 0.275 ± 0.1 after 72 h (p-value = 0.7626) of incubation. The zeta potential showed an increase from-28.43 ± 1.8 mV to -24.4 ± 1.05 mV after 24 h (p-value), to -19.47 ± 6.48 mV after 48 h (p-value= 0.0075) and decreased to -27.3 ± 2.52 mV after 72 h (p-value = 0.0243) of incubation.

After incubation at 37 °C, a significant size increase was observed from 658.5 ± 9.5 nm to 1335.67 ± 54.5 nm after 24 h (p-value<0.0001), to 1646.0 ± 68.1 nm after 48 h (p-value <0.0001) and to 1102.4 ± 169.6 nm after 72 h (p-value <0.0001) of incubation. No significant change in PDI was observed for the entire 72 h (p-values >0.05) of incubation. The zeta potential was found to have increased from -28.43 ± 1.8 mV to -19.7 ± 1.1 mV after 24 h (p-value = 0.0099), to -18.2 ± 1.5 mV after 48 h(p-value = 0.0019) and to -16.3 ± 1.4 after 72 h (p-value = 0.0002) of incubation. Therefore, AuNP 2 was stable in dH_20 at both 4 °C and at 37 ° C, but was not stable in LB at both 4 °C and at 37 ° C. LB seems to promote time dependentaggregation and deterioration of AuNP 2, resulting in the formation of AuNP clusters. AuNP 2 formed clusters of 658.5 ± 9.5 nm after being introduced into LB, these NP-clusters increased in size with time at 37 °C but show no significant changes in size when incubated at 4 °C.

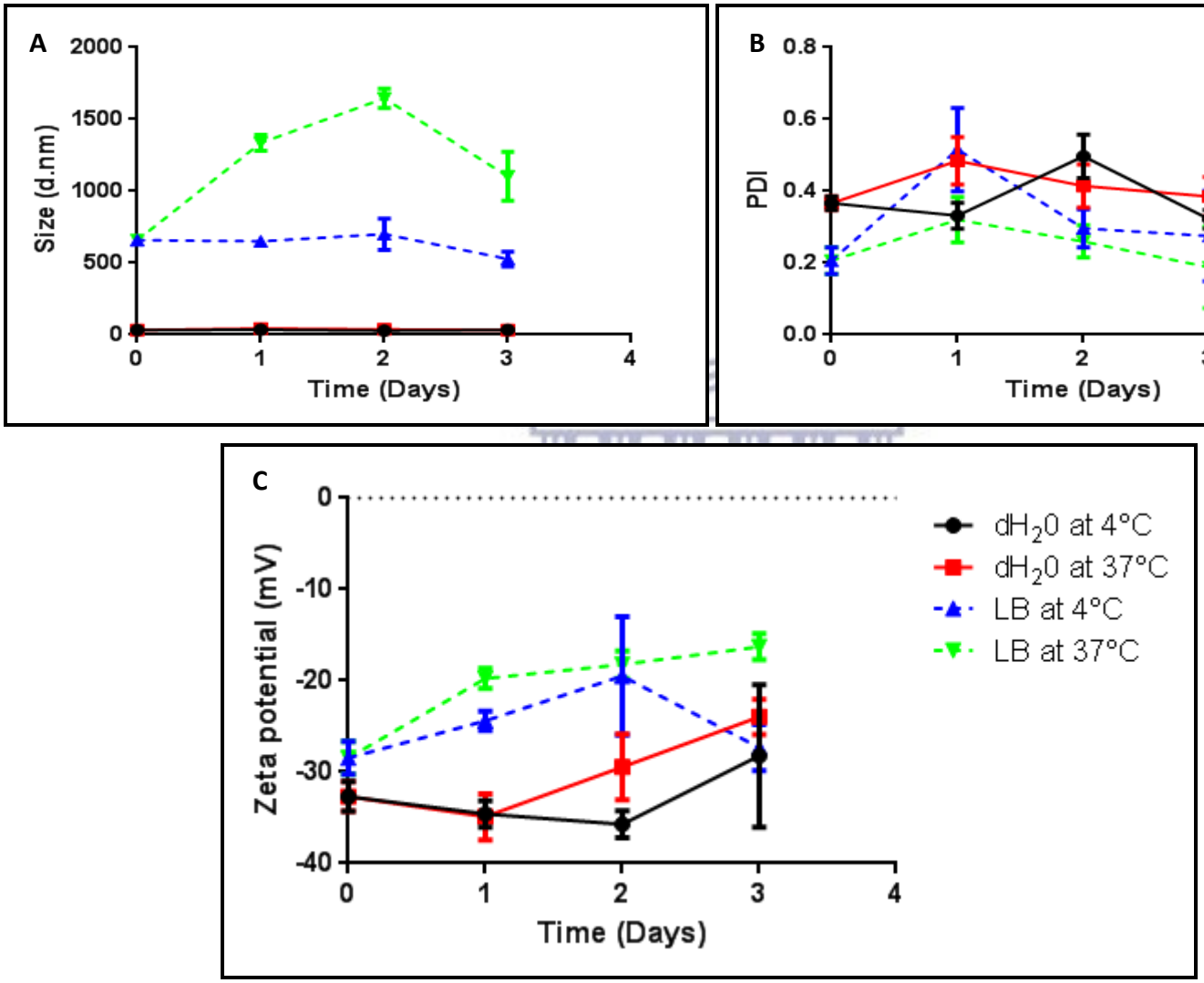

Figure 4.17: The stability of the of AuNP 2 in dH20 at 4 °C (-λ-) and 37 °C (-ν-) over 72 h of incubation, and the stability of AuNP 2 in lysogeny broth at 4 °C (-σ-)and at 37 °C (-τ-) over 72 h of incubation. Data is expressed in mean ± SD (n=3). (A)The hydrodynamic size, (B) PDI and (c) zeta potential of the AuNP.

4.5.8.5. The Stability of AuNP 3 in dH_2O at 4 °C and at 37 °C

The hydrodynamic size of UV treated AuNP 3 in dH_2O was found to be 21.71 ± 0.26 nm with a PDI of 0.175 ± 0.00 and a zeta potential of -30.7 ± 1.3 mV. The hydrodynamic size of AuNP 1 was measured again after 24 h, 48 h and 72 h of incubation at 4 ° C and at 37 ° C. At 4 °C (**Figure 4.19**), no significant difference was found in the hydrodynamic size of AuNP 3 after 24 h, 48 h and 72 h of incubation (p-values>0.9999). No significant difference was found in the PDI of AuNP 3 after 24 h (p-value>0.9999), 48 h (p-value = 0.9992) and 72 h (p-value>0.9999) of incubation. The zeta potential showed no significant changes after 24 h (p-value = 0.9988) and 48 h (p-value = 0.4455). However, a significant increase in zeta potential was observed from -30.67 ± 1.3 mV to -15.76 ± 9.08 mV after 72 h (p-value = 0.0006) of incubation. The increase in zeta potential is associated with loss of stability, therefore the results indicate that AuNP 3 was stable in dH_2O for at least 48 hours, but the quality of the AuNPs becomes compromised after 72 hours of incubation.

The hydrodynamic size of the UV treated AuNP 3 in dH_2O was thereafter measured at 37 °C (**Figure 4.19**). No significant difference in the hydrodynamic size of AuNP 3 was found after 24h (p-value = 0.9999), 48 h (p-value >0.9999) and 72 h (p-value >0.9999). The PDI showed an increase from 0.175 ± 0.00 to 0.979 ± 0.00 after 24 h (p-value <0.0001), and reduced to 0.474 ± 0.03 after 48 h (p-value <0.0001) and to 0.318 ± 0.00 after 72 h (p-value = 0.0114) of incubation. The zeta potential showed no significant changes after 24 h (p-value = 0.8639) and after 48 h (p-value = 0.1801) of incubation. However, the zeta potential showed a slight increase from -30.7 ± 1.3 mV to -20.4 ± 1.92 mV after 72 h (p-value = 0.0265) of incubation. The results suggest that at a temperature of 37 °C, AuNP 3 suspended in dH_2O maintained its overall hydrodynamic size, but began losing physical stability after 72 hours as shown by the increase in peta potential after 72 hours of incubation.

4.5.8.6. The Stability of AuNP 3 in LB at 4 °C and at 37 °C

The stability of AuNP 3 was investigated in LB by examining changes in hydrodynamic size, PDI and zeta potential after 24 h, 48 h and 72 h of incubation at 4 °C and at 37 °C. The hydrodynamic size showed an increase from 18.12 ± 2.7 nm to 510.47 ± 73.47 nm (p-value <0.0001) within 5 minutes after the AuNPs were added to LB. This increase in hydrodynamic size was accompanied by a colour change from a ruby-red colour to a navy blue colour. However, no significant increase in PDI was observed in this time period (p-value = 0.4617). The zeta potential increased from -30.7 ± 1.3 mV to -24.4 ± 2.1 mV (p-value = 0.0037). The results therefore indicated that the NP formed aggregates/clusters immediately after being introduced to LB. This hypothesis was validated using HR-TEM microscopy (**Figure 4.18**).

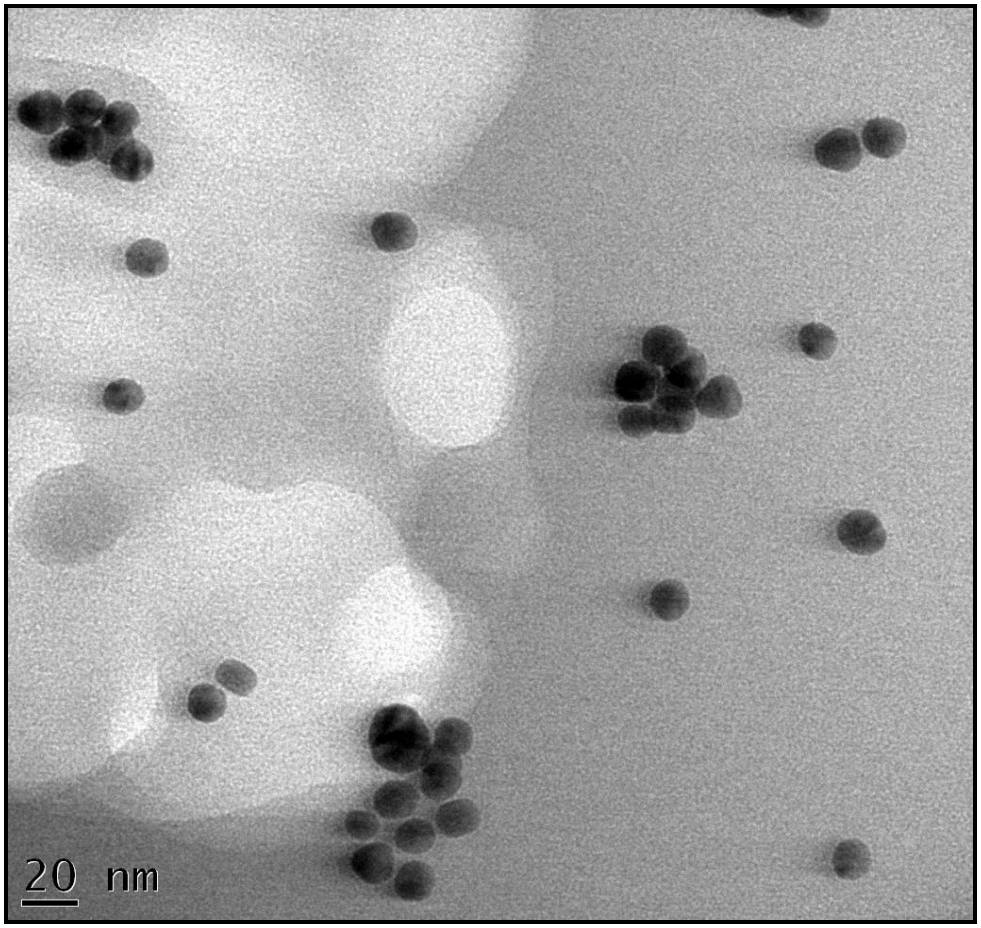

Figure 4.18: HR-TEM image at a 20 nm scale showing a cluster of AuNP 3 as a result of aggregation after re-suspending the NPs in LB for 5 minutes.

The hydrodynamic size, PDI and Zeta Potential of AuNP 3 clusters in LB were subsequently measured at 4 °C and 37 °C for 24 h, 48 h and 72 h. At 4°C, no significant change in the hydrodynamic size was evident after 24 h (p-value = 0.8964) of incubation. However, the hydrodynamic size showed significant increase after from 627.27 ± 26.09 nm to 1484.67 ± 360.68 nm after 48 h (P value <0.0001) and a decreased from 1484.67 ± 360.68 nm to 711.67 ± 71.03nm after 72 h (p-value <0.0001) of incubation, when compared to the negative control. The PDI showed an increased from 0.333 ± 0.05 to 0.532 ± 0.12 after 24 h (p-value < 0.0001) and a decrease to 0.286 ± 0.09 after 48 h (p-value= 0.8078) and to 0.202 ± 0.05 after 72 h (p-value = 0.0119) of incubation. The zeta potential showed no significant changes after 24 h (p-value = 0.4790), 48 h (p-value = 0.2417) and 72 h (p-value = 0.1592) of incubation. The results suggest that AuNP 3 lost their stability in LB and formed NP aggregates/clusters for the first 24 hours of incubation at 4 °C. However, the NP clusters maintained their level of stability for at remainder of the 72 h incubation period as indicated by the stable hydrodynamic size, PDI and zeta potential.

When incubated at 37 °C, the hydrodynamic size of AuNP 3 clusters increased from 510.47 ± 73.47 nm to 1303 ± 153.0 nm after 24 h (p-value = 0.0010), to 1026.6 ± 299.7 nm after 48 h (p-value 0.0335) and to 1170 ± 232.2 nm after 72 h (p-value = 0.0052) of incubation. The PDI increased from 0.333 ± 0.1 to 0.485 ± 0.0 after 24 h (p-value = 0.0025), to0.403 ± 0.0 after 48 h (p-value =0.3833) and to 0.290 ± 0.0 after 72 h (p-value = 0.8593). The zeta potential measurements showed no significant changes after 24 h (p-value = 0.4455), 48 h (p-value = 0.0.6052) and 72 h (p-value = 0.1592) of incubation. The increase in hydrodynamic size and increase in PDI suggested further aggregation of AuNP 3 clusters. However, the zeta potential indicated that the individual NPs had an acceptable level of stability.

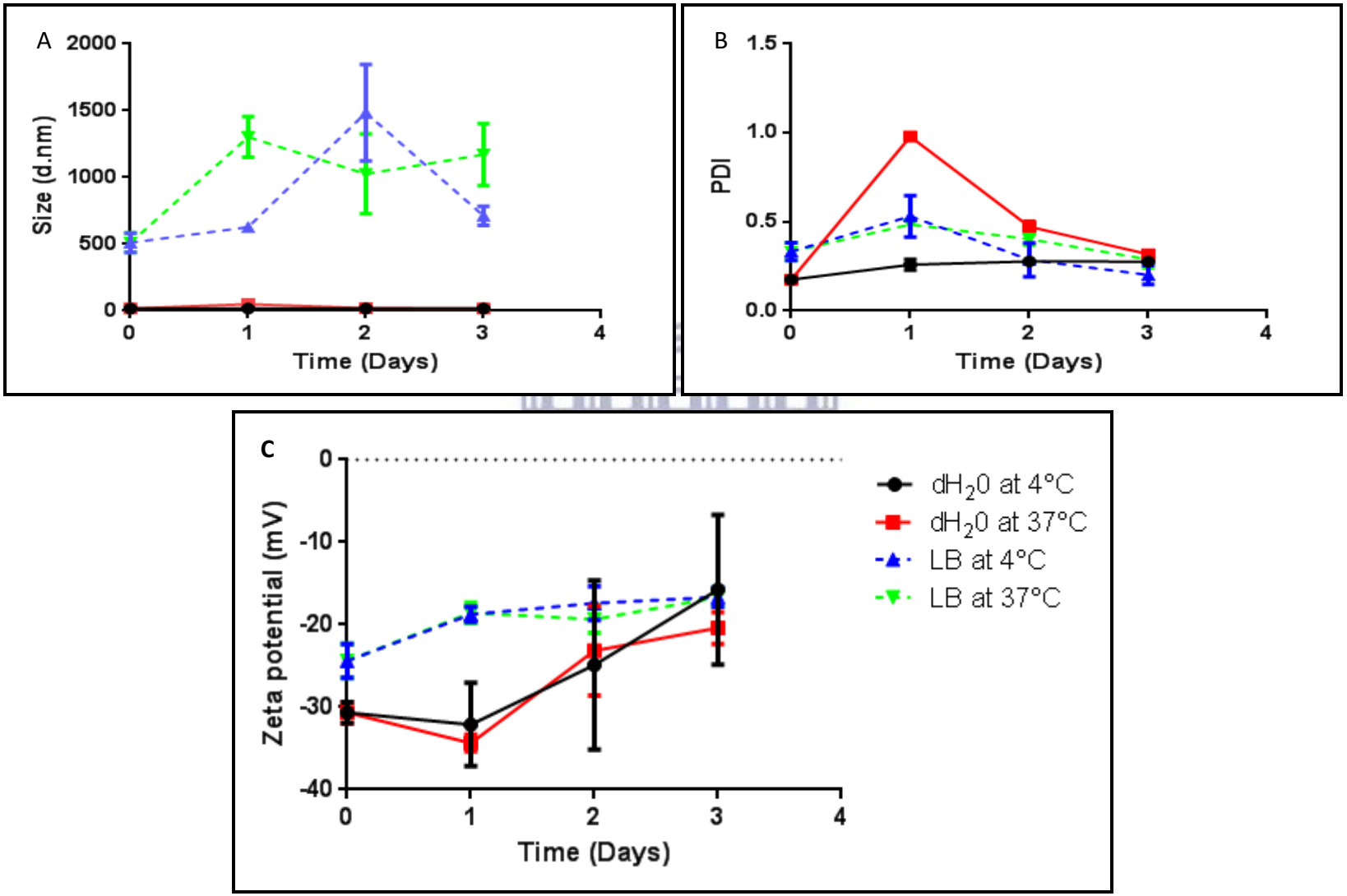

Figure 4.19: The stability of the of AuNP 3 in dH20 at 4 °C (-λ-) and 37 °C (-ν-) over 72 h of incubation, and the stability of AuNP 3 in lysogeny broth at 4 °C (-σ-)and at 37 °C (-τ-) over 72 h of incubation. Data is expressed in mean ± SD (n=3). (A) The size, (B) PDI and (C) zeta potential of the AuNP.

4.5.9. Discussion of Results

Three statistically different sizes of AuNPs with a fairly spherical morphology were prepared using the Turkevich/citrate reduction method. Each of the synthesized AuNPs showed a single λ_{max} absorbance peak near 520 nm, which is distinctive for spherical AuNPs (Lata *et al.,* 2014; Verma *et al.,* 2014). The Average core diameter of the prepared AuNPs was found to be 14.0 ± 2 nm, 28.2 ± 4 nm and 54.6 ± 7 nm with a zeta potential of -27.0 ± 6.28 mV,-32.7 ± 1.60 mV,-30.7 ± 2.1 mV, respectively. Each AuNP size exhibited a different shade of red in dH_2O as is characteristic for different sizes of spherical AuNPs (Verma *et al.,* 2014). In addition, the study also proved that the z-average can only be considered as an accurate measure of the hydrodynamic size if the NP sample under investigation is monomodal and monodispersed as previously stated (Lim *et al.,* 2013). Therefore, the results were found to support the theory that correlation between the absorption maxima and size of AuNPs can only be considered when working with monomodal/monodispersed AuNPs (Lim *et al.,* 2013).

Exposure of AuNPs to short wavelengths of UV light for 30 minutes was found to be a suitable method for the sterilization of the sAuNPs, as the method resulted in no significant changes on the physicochemical properties (hydrodynamic size, zeta potential and PDI) of the AuNPs. The stability of the UV treated AuNPs in dH_2O and in LB was investigated over a 72 h incubation period; the results indicated that the AuNPs in LB media formed clusters of increasing sizes over the 72 h of incubation but remained intact as single AuNPs within the clusters. The results therefore indicated that the AuNPs were unstable in LB at both 4 °C and 37 °C, this conclusion was supported by an increase in zeta potential and a colour change from red to a dark blue colour (due to aggregation) over the 72 h incubation period in LB. The AuNPs incubated at 37 °C were found to aggregate more when compared to AuNPs incubated at 4 °C, therefore suggesting that citrate capped sAuNPs are also sensitive to temperature induced aggregation.

Chapter 5: Determining the antibiotic activity of the AuNPs

5.1. Introduction

In recent years, Nanomaterials have become a promising contender to replace conventional materials due to their various applications in the fields of science and engineering. The exceptionality of NPs can be attributed the increased number of atoms at their grain boundaries and high surface-to-volume ratio (Shamaila *et al.,* 2016). NPs have proved to be essential materials in the advancement of an assortment of novel devices that are used in different physical, pharmaceutical, biomedical and biological applications (Azam *et al.,* 2009; Dykman and Khlebtsov, 2012; Zhou *et al.,* 2012).

Different types of metal NPs contain different metal elements and each uses numerous mechanisms to kill and/or inhibit the growth of specific microbes, thus rendering the development of resistance improbable (Shamaila *et al.,* 2016). These include NPs containing zinc (Zn), copper (Cu), titanium (Ti), magnesium (Mg), silver (Ag), and gold (Au). Among these NPs, gold NPs are commonly used as a catalyst for gene therapy, diagnostic, medical therapy and biological purposes (Giasuddin *et al.,* 2012; Jain *et al.,* 2012; Misbahi, 2010).

The antibiotic activity of NPs is primarily based on the NP size (Yugang and Changhua, 2011). During the preparation of NPs, a number of reducing agents, stabilizers, and solvents can be utilized to control the size and shape of the resulting NPs (Das *et al.,* 2011). In general, the size of a nonspherical nanomaterial is defined as an equivalent diameter of a spherical particle whose selected physical properties, *e.g.* diffusivity, are equivalent to those of the nanomaterial in the same environment (Powers *et al.,* 2006; Shekunov *et al.,* 2007). One frequently adopted example is the hydrodynamic diameter of a molecule, which is the effective size calculated from the diffusion coefficient using the Stokes–Einstein relationship (Lin *et al.,* 2014).

Previous studies have investigated the antimicrobial activity of AuNPs against human bacterial pathogens (Zhou *et al*., 2012; Ali *et al*., 2011). However, these studies published results that were inconclusive for the zone of inhibition for *E. coli* and *S. aureus* (Zhou *et al*., 2012; Ali *et al*., 2011). A recent study investigated the efficiency of different sizes of pure sAuNPs against enteric bacteria (*E. coli, S. aureus, Bacillus subtilis* and *Klebsiella pneumoniae*) at different concentrations after 24 hours of incubation (Shamaila *et al.,* 2016). The antibacterial activity of the AuNPs on the gram-positive and gram-negative bacteria was observed to have been dependent on the concentration of the AuNPs and was demonstrated to increase as the average size of the NPs decreased (Shamaila *et al.,* 2016). These results therefore suggested that the antibacterial activity was dependent on the size and concentration of the AuNPs.

Micro dilution tests can be used to determine MIC endpoint and a variety of viewing devices are available that can read micro dilution tests and record the results with high capacity to differentiate growth in different wells. Furthermore, a number of colorimetric methods based on the use of dye reagents such as Tetrazolium salts, 3-(4, 5- dimethylthiazol-2-yl)-2, 5-diphenyl tetrazolium bromide (MTT) and 2, 3-bis {2-methoxy-4-nitro-5-[(sulfenylamino) carbonyl]-2H- tetrazolium-hydroxide} (XTT), are available and are often used to determine MIC endpoint for antifungal and antibacterial micro dilution assays (Al-Bakri and Afifi, 2007; Liang *et al.,* 2012; Monteiro *et al.,* 2012; Kuhn *et al.,* 2003). The Alamar blue dye (resazurin) is another effective growth indicator that is also commonly used for this purpose (Balouiri *et al.,* 2016).

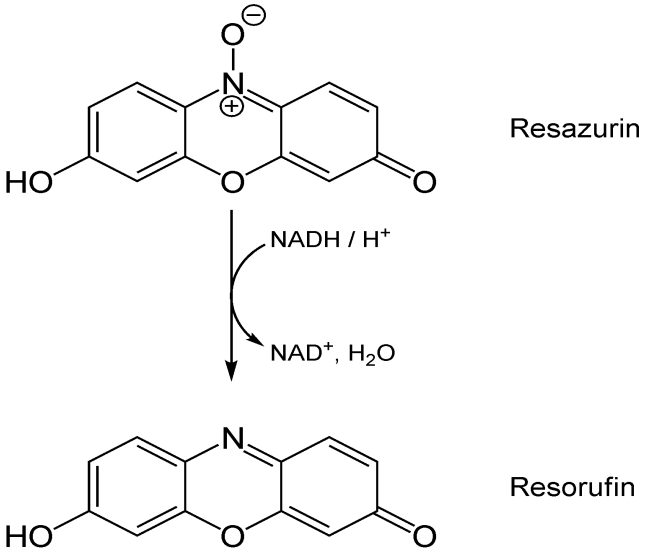

Figure 5.1: Intracellular reduction of resazurin to resorufin using NADH (Shahangian, Ash, Rollins, 1984).

The Alamar blue is a commonly used cell viability reagent used to assess cell health. The principle of this assay is that soluble resazurin dye can be reduced by healthy cells into fluorescent resorufin, and the fluorescence (excitation 535 nm, emission 590 nm) of this dye can then be recorded (Balouiri *et al.,* 2016). Resazurin (blue and nonfluorescent) is reduced to resorufin (pink and highly fluorescent) which is further reduced to hydroresorufin (colourless and non fluorescent). This reduction can occur intracellularly via enzyme activity or in the medium as a chemical reaction (O'Brien *et al.,* 2000).

The 'resazurin reduction test' has been used for approximately 50 years to examine bacterial and yeast contamination of milk, and for assessing semen quality (O'Brien *et al.,* 2000). The dye is widely regarded as a very simple and versatile approach for measuring bacterial growth, cell proliferation and cytotoxicity. This dye presents numerous advantages over other cytotoxicity or proliferation tests but has also been observed to present several drawbacks (O'Brien *et al.,* 2000). In a previous study, tests using numerous toxicants in different cell lines and rat primary hepatocytes showed an accumulation of the fluorescent product of Alamar Blue in the medium which could lead to an overestimation of cell population (O'Brien *et al.,* 2000). In addition, the extensive reduction of Alamar Blue by metabolically active cells led to a final non-fluorescent product, thus resulting in an underestimation of cellular activity (O'Brien *et al.,* 2000).

These and other similar assays have been widely used in a large number of *in vivo* and *in vitro* experiments which are designed to rapidly and efficiently assess the toxicity of NPs. However, due to the unique physicochemical properties and increased reactivity of NPs, these materials are prone to interfere with spectrophotometric and spectrofluorometric assays (Ong *et al.,* 2014). A number of NPs have been reported to interfere with commonly used tests such as the lactate dehydrogenase (LDH) cytotoxicity assay, Alamar blue, and tetrazoliumbased assays (e.g. MTS and MTT) (Han *et al.,* 2011; Holder *et al.,* 2012; Kroll *et al.,* 2012; MacCormack *et al.,* 2012). These assays consist of dyes or proteins that have potential to interact with NPs, upon binding to the proteins and dyes, NPs can alter the structure and thus alter the function of the dyes and/or proteins involved. It is estimated that this process occurs in common toxicity assays. The presence of NPs in assays may adversely influence these reactions

and cause significant changes in enzyme activity (Asuri *et al.,* 2006; Fei and Perrett, 2009; Kane and Stroock, 2007), fluorescence, and/or the absorbance characteristics of indicator molecules (Hedderman *et al.,* 2004; Ramakrishna and Ghosh, 2001).

The activity of AuNPs is known to depend on composition, surface modification, intrinsic properties, and the bacterial species (Hajipour *et al.,* 2012). The interaction between AuNPs and fluorescent dye molecules has been receiving increased attention due to the fascinating optical and electronic interactions of the AuNPs and the NPs have been found to quench the fluorescence of perylene diimide, a multi-purpose and highly fluorescent dye commonly used as high-grade industrial paint, depending on their size and shape. Spherical AuNPs were found to be more effective at quenching the fluorescence of perylene diimide when compared to rod shaped AuNPs (Xue *et al.,* 2013). Therefore, it is important to investigate the quenching potential of AuNPs before employing the NPs in any colorimetric assay based on the use of any dye reagent.

5.2. Objectives

The objective of this chapter was to determine the effect of size, concentration and exposure time on the antibacterial activity of spherical AuNPs on *E. coli*, *S. aureus* and *MRSA*. To develop the assay to determine the antibacterial activity, the quenching effect of the AuNPs on Alamar blue was also determined.

5.3. Materials & methods

5.3.1. Reagents and materials

Gold (III) chloride tri-hydrate ($HAuCl_4 \bullet 3H_2O$) ACS, (99.9 + %) was purchased from Sigma Aldrich (South Africa), tri-Sodium Citrate ($Na_3\ C_6H_5O_7.\ 2H_2O$) and lysogeny broth were purchased from Merck Laboratory Supplies (South Africa), *MRSA (ATCC 33591), E. coli (ATCC 25922) and S. aureus (ATCC 29213)* were procured from ATCC (USA). Alamar blue was purchased from Thermo Fisher Scientific (South Africa). Ultra-purified distilled water (18.2 MΩ cm, Millipore) was used in all experiments.

5.3.2. Instrumentation

Gold nanoparticles were sterilized using a UV chamber (Ultra-Violet Products, Inc, USA). All bacteria work was conducted inside an ethanol sterilized Laminar Flow (Labotec, South Africa). The absorbance and fluorescence readings were determined using the POLARstar Omega plate reader (BMG LABTECH, Germany).

5.4. Methods

Fresh sub-cultures of *MRSA, E. coli* and *S. aureus* were prepared by scraping the top of the tubes of frozen stocks with a sterile loop and aseptically streaking the bacteria on Mueller-Hinton agar plates without thawing the tube. The agar plates were then incubated for 18-24 hours. After the incubation process, a single colony of each bacterium was inoculated into fresh nutrient broth medium (LB) and incubated for 16 to 20 hours to obtain a day 1 working stock. The absorbance of each bacterial suspension was observed at 450 nm and the turbidity was adjusted to obtain a turbidity corresponding to a 0.5 McFarland standard, thus resulting in a suspension containing approximately 1 to 2 X 10^8 samples of bacterium (Pfaller *et al.,* 2004).

5.4.1. Determining the concentration of the AuNPs

The concentration of the sAuNPs was determined from the UV-Vis spectra using the Beer-Lambert law as previously described (Haiss *et al.,* 2007). Metallic NPs are known to strongly interact with light at specific wavelengths and their unique extinction peaks on ultraviolet-visible (UV-Vis) spectra can be utilized to calculate NP concentrations via Beer-Lambert law (Haiss *et al.,* 2007). The data of $\varepsilon_{450}(d)$ in **Table 5.1** can be used to calculate the concentration *(C)* of sAuNPs in mol per litre from the absorption (*A)* at 450 nm for a standard path length *l* of 1 cm according to: $\boldsymbol{C = A_{450}/\varepsilon_{450}}$. Where ε is the molar extinction coefficient at the wavelength of maximum extinction (M^{-1} cm^{-1}) and *d* is the diameter (nm) of AuNPs (Haiss *et al.,* 2007).

5.4.2. Determining the quenching effect of the AuNPs on the fluorescence of Alamar blue

To investigate the quenching effect of sAuNPs on Alamar blue, a 100 µl sample of Alamar blue was mixed with a 1000µl of a 0.5 McFarland standard (OD = 0.08) of *E. coli* solution in three sterile 2 ml Eppendorf tubes and the mixtures was incubated at 37 °C for 1 to 4 hours until the colour changed from dark blue to pink. After the incubation, the mixtures were centrifuged at 4000 rpm at 25 °C. The supernatants were removed using 5 ml sterile syringes and passed through 0.2 µm membrane filters to remove any remaining bacteria.

This protocol was adapted from a previous study where cells were used to reduce tetrazolium dye to formazan in order to investigate the interference of single walled carbon nanotubes (SWCNTs) on the MTT assay (Davis *et al.,* 2007). The fluorescence readings of the reduced Alamar blue containing 0.150 nM, 0.075 nM and 0.038 nM of AuNPs in a final plate-well volume of 100 µl were measured at 530-560 nm (excitation wavelength) and 590 nm (emission wavelength). To calculate the normalization of Alamar blue, the fluorescence readings of Alamar blue samples with 0.150 nM, 0.075 nM and 0.038 nM were subtracted from the fluorescence reading of the negative control samples (Alamar blue without AuNPs).

Table 5.1: Molar decadic extinction coefficient (ε) at λ = 450 nm and the corresponding theoretical extinction efficiencies for sAuNPs in water with diameter (d) ranging from 2 to 100 nm (Haiss *et al.,* 2007).

d/ nm	ε_{450}/ $M^{-1}cm^{-1}$	*d*/ nm	ε_{450}/ $M^{-1}cm^{-1}$	*d*/ nm	ε_{450}/ $M^{-1}cm^{-1}$	*d*/ nm	ε_{450}/ $M^{-1}cm^{-1}$	*d*/ nm	ε_{450}/ $M^{-1}cm^{-1}$	*d*/ nm	ε_{450}/ $M^{-1}cm^{-1}$
2	4.25E+05	19	4.60E+08	36	3.52E+09	53	1.19E+10	70	2.71E+10	87	4.78E+10
3	1.49E+06	20	5.41E+08	37	3.84E+09	54	1.26E+10	71	2.82E+10	88	4.91E+10
4	3.62E+06	21	6.31E+08	38	4.18E+09	55	1.33E+10	72	2.93E+10	89	5.04E+10
5	7.20E+06	22	7.31E+08	39	4.54E+09	56	1.41E+10	73	3.05E+10	90	5.17E+10
6	1.26E+07	23	8.42E+08	40	4.92E+09	57	1.48E+10	74	3.16E+10	91	5.30E+10
7	2.03E+07	24	9.64E+08	41	5.32E+09	58	1.57E+10	75	3.28E+10	92	5.43E+10
8	3.07E+07	25	1.10E+09	42	5.74E+09	59	1.65E+10	76	3.40E+10	93	5.56E+10
9	4.43E+07	26	1.24E+09	43	6.18E+09	60	1.73E+10	77	3.52E+10	94	5.69E+10
10	6.15E+07	27	1.40E+09	44	6.65E+09	61	1.82E+10	78	3.64E+10	95	5.82E+10
11	8.27E+07	28	1.58E+09	45	7.13E+09	62	1.91E+10	79	3.77E+10	96	5.94E+10
12	1.09E+08	29	1.76E+09	46	7.65E+09	63	2.00E+10	80	3.89E+10	97	6.07E+10
13	1.39E+08	30	1.96E+09	47	8.18E+09	64	2.10E+10	81	4.02E+10	98	6.19E+10
14	1.76E+08	31	2.18E+09	48	8.74E+09	65	2.19E+10	82	4.14E+10	99	6.31E+10
15	2.18E+08	32	2.41E+09	49	9.32E+09	66	2.29E+10	83	4.27E+10	100	6.44E+10
16	2.67E+08	33	2.66E+09	50	9.92E+09	67	2.40E+10	84	4.40E+10		
17	3.24E+08	34	2.93E+09	51	1.06E+10	68	2.50E+10	85	4.53E+10		
18	3.87E+08	35	3.21E+09	52	1.12E+10	69	2.61E+10	86	4.65E+10		

5.4.3. Investigating the effect of size, concentration and exposure time on the antibacterial activity of spherical AuNPs.

The effect of sAuNPs on the growth of *MRSA, E. coli* and *S. aureus* was examined via broth micro-dilution using the Alamar blue dye as an indicator of bacterial cell health according to The Clinical & Laboratory Standards Institute (CLSI) standards. A two-fold serial dilution of each sAuNP size with fresh nutrient broth (LB) in a Greiner 96 well plate was performed, followed by the addition of a 1:2 dilution of the bacterial culture to sAuNPs suspended in broth media. At the end of the dilution process, bacterial samples containing 0.150 nM, 0.075 nM and 0.038 nM of sAuNPs were obtained. Untreated *MRSA, E. coli* and *S. aureus* cultures equivalent to a 0.5 McFarland standard were used as the negative controls while *MRSA, E. coli* and *S. aureus* cultures treated with 50 µg/ml of ampicillin were used as positive controls. The bacterial cultures containing the sAuNPs were incubated at 37 ^{0}C for 24, 48 and 72 hours in an ambient air incubator.

After incubation, bacterial growth was evaluated by measuring the turbidity at 450 nm using the POLARstar Omega plate reader, based on the principle that turbidity is directly proportional to bacterial growth. Thereafter, 10µl of Alamar blue was added to each well. Alamar blue is light sensitive; therefore, the 96 well plates were covered in aluminum foil and incubated for 1 to 4 hours at 37°C. The fluorescence readings were read at 530 -560 (excitation wavelength) and 590 nm (emission wavelength), while the absorbance readings were read at 570nm (630nm reference wavelengths). The data was expressed as the percentage growth inhibition.

$$100 - \left[\frac{\text{Relative Fluorescence units (RFU) of bacteria with AuNPs}}{\text{Relative Fluorescence units (RFU) of bacteria with no AuNPs}} \text{ X } 100 \right]$$

The determined fluorescence quenching values of the sAuNPs (**figure 5.7**) were substracted from the final fluorescence readings to compensate for the fluorescence quenching of the different concentrations of the sAuNPs**.**

5.4.4. Statistical Analysis

GraphPad Prism 6 was used to compare the dose– responses of each bacterial strain to each AuNP size obtained using the Alamar blue method. The results of both the fluorescence quenching and the antibacterial activity assays were aggregates of three independent experiments; the average of each independent experiment was calculated and used to calculate the p-values. In statistical significance testing, the p-value is the probability of obtaining a test statistic result similar to the one that was actually observed, assuming that the null hypothesis is true.

In a statistical test, sample results are compared to the negative control by way of two competing hypotheses: the null hypothesis is a neutral statement about a population, such as "no difference" between two groups, the alternative (or research) hypothesis is the statement that “there is a difference” between two groups. If the p-value is less than or equal to a threshold value (traditionally 5% or 1%), it suggests that the observed data is inconsistent with the theory that the null hypothesis is true, and thus that hypothesis must be rejected and the other hypothesis accepted as true (Ferreira and Patino, 2015). Traditionally, the cut-off value to reject the null hypothesis is 0.05. Thus, a p-value less than 0.05 indicate a significant difference between two groups (Ferreira and Patino, 2015). The p-value was calculated taking into account both the average mean and the standard deviation of the parameters being compared.

5.5. Results and Discussion.

5.5.1. Determining the quenching effect of the AuNPs on the fluorescence of Alamar blue.

It was confirmed that the reduced form of Alamar blue strongly absorbs at a UV-Vis range of 500-600 nm (**Figure 5.2**). This UV-Vis absorption range was also found to be the same range where AuNP 1, AuNP 2 and AuNP 3 also absorb (**Figure 4.3**). Therefore, mixing the Alamar blue with different concentrations (0.150 nM, 0.075 nM and 0.038 nM) of the AuNPs resulted in absorbance interferences. The absorbance interferences where observed to increase with the increase in AuNP concentration, therefore consequently interfering with the OD readings of the Alamar blue assay **(Figure 2, 3 and 4 in the Appendix)**.

These results corresponded with previously published results, where iron/graphite magnetic particles, superparamagnetic magnetite/silica nanoparticles, bare and PEGylated silica nanoparticles and magnetic composites magnetite/FAU zeolite were observed to have strong absorbance at 525 nm; the same wavelength used in MTT assays, in culture medium in the absence of cells (Diaz *et al*., 2008). This absorbance was found to increase with the NP concentration and as a result greatly interfere with the MTT assay results (Diaz *et al*., 2008). As a result of the absorbance interference, fluorescence was used to measure the antibacterial activity of the sAuNPs and the statistical significance of the results was analysed using two-way ANOVA.

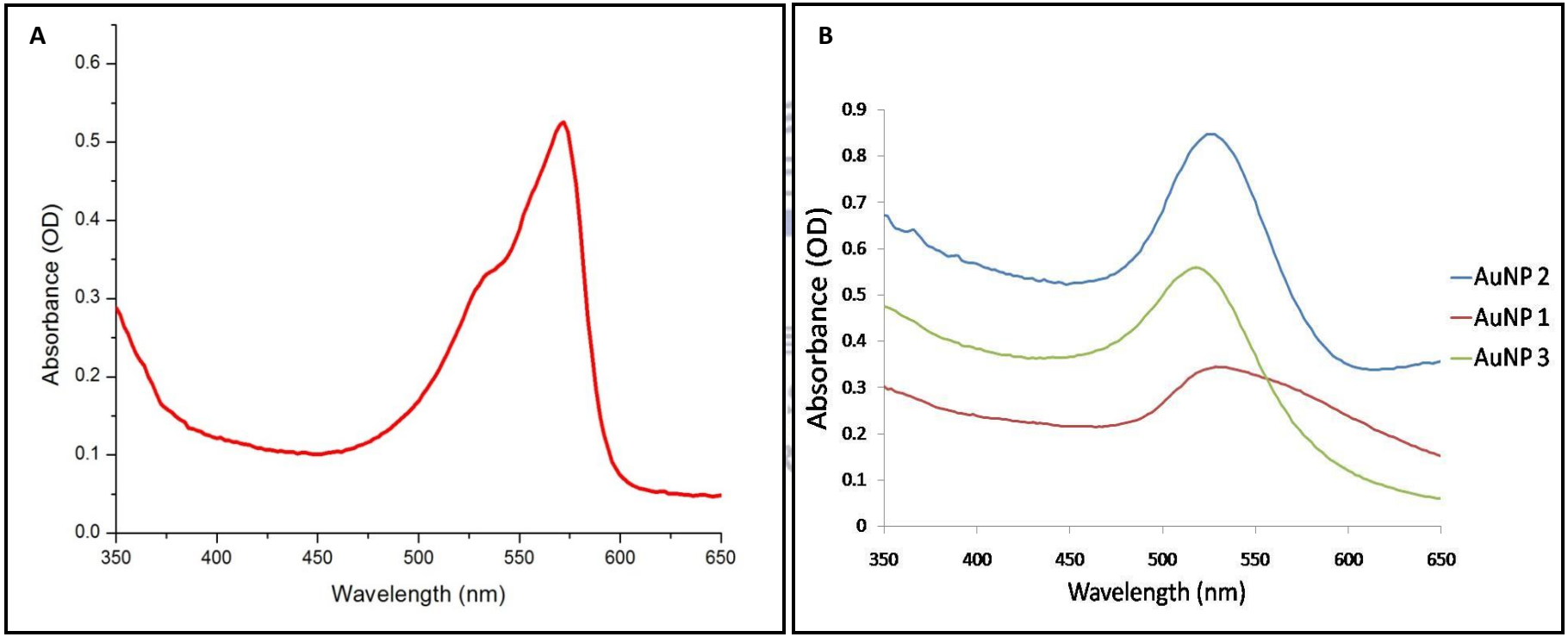

Figure 5.2: The UV-vis spectrum of the reduced form of (A) Alamar blue dye (resorufin), and (B) the UV-vis spectrum of the sAuNPs measured at an absorbance range of 350-650 nm. Both the sAuNPs and the resorufin absorb highly at the UV range of approximat.

5.5.1.1. Determining the quenching effect of the AuNP 1.

AuNP 1 clusters were observed to have quenched 27.2 (± 4.26) % of Alamar blue fluorescence at a concentration of 0.038 nM (p-value < 0.0001), 18.4 (± 6.41) % at a concentration of 0.075 nM (p-value = 0.0026) and 30.8 (± 4.01) % at a concentration of 0.150 nM (p-value < 0.0001), after 3 hours of incubation at room temperature when compared to the negative control (resorufin with no sAuNPs) (**Figure 5.3**). No significant difference was observed between the fluorescence quenching efficacy of AuNP 1 clusters with a concentration of 0.038 nM and the fluorescence quenching of AuNP1 clusters at a concentration of 0.075 nM (p = 0.5063). No significant difference was observed between the quenching efficacies of AuNP 1 clusters with a concentrationof 0.038 nM and those with a concentration of 0.150 nM (p-value > 0.9999), and no difference was observed between AuNP 1 clusters with a concentration of 0.075 nM and those with a concentration of 0.150 nM (p-value = 0.0803).

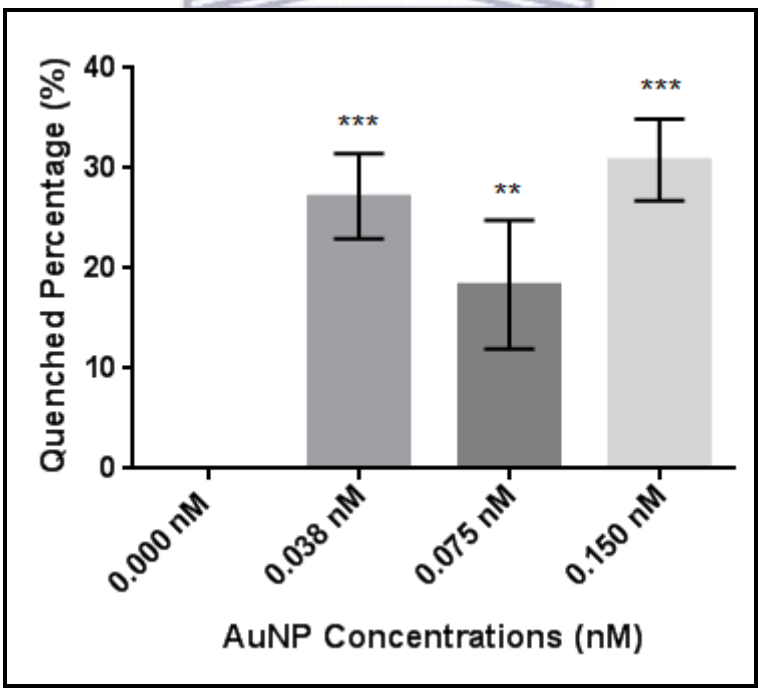

Figure 5.3: Comparing the quenching percentage of 0.038 nM, 0.075 nM and 0.150 nM of AuNP 1 on the fluorescence of Alamar blue after 3 hours of incubation at 25 °C. Data is expressed in mean ± SD (n = 3). Statistical significance was indicated by * (p-value <0.05), ** (p-value <0.01) and *** (p-value <0.001).

The results therefore, showed no significant difference between the quenching efficacy of AuNP 1 at the three utilized concentrations (0.038 nM, 0.075 nM and 0.150 nM). However, the quenched fluorescence percentage and the p-values indicate that AuNP 1 clusters at a concentration of 0.150 nM showed more fluorescence quenching potential when compared to the lower concentrations, though statistically insignificant. A possible reason for the lack of significant difference between the quenching efficacies of the three concentrations of could possibly be due to the small concentration range used.

5.5.1.2. Determining the quenching effect of the AuNP 2.

AuNP 2 clusters were observed to have quenched 27.7 (± 3.65) % of Alamar blue fluorescence at a concentration of 0.038 nM (p-value = 0.0002), 23.17(± 8.75) % at a concentration of 0.075 nM (p-value = 0.0011) and 34.2 (± 7.00) % at a concentration of 0.150 nM (p-value <0.0001) after 3 hours of incubation at room temperature (**Figure 5.4**), when compared to the negative control (Alamar blue with no sAuNPs). No significant difference was observed between the fluorescence quenching efficacies AuNP 2 clusters at a concentration of 0.038 nM and AuNP 2 clusters with a concentration of 0.075 nM (p-value = 0.9314). No significant difference was observed between the fluorescence quenching efficacies of AuNP 2 clusters with a concentration of 0.038 nM and a concentration of 0.150 nM (p = 0.7291). No significant difference was observed between the fluorescence quenching of AuNP 2 clusters with a concentration of 0.075 nM and those with a concentration of 0.150 nM (p-value 0.1962).

Therefore, no significant difference was observed between the quenching effects of the three concentrations of AuNP 2 clusters. However, though statistically insignificant, the highest concentration (0.150 nM) of the AuNP 2 clusters showed the highest fluorescence quenching percentage and a larger statistical difference when compared to the negative control. These results were parallel to the results obtained in the quenching study of AuNP 1, the results therefore suggest that the sAuNPs potentially quenched the fluorescence of Alamar blue in a concentration dependent manner. As with AuNP 1 clusters, the insignificant difference between the quenching effects of each concentration used were possibly due to the short concentration range of the sAuNPs employed in this study.

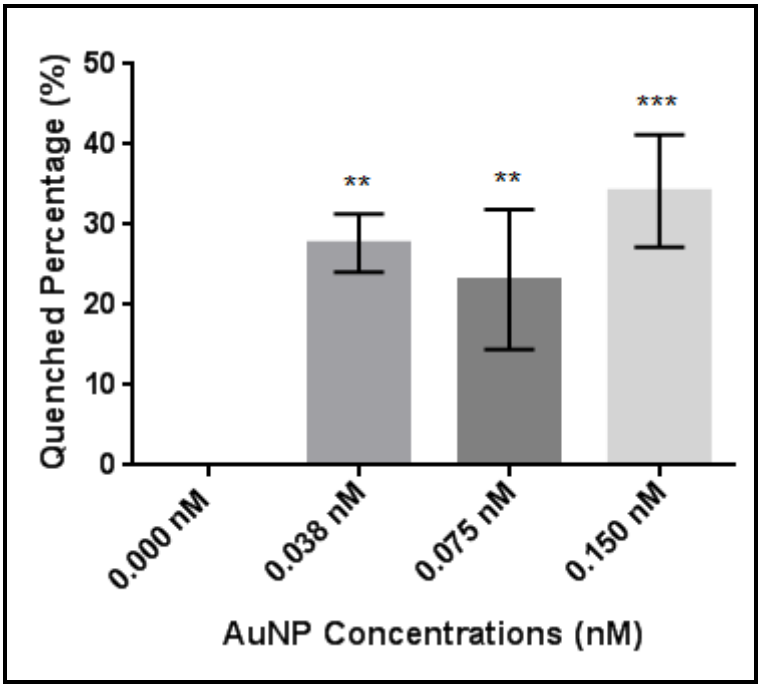

Figure 5.4: Comparing the quenching percentage of 0.038 nM, 0.075 nM and 0.150 nM of AuNP 2 on the fluorescence of Alamar blue after 3 hours of incubation at 25 °C. Data is expressed in mean ± SD (n = 3). Statistical significance was indicated by * (p-value <0.05), ** (p-value <0.01) and *** (p-value <0.001).

5.5.1.3. Determining the quenching effect of the AuNP 3.

The results showed that AuNP 3 clusters were observed to have quenched 18.17 (±2.81) % at a concentration of 0.038 nM (p-value = 0.0134), 12.73 (± 5.15) % at 0.075 nM (p-value = 0.1231) and 31.0 (± 10.76) % at a concentration of 0.150 nM (p-value < 0.0001) of alamar blue fluorescence after 3 hours of incubation at room temperature (**Figure 5.5**), when compared to the negative control. No significant difference was observed between the quenching efficacy of AuNP 3 clusters with concentrations of 0.038 nM and 0.075 nM (p = 0.8759). No significant difference was observed between the AuNP clusters with a concentration of 0.038 nm and those with a concentration of 0.150 nm (p-value = 0.1200). However, a significant difference was observed between the fluorescence quenching efficacy of AuNP 3 clusters with concentrations of 0.075 nm and that of AuNP 3 clusters with a concentration of 0.150 nm (p-value 0.0131). The results showed that AuNP 3 clusters at a concentration of 0.150 nm had more fluorescence quenching activity when compared to AuNP 3 clusters with concentrations

of 0.038 nM and 0.075 nM. These results therefore suggest that AuNP 3 potentially quenches the fluorescence of Alamar blue in a concentration dependent manner.

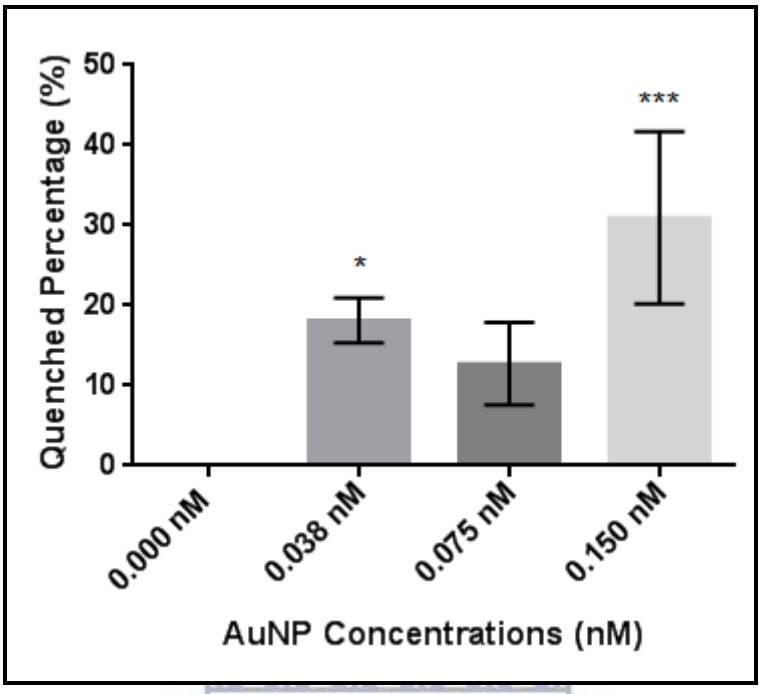

Figure 5.5: Comparing the quenching percentage of 0.038 nM, 0.075 nM and 0.150 nM of AuNP 3 on the fluorescence of Alamar blue after 3 hours of incubation at 25 °C. Data is expressed in mean ± SD (n = 3). Statistical significance was indicated by * (p-value <0.05), ** (p-value <0.01) and *** (p-value <0.001).

These results were therefore comparable to the results obtained in a previous study, were carbon black NPs were observed to quench and decrease the fluorescence of MTT as the concentration of carbon black increased (Aam *et al.,* 2007).

5.5.1.4. Comparing the fluorescence quenching efficacy of the sAuNPs.

When comparing the fluorescence quenching efficacies of the sAuNps (**Figure 5.6**), no significant differences were observed between the clusters of AuNP 1 and AuNP 2 clusters (p-value = 0.9996), between clusters of AuNP 1 and AuNP 3 (p-value = 0.2697) clusters as well as between the clusters of AuNP 2 and AuNP 3 (p-value = 0.2298) clusters at a concentration of 0.038 nM. At a concentration of 0.075 nM, no significant difference was observed between the fluorescence quenching efficiency of AuNP 1 and AuNP 2 clusters (p-value = 0.7517), between clusters of AuNP 1 and AuNP 3 (p-value = 0.6424) and between clusters of AuNP 2 and AuNP 3 (p-value = 0.1696) at a concentration of 0.075 nM. Furthermore, no significant differences were observed

between the fluorescence quenching efficacies of AuNP 1 and AuNP 2 clusters (p = 0. 8932), between AuNP 1 and AuNP 3 (p-value >0.9999) and between AuNP 2 and AuNP 3 clusters (p = 0.9039) at a concentration of 0.150 nM as well. These results suggested that there was no significant difference between the fluorescence quenching efficacies of AuNP 1, 2 and 3. Thus, suggesting that the fluorescence quenching of sAuNPs was not dependenton the size of the AuNPs.

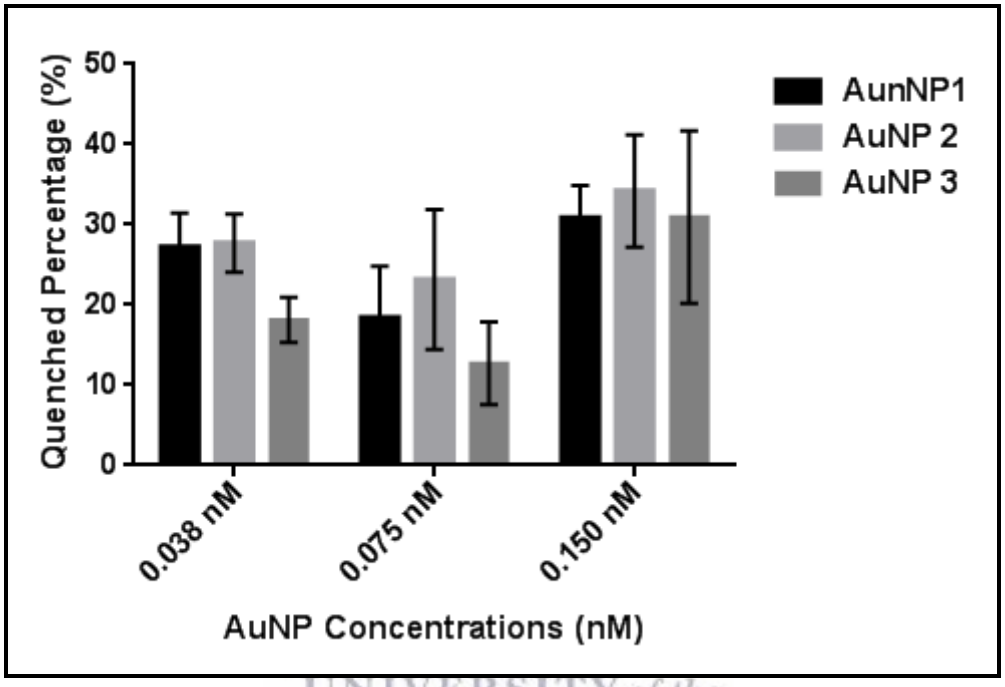

Figure 5.6: A comparison of the quenching efficacy of AuNP1, AuNP 2 and AuNP 3 on the fluorescence of Alamar blue after 3 hours of incubation at 25 °C. Data is expressed in mean ± SD (n=3). Statistical significance was indicated by * (p-value <0.05), ** (p-value <0.01) and *** (p-value <0.001).

Therefore, the observed results were not in line with the results obtained in a recently published study, where organo-soluble decane thiol monolayer-protected AuNPs of different shapes and sizes were homogenously mixed with strong fluorescent perylene diimide (PDI) dye molecules in both solution and solid states (Xue *et al.,* 2013). The effect of the doped AuNPs on PDI was investigated by UV–vis, fluorescence, transmission electron microscopy, scanning electron microscopy, and Raman experiments. The AuNPs were found to modify the strong fluorescence properties of PDI in a size and shape dependent manner, with sAuNPs having a higher quenching efficacy when compared to rod shaped AuNPs (Xue *et al.,* 2013).

In the same study, the smallest sAuNPs (2.6 nm) displayed the strongest quenching effect when compared to larger sAuNPs (34.2 nm and 102.6 nm) (Xue *et al.,* 2013). A possible reason why the sAuNPs in the current study did not show any size dependentquenching efficacies could is due to the size range of the sAuNPs. The published study used a wider average size range (2.6 nm – 102.6 nm) compared to the current study (14.03 nm – 53.61 nm); therefore, the size range used in the current study could have been too narrow and therefore fell in a range of sAuNPs that have similar fluorescence quenching efficacies. In addition, the sAuNP used in this study by Xen *et al* were protected from aggregation by a decane thiol monolayer, where as the sAuNPs in the current study were capped with citrate. Citrate is known to be a weak capping agent (Lin *et al.,* 2013).

Aggregation has been reported to reduce the surface area of the individual NPs involved (Lin *et al.,* 2013). Therefore, an additional reason could be that the effect of size on the fluorescence quenching activity of the sAuNPs was nullified by the aggregation process, which could have reduced the amount of free binding space for the dye molecule, altering the activity of the sAuNPs in the process. However, the results showed that the clusters of citrate-capped sAuNPs of an average size range of 14.03 nm to 53.61 nm had a high quenching activity on the fluorescence of Alamar blue and also supported the theory that determining potential sources of interference is an essential issue in the preliminary study of nanotoxicology as these interferences can greatly distort the results obtained, which can subsequently result in false positive or false negative results (Kong *et al.,* 2011). Due to the discovered quenching of Alamar blue fluorescence, the percentage quenching values of each sAuNP were taken into account in the determination of the efficacy of the NPs against the bacteria.

5.5.2. Investigating the effect of size, concentration and exposure time on the antibacterial activity of spherical AuNPs.

5.5.2.1. The efficacy of AuNP 1 against *E. coli, S. aureus* and *MRSA*

AuNP 1 clusters at a concentration of 0.038 nM were found to have no significant effect on the growth of *E. coli* after both 24 hours ($p = 0.4538$) and 48 hours ($p = 0.9994$), as well as after 72 hours of incubation ($p = 0.9894$) with the pathogen. The sAuNP clusters

where observed to have negligibly induced the growth of *E. coli* by 18.1 (± 12.1) % and 4.0 (± 5.8) % after 24 hours and 48 hours, respectively. The NPs were then observed to have significantly inhibited 6.6 (± 19.6) % of *E. coli* growth after 72 hours of exposure **(Figure 5.7).** At a concentration of 0.075 nM, AuNP 1 clusters was found to have a significant growth inducing effect on *E. coli* after 24 hours of incubation, resulting in *E. coli* growing to 41.8 (± 29.4) % (p-value = 0.0031) higher than the negative control. However, the induced growth was found to have reduced to only 5.1 (± 11.1) % above the negative control after 48 hours (p-value = 0.9974). The growth of *E. coli* was only inhibited by 27.5 (± 8.4) % after 72 hours (p-value = 0.0842) of incubation.

The sAuNP clusters were therefore found to have no significant effect on the growth of *E. coli* after 48 hours and 72 hours of incubation when compared to the negative control at a concentration of 0.075 nM. At a concentration of 0.150 nM, AuNP 1 clusters was found have negligible growth inhibiting effects on *E. coli* and only managed to inhibit the growth of *E. coli* by 17.0 (± 13.0) % (p-value = 0.5269) and by 25.9 (± 18.5) % (p-value = 0.1178) after 24 hours and 48 hours of exposure, respectively. However, the NP clusters were found to have significantly inhibited 39.6 (± 9.5) % (p-value = 0.0053) of bacterial growth after 72 hours of incubation when compared with the negative control.

The results therefore suggested that AuNP 1 clusters at 0.150 nM had a time dependent growth inhibition activity against *E. coli*. However, the efficiency of AuNP 1 clusters against the growth of *E. coli* was also found to weaken as the concentration of NP clusters decreased; therefore, suggesting that the growth inhibition effect of AuNP 1 clusters was also dependent on the concentration. These results were parallel to previously published data, where *E. coli* DH5 α was treated with sAuNPs with a core diameter of 20 nm synthesized from *Bacillus clausii* (Zhang *et al.,* 2016).

The CFU results of the study revealed that the viability of *E. coli* decreased as the concentrations of the AuNPs increased after 12 hours of incubation. The same study also found that the AuNPs had no significant effect on cell viability at very low concentrations (Zhang *et al.,* 2016). *S. aureus* was then exposed to AuNP 1 clusters with concentrations of 0.038 nM, 0.075 nM and 0.150 nM for 72 hours at 37 °C. The AuNP 1 clusters at a concentration of 0.038 nM were observed to have slightly induced the growth of *S. aureus* by 19.6 (±3.6) %, 7.5 (± 3.4) % and 23.0 (± 15.8) % after 24 hours of

(p-value = 0. 3690), 48 hours (p-value = 0.9805) and 72 hours (p-value = 02097) of incubation, respectively.

At a concentration of 0.075 nM, AuNP1 clusters were observed to have no significant effect on the growth of *S. aureus* after 24 hours (p-value = 0.9967), 48 hours (p-value> 0.9999) and after 72 hours (p-value = 0.9093) of incubation. The AuNP clusters were observed to have slightly induced the growth of the bacteria by 5.4 (± 7.0) %, 0.2 (± 7.0) % and 10.4 (± 11.7) % after 24, 48 and 72 hours of exposure, respectively. AuNP 1 clusters at a concentration of 0.150 nM were also found to have no significant growth inhibiting effect on *S. aureus* after 24 hours (p-value = 0.5316), 48 hours (p-value = 0.8523) and after 72 hours (p = 0. 9277) of incubation. The sAuNP clusters slightly increased the growth of the bacteria by 17.0 (± 9.9) %, 11.8 (± 3.7) % after 24 hours and 48 hours of incubation. However, after 72 hours of exposure, the NP clusters were found to have slightly inhibited the growth of *S. aureus* by 9.9 (± 36.9) %, which suggests that the NP clusters might have a potential time-dependent activity. Nonetheless, the results showed that the sAuNP clusters had a negligible effect on the growth of *S. aureus* at a concentration of 0.038 nM, 0.075 nM and 0.150 nM.

When *MRSA* was exposed to 0.038 nM of AuNP 1 clusters, the growth of *MRSA* was observed to have been significantly increased by 18.7 (± 13.8) %, 18.0 (± 15.1) % and 18.2 (± 10.0) after 24 hours (p-value = 0.1023), 48 hours (p-value = 0.1252) and 72 hours (p-value = 0.1183) of incubation, respectively. At 0.075 nM, the sAuNP clusters were found to show statistically negligible growth inducing effects on the growth of *MRSA*, slightly inducing the growth of the bacteria by 11.0 (± 12.2) %, 7.7 (± 11.4) % and 9.1 (± 3.3) % after 24 hours (p-value = 0.6147), 48 hours (p-value = 0.8848) and 72 hours (p-value = 0.7839) of exposure, respectively. At 0.150 nM, AuNP 1 clusters showed no significant growth inhibiting activity on *MRSA* after 24 hours (p-value = 0.9977), 48 hours (p-value = 0.5734) and 72 hours (p-value = 0.0784) of incubation and were observed to have inhibited bacterial growth by 3.5 (± 9.3) %, 11.4 (± 5.9) % and 19.6 (± 6.4) %, respectively; when compared to the negative control (only inducing bacterial growth). Similar to the lower concentrations, the results showed a time-dependent increase in the percentage growth of *MRSA* by AuNP 1 clusters at a concentration of 0.150 nM.

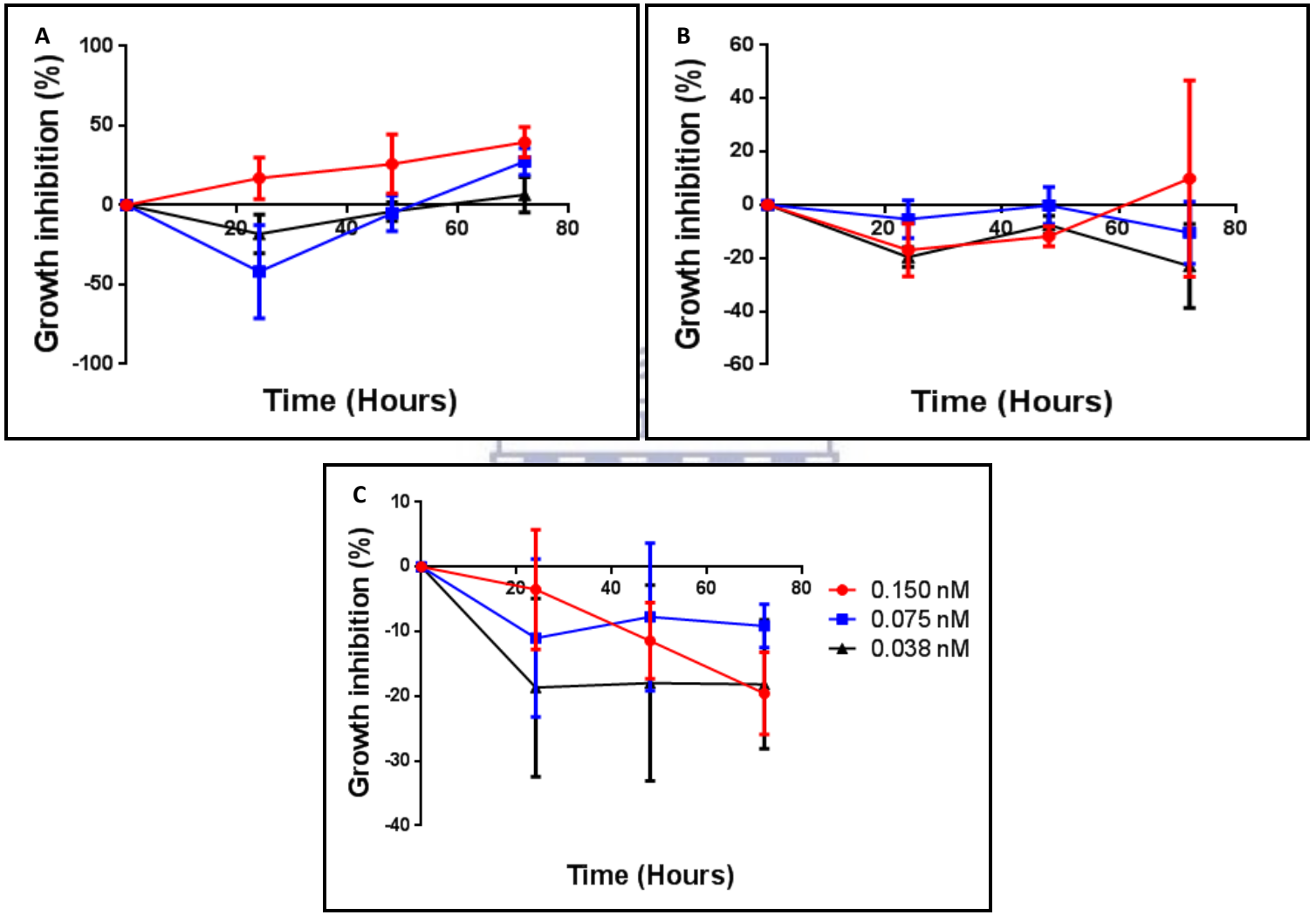

Figure 5.7: The percentage growth inhibition of (A) *E.coli,* (B) *S. aureus* and (C) *MRSA* treated by different concentrations of AuNP 1 after 72 hours of incubation. Data is expressed in mean ± SD (n = 3).

AuNP 1 clusters (14.0 ± 1.67 nm) showed concentration- and time dependent antibacterial activity, with a minimum inhibitory concentration (MIC) of 0.150 nM against *E. coli* with lower concentration inducing an increase in the growth of *E. coli*. The results also indicated that AuNP 1 clusters at 0.075 nM and 0.038 nM induce an increase in the growth of *E.coli, S aureus* and *MRSA*. These results were parallel to previously published results where spherical AgNPs of 11 nm were observed to exert their antibiotic activity in a dose- and time-dependent manner against MDR-*Pseudomonas aeruginosa* and *S. aureus* with MICs of 1 and 2 µg/ml, respectively (Beyth *et al.,* 2015). The effect of 50 ng/ml of Ampicillin on *E. Coli, S. Aureus* and *MRSA* can be found on **Figure 5** of the Appedix, the results where not compared with those of the AuNPs due to the difference in chemical composition between AuNPs and Ampicillin.

5.5.2.2. The efficacy of AuNP 2 against *E. coli, S. aureus* and *MRSA*

At 0.038 nM, AuNP 2 clusters were observed to have no statistically significant effect on the growth of *E. coli* and were found to induce an increase in the growth of *E. coli* by 28.5 (± 29.8) % after 24 hours (p-value = 0.6423), by 34.5 (± 4.2) % after 48 hours (p-value = 0.4327) and by 6.1 (± 24.8) % after 72 hours (p-value = 0.9998) of incubation when compared to the negative control **(Figure 5.8)**. At 0.075 nM, AuNP 2 clusters also had no statistically significant growth inhibition effect against *E. coli* and were observed to have induced an increase in the growth of the bacteria by 33.3 (± 25.3) % after 24 hours (p-value = 0.4706), and by 20.6 (± 10.8) % after 48 hours (p-value = 0.8849) of incubation. However, after 72 hours of incubation, AuNP 2 clusters were found to have induced a significant increase in the growth of *E. coli* by 65 (± 57.9) % (p-value = 0.167), when compared to the negative control.

At a concentration of 0.150 nM, AuNP 2 clusters also showed no statistically significant activity on the growth of *E. coli.* The growth of *E .coli* was found to have been reduced by 10.4 (± 17.9) % after 24 hours (p-value = 0.9958), increased by 21.9 (± 24.9) % after 48 hours (p-value = 0.8523) and again reduced 30.1 (± 16.9) % after 72 hours (p-value = 0.5844) of incubation when compared to the negative control. The results indicated that AuNP 2 clusters had negligible growth inhibiting effects on the growth of *E. coli* at the tested concentrations, but showed potential time and concentration dependent growth inhibiting potential at 0.150 nM.

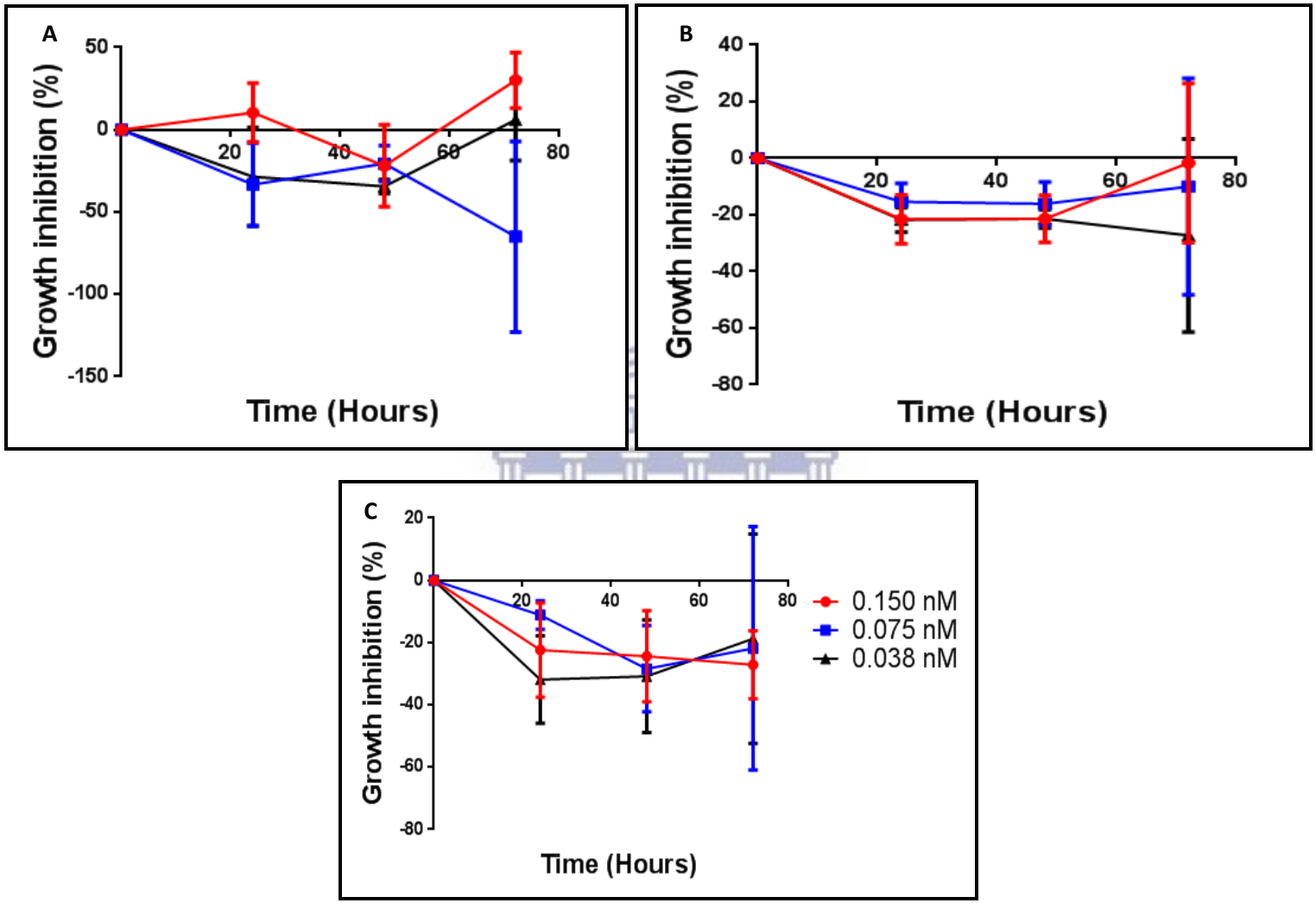

Figure 5.8: The percentage growth inhibition of (A) *E.coli,* (B) *S. aureus* and (C) *MRSA* treated with different concentrations of AuNP 2 for 72 hours. Data is expressed in mean ± SD (n = 3).

No statistically significant growth inhibiting activity was observed after exposing *S. aureus* to 0.038 nM of AuNP 2 clusters, sAuNP clusters were found to have induced a statistically insignificant increase in the growth of *S. aureus* by 21.7 (± 4.4) % after 24 hours (p-value = 0.6013), 21.4 (± 3.3) % after 48 hours (p-value = 0.6192) and by 27.3 (± 34.1) % after 72 hours (p-value = 0.3472) of exposure, when compared to the negative control. At a concentration of 0.075 nM, the AuNP 2 clusters where found to have induced a statistically negligible increase on the growth of *S. aureus* by 15.4 (± 6.6) % after 24 (p = 0.8749) hours, by 16.1 (± 7.7) % after 48 hours (p = 0.8522) and by 10 (± 38.3) % after 72 hours (p = 0.9824) of exposure. At 0.150 nM, the sAuNP clusters showed no statistically significant growth inhibiting activity on *S. aureus,* but were found to have induced a statistically insignificant increase in the growth of *S. aureus* by 21.6 (± 8.6) % after 24 hours (p = 6095), 21.4 (± 8.3) % after 48 hours (p = 0.6176) and by 1.7 (28.1) % after 72 hours (p > 0.9999). The results therefore, suggested that the concentrations of AuNP 2 clusters used in this study had no significant impact on the growth of *S. aureus* and could therefore mean that higher concentrations of AuNP 2 clusters were required to produce any statistically noteworthy growth inhibiting activity.

The sAuNP clusters also showed no statistically significant impact on the growth of *MRSA* at a concentration of 0.038 nM and where observed to have induced an increase in the growth of *MRSA* by 31.9 (± 14.1) % after 24 hours (p = 0.2268), by 30.8 (± 18.1) % after 48 hours (p = 0.2582) and by 18.7 (± 33.6) % after 72 hours (p = 0.7720) of exposure. At 0.075 nM, AuNP 2 clusters were also found to lack any statistically significant activity on the growth of *MRSA* and were observed to have induced a statistically negligible increase in the growth of *MRSA* by 11.2 (± 4.6) % after 24 hours (p-value = 0.9748), by 28.4 (± 13.8) % after 48 hours (p-value = 0.3405) and by 21.8 (± 39.0) % after 72 hours (p-value = 0.6326) of incubation at 37 °C, when compared to the untreated sample. The sAuNP clusters also showed a lack of statistically significant inhibition activity against the growth of *MRSA* at a concentration of 0.150 nM and were found to have induced a statistically negligible increase in the growth of *MRSA* by 22.4 (± 15.2) % after 24 hours (p-value = 0.6059), by 13.1 (± 14.6) % after 48 hours (p-value

= 0.5137) and by 27.1 (± 10.9) % after 72 hours (p-value = 0.3934) of incubation, when compared to the negative control.

5.5.2.3. The efficacy of AuNP 3 against *E. coli, S. aureus* and *MRSA*

E.coli, S. aureus and *MRSA* were all exposed to 0.038 nM, 0.075 nM and 0.150 nM of AuNP 3 clusters for an incubation period of 72 hours as illustrated on **Figure 5.9**. At a concentration of 0.038 nM, the NP clusters showed no statistically significant activity on the growth of *E. coli* and were found to have induced an increase in the growth of *E. coli* by 47.3 (±58.9) % after 24 hours (p-value = 0.1950), by 22.8 (± 6.4) % after 48 hours (p-value = 0.8764) and by 7.1 (± 14.1) % after 72 hours (p-value = 0.9998) of exposure, when compared to the negative control. At 0.075 nM, the sAuNP clusters were still observed to exert statistically negligible activity on the growth of *E. coli* and were observed to have induced an increase in the growth of *E. coli* by 39.0 (± 48.2) % after 24 hours (p-value = 0.3872), by 12.4 (± 15.1) % after 48 hours (p-value = 0.9933) and by 10.4 (± 10.3) % after 72 hours (p-value = 0.9974) of incubation at 37°C.

At a concentration of 0.150 nM, the NP clusters were also observed to lack any statistically significant activity on the growth of *E. coli* after the 72 hour incubation period and were found to have induced a reduction in the growth of *E. coli* by 19.3 (± 19.0) % after 24 hours (p-value = 0.9388), and by 32.7 (± 9.3) % after 48 hours (p-value = 0.5867) of incubation. The NP clusters were then observed to have induced an increase in the growth of *E. coli* by 32.3 (± 36.0) % after 72 hours (p-value = 0.5999) of incubation, when compared to the negative control.

AuNP 3 clusters were found to lack statistically significant activity against the growth of *S. aureus* at a concentration of 0.038 nM and were observed to have induced an increase in the growth of *S. aureus* by 24.7 (± 4.6) % after 24 hours (p = 0.0938), by 11.7 (± 2.0) % after 48 hours (p = 0. 7992) and by 13.8 (± 28.9) % after 72 hours (p = 0.6569) of exposure when compared to the negative control. At a concentration of 0.075 nM, the NP clusters were also observed to lack statistically significant activity on the growth of *S. aureus* and were observed to have induced an increase in the growth of *S. aureus* by 15.9 (± 8.0) % after 24 hours (p-value = 0.4997), by 4.3 (± 8.0) % after 48 hours (p-value = 0.9983) and by 13.8 (± 15.9) % after 72 hours (p-value = 0.8562) of incubation, when compared to the untreated sample.

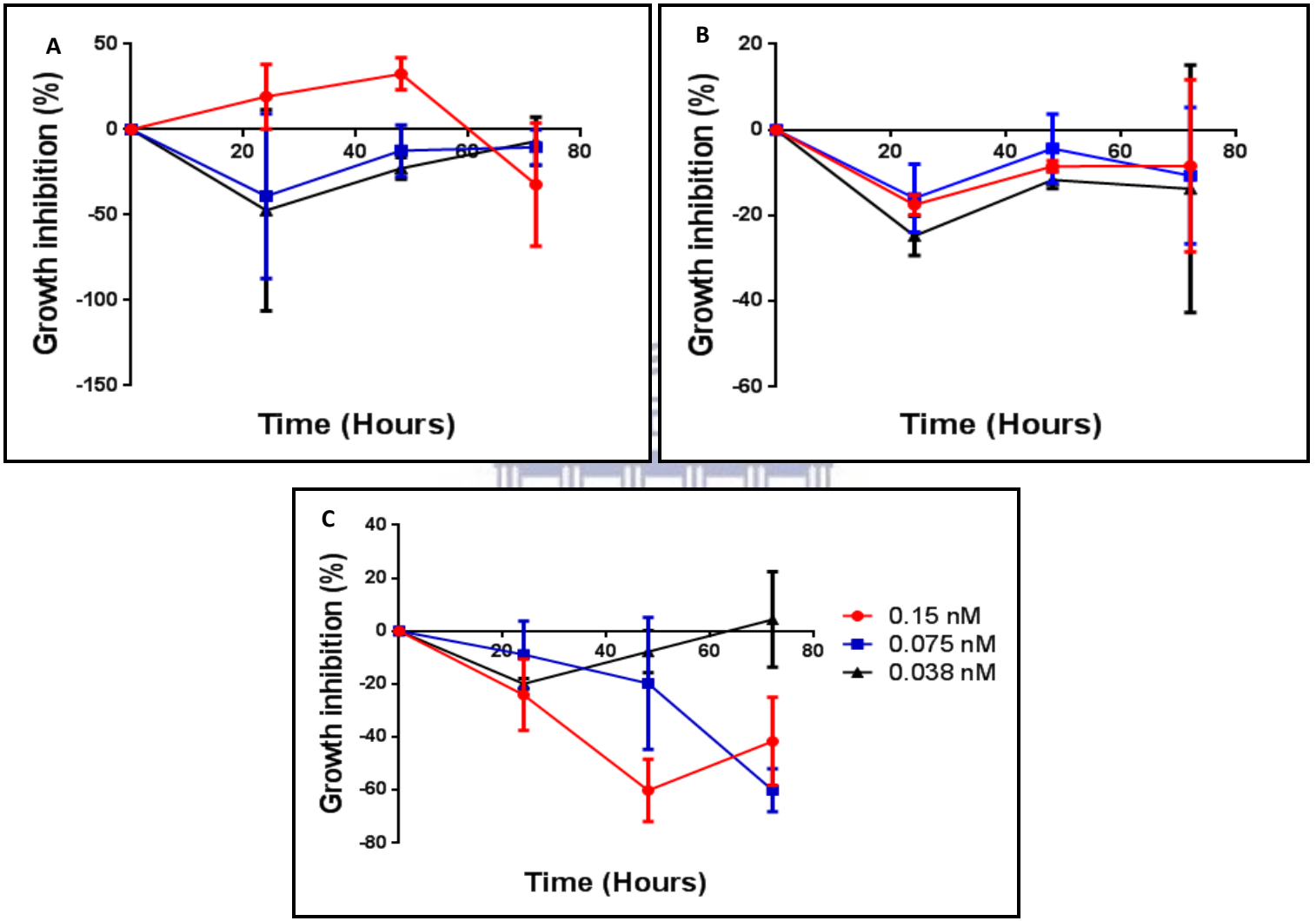

Figure 5.9: The percentage growth inhibition of (a) *E.coli*, (b) *S. aureus* and (c) *MRSA* treated with different concentrations of AuNP 3 for 72 hours. Data is expressed in mean ± SD (n = 3).

At a concentration of 0.150 nM, the sAuNP clusters also showed no statistically significant activity on the growth of *S. aureus* after the 72 hour incubation period and were found to have induced an increase in the growth of *S. aureus* by 17.5 (± 2.3) % after 24 hours (p-value = 0.3936), by 8.5 (± 1.3) % after 48 hours (p-value = 0.9450) and by 8.4 (± 20.1) % after 72 hours (p-value = 0.9479) of exposure, when compared to the negative control. The results thus indicated that AuNP 3 clusters had negligible impact on the growth of *S. aureus* at a concentration of 0.038 nM, 0.075 nM and 0.150 nM.

When exposed to *MRSA* at a concentration of 0.038 nM, AuNP 3 clusters were observed to lack statistically significant activity on the growth of *MRSA* but were found to have induced an increase in the growth of *MRSA* by 19.9 (± 2.0) % after 24 hours (p-value = 0.3111), by 7.7 (± 7.9) % after 48 hours (p-value = 0.9726) and by 4.4 (± 18.0) % after 72 hours (p-value = 0.9986) of exposure. At 0.075 nM, the sAuNP clusters were also observed to lack statistically significant activity on the growth of *MRSA* after 24 hours (p-value = 0.9485) and 48 hours (p-value = 0.3200). The NP clusters were observed to have induced an increase in the growth of *MRSA* by 8.8 (± 12.7) % and by 19.7 (± 24.9) %, respectively. However, the NP clusters were found to have induced a statistically significant increase on the growth of *MRSA* by 60.0 (± 8.1) % after 72 hours (p-value <0.0001) of exposure.

At a concentration of 0.150 nM, the NP clusters were found to have no significant impact on the growth of *MRSA* and were observed to have induced an increase in the growth of *MRSA* by 24.1 (± 13.4) % after 24 hours (p-value = 0.1426) of exposure. However, the NPs were observed to have significantly induced an increase in the growth of *MRSA* by 60.1 (± 8.13) % after 48 hours (p-value < 0.0001) of exposure, this induced increase was found to have decreased to 41.6 (± 16.6) % after 72 hours (p-value = 0.0023) of exposure, when compared to the negative control. This sudden decrease in the growth percentage of *MRSA* after 72 hours of incubation was predicted to have been due to the depletion of nutrients in the LB media. Overall, the results suggested that AuNP 3 clusters had statistically negligible growth inhibition activity on *MRSA* at 0.038 nM, but showed statistically significant time-dependent growth inducing activity at 0.150 nM, and 0.075 nM.

In summary, clusters of AuNP 1, AuNP 2 and AuNP 3 were observed to be more effective at inhibiting the growth of *E. coli* when compared to *S. aureus* and *MRSA*, thus, indicating that the sAuNP clusters had more growth inhibiting activity against gram negative bacteria when compared to gram positive bacteria. A possible explanation to why the sAuNP clusters were more effective against the Gram negative bacteria as compared to the Gram-positive bacteria could be due to the differences in the cell wall structure of Gram-positive bacteria and Gram-negative bacteria. The cell wall of Gram-positive bacteria contains a thick layer (approximately 20–50 nm in width) of peptidoglycan (PG), which is attached to teichoic acids that are unique to the wall of Gram-positive bacteria (Scott and Barnett, 2006). On the other hand, the cell walls of Gram-negative bacteria are more complex, both structurally and chemically. These cell walls consist of of a thin PG layer and contain an outer membrane, which covers the surface membrane (Hajipour *et al.,* 2012).

Therefore, a possible explanation to why the Gram-negative bacteria was observed to be more susceptible to the NPs could be in-part due to the thickness of the PG layer, which is 50% higher in Gram-positive when compared to Gram-negative bacteria (Umadevi *et al.,* 2011). Therefore, larger doses of the sAuNP clusters might be required for the Gram-positive bacteria, or more exposure time might be required for the NPs to pass through the thick PG layer of the Gram-positive bacteria. AuNP 1 clusters were observed to be more efficient at inhibiting the growth of *E. coli* when compared to clusters of AuNP 2 and AuNP 3, and the antibiotic activity of AuNP 1 clusters was observed to be both concentration-and time-dependent with an MIC of 0.150 nM against *E .coli* that was only effective after 72 hours of exposure. The results therefore aligned and further substantiated previously published results where the *in vitro* mechanisms of two different sizes of sAuNPs were demonstrated using the turbidity of the nutrient broth and by taking optical density (OD) values from the spectrophotometer with a 600 nm filter. The study found that G1 AuNPs, which had a smaller size (6–34 nm), reduced the growth of *S. aureus* from 75.19% to22.4%, whereas the growth of *E. coli* was reduced from 74.3% to 6.2%. Thus, for complete inhibition of *S. aureus*, a larger dose was required.

On the other hand, the reduction in growth by G2 AuNPs (20-40 nm) on *S. aureus* was up to 23.7% whereas *E. coli* was reduced up to 6.2 % therefore concluding that the sAuNPs had more antibacterial activity against Gram-negative bacteria (Shamaila *et al.,* 2016). Upon aggregation, NP transport dynamics, such as diffusion and sedimentation, have been reported to become distorted compared to those of stable, dispersed NPs.Therefore, aggregation results in a larger hydrodynamic radius, and the aggregates typically become susceptible to sedimentation, whereas single small NPs characteristically only display Brownian motion (Moore *et al.,* 2015). Though displaying a larger hydrodynamic radius, NP aggregates do not behave the same as large single dispersed particles. Aggregation has been reported to interfere with the cytotoxicity of NPs as the surface area of the NP aggregates radically changes compared to monodispersed NPs, which may greatly alter the interaction between NP aggregates and cells. In the absence of external forces, the NP aggregates have a random assortment and exhibit an arbitrary shape and an amorphous structure (Moore *et al.,* 2015). Therefore, the role of particle size on the growth inhibiting activity of the NPs could not be well investigated as the sAuNPs were found to unstable and were thus prone to severe aggregation when mixed with LB media.

In addition, the low concentrations (0.075 nm and 0.075 nm) of the AuNPs resulted in enhanced bacterial proliferation. A possible explaination for the enhanced bacterial proliferation could be “Stress-Proliferation”, as bacteria have been found to modulate their own growth and proliferation to increase their chances of survival under stressful conditions, such as antibiotic treatment (Heinrich *et al.,* 2015). The results in this study were therefore parallel to the results obtained in a previous study, where it was also found that AuNPs stabilized with a weakly bound negatively charged capping agent (citrate) tend to aggregate more when compared to those with a strongly bound capping agent (poly(allylamine)hydrochloride). The increased aggregation also resulted in reduced surface area which reduced the interactions between the NPs and the bacteria, thus reducing the bacterial growth inhibitory interactions (Zhou *et al*., 2013).

Chapter 6: Conclusion

The objectives of this study were to synthesize sAuNPs of three different sizes (i.e. AuNP1, AuNP 2 and AuNP 3), characterize the physicochemical properties of the three AuNPs, and to investigate the growth inhibition efficiency of the AuNPs on the growth of *E. coli, S. aureus* and *MRSA*. It was hypothesized that sAuNPs synthesized using the citrate reduction method would show size- and concentration-dependentgrowth inhibiting activity against bacteria. The three AuNP samples were successfully synthesized using the Turkevich/citrate reduction method, washed and later suspended in dH_20. Each of the synthesized AuNPs showed a single λ_{max} absorbance peak near 520 nm, which is distinctive for spherical AuNPs; the morphology was later confirmed using HR-TEM. The average core diameters of AuNP 1, AuNP 2 and AuNP 3 were measured and found to be 14.0 ± 2 nm, 28.2 ± 4 nm and 54.6 ± 7 nm with zeta potentials of -27.0 ± 6.28 mV, -32.7 ± 1.60 mV and -30.7 ± 2.1 mV, respectively.

The study found that the z-average size can only be considered an accurate measure of the hydrodynamic size if the NP sample under investigation is monomodal and monodispersed as previously stated (Lim *et al.,* 2013). Therefore the correlation between the absorption maxima and size of AuNPs can only be considered when working with monomodal AuNPs. The stability of the AuNPs in dH_2O and in LB was also investigated over a period of 72 hours at a temperature of 4 and 37 ° C; the results suggested that the AuNPs formed clusters in LB media over time. Therefore, indicating that the AuNPs were unstable in LB at both 4 and 37 ° C, respectively. In conclusion, the synthesized AuNPs showed an acceptable amount of uniformity, fair stability in dH_20, and all the three AuNP samples showed a reasonably spherical morphology in dH_2O. However, the AuNPs showed poor stability in LB as indicated by dark blue colour change (due to aggregation of GNPs) and increase in zeta potential over time.

The quenching efficacies of the AuNP clusters on fluorescence of Alamar blue were successfully examined and the quenching of the NP clusters were found to be concentration dependent, but no relationship between NP size and quenching efficacy were observed. A possible reason for this was suggested to be the aggregation of the NPs in LB media, which could have nullified the effect of size on the quenching of fluorescence by the AuNPs as the NPs formed clusters.

On the other hand, clusters of sAuNPs with core-diameter of 54.6 ± 7.2 nm were observed to have exhibited growth inhibiting activity against *E. coli*, and growth inhibition potential against *S. aureus* and *MRSA* when compared to clusters of sAuNPs with core-diameters of 28.2 ± 3.9 nm and 14.0 ± 1.7 nm. Therefore the NPs were observed to be more effective against Gram-negative bacteria than Gram-positive. The mechanism of the growth inhibition activity was found to be size-and dose-dependent. Therefore, the antibacterial mechanism of the AuNPs against the three pathogenic bacteria demonstrated that sAuNPs have a potential to be the next therapy against Gram-negative bacteria. In conclusion, the results were partially aligned with the hypothesis. As the growth inhibiting activity of the NPs was found to be potentially dependent on both concentration and on exposure time. However, the role of size on the growth inhibiting activity of the AuNPs against *E. coli, S. aureus* and *MRSA* were hindered by the inability of the NPs to maintain discrete NP sizes in LB media. In addition, the three bacterial showed enhanced proliferation as a survival strategy to overcome the antibiotic stressful conditions caused by the low concentrations of the AuNPs.

Future objectives of this study would be to stabilize and therefore prevent the aggregation of the sAuNPs, to examine the influence of size on the uptake of the sAuNPs by *E. coli, S. aureus* and *MRSA* and to investigate the role that sAuNP uptake plays in the time- and dose-dependent antibacterial activity of the NPs. In addition, nanotoxicity is generally regarded and has been found to be triggered by the induction of oxidative stress by free radical formation in biological systems including bacteria (Hajipour *et al.,* 2012). Therefore, it is also essential to examine the role of ROS production in the growth inhibition activity of the sAuNP against *E. coli, S. aureus* and *MRSA*.

Chapter 7: References

Aam B B and Fonnum F (2007). 'Carbon black particles increase reactive oxygen species formation in rat alveolar macrophages *in vitro*'. *Archives of Toxicology*, vol. 81:p. 441–446.

Acar J F, Moulin G, Page S W, and Pastoret P P (2012). 'Antimicrobial resistance in animaland public health: introduction and classification of antimicrobial agents'. *Revue scientifique et technique (International Office of Epizootics),* vol. 31: no. 1, p. 15-21.

Agnihotri S M, Ohshima H, Terada H, Tomoda K and Makino K (2009).'Electrophoretic Mobility of Colloidal Gold Particles in Electrolyte Solutions'. *Langmuir*, vol. 25: no. 8, p 4804–4807.

Ahmad S and Mokaddas E (2010). 'Recent advances in the diagnosis and treatment of multidrug-resistant tuberculosis'. *Respiratory Medicine CME,* vol. 3: p. 51-61.

Ali D M, Thajuddin, N, Jeganathan K, and Gunasekaran M (2011). 'Plant extract mediated synthesis of silver and gold nanoparticles and itsantibacterial activity against clinically isolated pathogens'. *Colloids and Surfaces B: Biointerfaces,* vol. 85: p.360–365.

Al-Bakri A G, and Afifi F U (2007). 'Evaluation of antimicrobial activity of selected plant extracts by rapid XTT colorimetry and bacterial enumeration'. *Journal of Microbiology: Methods,* vol. 68: p.19–25.

Andersen P, Askgaard D, Ljungqvist L, and Bennedsen J, Heron I (1991). 'Proteins released from *Mycobacterium tuberculosis* during growth'. *Infection Immunity,* vol. 59: p. 1905-1910.

Ashida H, Mimuro H, Ogawa M, Kobayashi T, Sanada T, Kim M, and Sasakawa C (2011). 'Cell death and infection: A double-edged sword forhost and pathogen survival'. *Journal of Cell Biology,* vol. 195: no. 6, p. 931-942.

Asuri P, Bale S S, Karajanagi K S, and Kane RS (2006). 'The protein–nanomaterial interface'. *Current Opinion in Biotechnology,* vol. 17: p. 562–568.

Azam A, Ahmed F, Arshi N, Chaman M, and Naqvi A H (2009). 'One step synthesis and characterization of gold nanoparticles and their antibacterial activities against *E. coli'*. *International Journal of Theoretical and Applied Science,* vol.1: p. 1–4.

Baek, Y W and An, Y J (2011). 'Microbial toxicity of metal oxide nanoparticles (CuO, NiO, ZnO, and Sb_2O_3) to *Escherichia coli, Bacillus subtilis, and Streptococcus aureus'*. *Science of the* Total Environment, vol. 409: p. 1603–1608.

Baoum A, Dhillon N, Buch S, and Berkland C (2010). 'Cationic surface modification of PLG nanoparticles offers sustained gene delivery to pulmonary epithelial cells'*. Journal of Pharmaceutical Science,* vol. 99: p. 2413–2422.

Balouiri M, Sadiki M and Ibnsouda S K (2015). 'Methods for in vitro evaluating antimicrobial activity: A review'. *Journal of Pharmaceutical Analysis,* vol. 6: p. 71–79.

Barger A, Fuhst C and Wiedemann B (2003).' Pharmacological indices in antibiotic therapy'. *Journal of Antimicrobial Chemotherapy,* vol. 52: p. 893–898.

Baudot C, Tan CM, and Kong JC (2010). 'FTIR spectroscopy as a tool for nano-material characterization'. *Infrared Physical Technology*, vol. 53, p. 434–438.

Bbosa G S, Mwebasa N, Odda J, Kyegombe D B, and Ntale M (2014). 'Antibiotics/antibacterial drug use, their marketing and promotion during the post-antibiotic golden age and their role in emergence of bacterial resistance'. *Health,* vol. 6: no.5, p. 410-425.

Berciano-Guerrero M A, Montesa-Pino A, Castaneda-Penalvo G and Flores J R (2014) Nanoparticles in Melanoma. Viewed on 8 August 2017, from https://www.researchgate.net/publication/264093769_Nanoparticles_in_Melanoma

Beyth N, Houri-Haddad Y, Domb A, Khan W, and Hazan R (2015), 'Alternative antimicrobial approaches: Nano-Antimicrobial materials. Viewed on June 2017, from http://dx.doi.org/10.1155/2015/246012

Biju V, Itoh T, and Ishikawa M (2010). 'Delivering quantum dots to cells: bioconjugated quantum dots for targeted and nonspecific extracellular and intracellular imaging'. *Chemistry Society Review,* vol. 39: p. 3031–3056.

Bonnell D (2001). 'Scanning probe-microscopy and spectroscopy: theory, techniques, and applications'. *Wiley-vch*. Vol. 1: p. 1-110.

Boukari H and Sackett DL (2008). 'Fluorescence correlation spectroscopy and it's application to the characterization of molecular properties and interactions'. *Methods for Cell Biology,* vol. 84: p. 659–678.

Brand R (2008). 'Marketing drugs: Debating the real cost: Concern about close ties between doctors and pharmaceutical firms are prompting new financial disclosure laws and education efforts'. *State Legis*, vol. 34: p. 26-29.

Briscoe C J and Hage D S (2009). 'Factors affecting the stability of drugs and drug metabolites in biological matrices'. *Bioanalysis.*, vol. 1: p. 205–220.

Buzea C, Pacheco I, Robbie K. Nanomaterials and nanoparticles (2007). 'Sources and toxicity'. *Biointerphases*, vol. 2: p. 17–71.

Cegedim (2013) U.S. Pharmaceutical Company Promotion Spending. Viewed on 10 January 2017, from http://www.skainfo.com/health_care_market_reports/2012_promotional_spending.pdf.

Chapman HN, Fromme P, Barty A, White TA, Kirian RA, and Aquila A, (2011). 'Femtosecond X-ray protein nanocrystallography'. *Nature,* vol. 470: p. 73–77.

Chen Y S, Hung Y C, Liau I and Huang G S (2009). 'Assessment of the *in vivo* toxicity of gold nanoparticles'. *Nanoscale Research Letters,* vol. 4: no. 8, p. 858-864.

Chow M K and Zukoski C F (1994). Gold solution formation mechanisms- role for colloidal stability. *Journal of Colloid Interface Science*, vol. 165: no. 97, p.1-99.

Crist RM, Grossman JH, Patri AK, Stern ST, Dobrovolskaia MA, and Adiseshaiah PP (2013). 'Commonpitfalls in nanotechnology: lessons learned from NCI's nanotechnology characterizationlaboratory'. *Integrative Biology,* vol. 5: p. 66–73.

Das M, Hwan Shim K, Seong S A. An1 Y and Dong Kee Y (2011). 'Review on Gold Nanoparticles and Their Applications'. *Toxicology and Environmental Health Sciences,* vol. 3: no. 4, p. 193-205.

Davis R R, Lockwood P E, Hobbs D T, Messer R L, Price R J, and Lewis J B (2007). '*In vitro* biological effects of sodium titanate materials'. *Journal of Biomedical Materials Research part B*, vol. 83: p.505–511.

De Clercq E (2004). 'Antivirals and Antiviral Strategies'. *Nature Reviews Microbiology,* vol. 1, p. 13–25.

Decuzzi P, Pasqualini R, Arap W, Ferrari M (2009). 'Intravascular delivery of particulate systems: doesgeometry really matter?'. *Pharmaceutical Research,* vol. 26, p. 235–243.

Devi L S and Joshi S R (2012). 'Antimicrobial and synergistic effectsof silver nanoparticles synthesized using: Soil fungi of high altitudes of Eastern Himalaya'. *Micobiology,* vol. 40:p. 27–34.

Diaz B, Sanchez-Espinel C, Arruebo M, Faro J, Miguel E D, Magadan S, Yague C, Fernandez-Pucheco R, Ibarra MR, Santamaria J, and Gonzalez-fernandez A (2008). 'Assessing methods for blood cell cytotoxic response to inorganic nanoparticles and nanoparticles aggregates'. *Small Journal,* vol. 10: no. 10, p. 1-10.

Dube A and Ebrahim N (2017) The nanomedicine landscape of South Africa. Viewed on 8August 2017, fromhttps://www.degruyter.com/view/j/ntrev.ahead-of-print/ntrev-2016-0108/ntrev-2016-0108.xml?format=INT

Dykman L and Khlebtsov N (2012). 'Gold nanoparticles in biomedical applications: recent advances and perspectives'. *Chemical Society Rev*iews, vol. 41: p. 2256-2282.

Encyclopædia-Britannica (2013) Antibiotic resistance: Mechanismsof antibiotic resistance. Encyclopædia Britannica Online. http://www.britannica.com/EBchecked/media/129670/There-are-multiple-mechanisms-by-which-bacteria-can-develop-resistance.

Escalante P (2 June 2009). "In the clinic. Tuberculosis". *Annals of internal medicine,* vol. 150: no. 11, p. 61–614.

Fei L and Perrett S (2009). 'Effect of nanoparticles on protein folding andfibrillogenesis'. *International Journal of Molecular Sciences,* vol.10: p. 646–655.

Ferrari M (2008). 'Nanogeometry: beyond drug delivery'*. Nature Nanotechnology,*vol. 3: p. 131–132.

Ferreira J C and Patino C M (2015). 'What does the p value really mean?'. *Brazilian Journal of Pulmonology,* vol. 41: no. 5, p. 485-485.

Feynman R.P. (February 1960). There's Plenty of Room atthe Bottom. *Engineering and Science magazine*, vol. 23: no. 5.

Free billion investment guide (2017) Understanding gold nanoparticles cancer research. Viewed on 5 july 2017, from http://www.free-billion-investment-guide.com/cure-for-cancer.html

Furuya E Y and Lowy F (2006). 'Antimicrobial-resistantbacteria in the community setting'.*Nature Reviews Microbiology*, vol. 4: p. 36-45.

Gao X F, Yang Z W, and Li J (2011). 'Adjunctive therapy with interferon-gamma for the treatment of pulmonary tuberculosis: a systematic review'. *International Journal of Infectious Diseases,* vol. 15: p. 594–600.

Garry G, Graham G, Champion D, and Ziegler J (1994). 'The cellular metabolism andeffects of gold complexes, Metal', *Based Drugs*, vol. 1: p. 395–404.

George S, Lin S, Ji Z, Thomas CR, Li L, and Mecklenburg M (2012). 'Surface defects on plate-shaped silvernanoparticles contribute to its hazard potential in a fish gill cell line and zebrafish embryos'. *American Chemical Society: Nano*technology, vol. 6: p. 3745–3759.

Giasuddin A S M, Jhuma K A, and Haq A M M (2012). 'Use of Gold Nanoparticles in Diagnostics, Surgery and Medicine: A Review'. *Bangladesh Journal of Medical Biochemistry*. vol.5: p. 56–60.

Giersig M and Mulvaney P (1993). 'Preparation of ordered monolayers by electrophoretic deposition'. *Langmuir,* vol. 9: p. 3408-3413.

Grillo B L (2014) Synthesisand Alignment of gold nanorodsfor optical applications. Viewed on 5 November 2016, from https://www.ideals.illinois.edu/bitstream/handle/2142/49460/Bethany_Grillo.pdf?sequence=1.

Guerrero-Martinez A, Barbosa S, Pastoriza-Santos I, Liz-Marzan L M, and Curr O P. (2011). 'Colloid Interface'. *Science*, vol.16: p. 118–127.

Haiss W, Thanh N T K, Aveyard J, and Fernig D G (2007). 'Determination of Size and Concentration of Gold Nanoparticles from UV-Vis Spectra'. *Analytical Chemistry*, vol. 79: no. 11, p. 4215-4221.

Hajipour M J, Fromm K M, Ashkrran A A, De Aberasturi D J, De Larramendi I R, Rojo T, Serpooshan V, Parak W J, and Mahmoudi M (2012). 'Antibacterial properties of nanoparticles', *Trends in Biotechnology,* p. 1-13.

Han X, Gelein R, Corson N, Wade-Mercer P and Jiang J (2011). 'Validation of an LDH assay for assessing nanoparticle toxicity'. *Toxicology,* vol. 287: p. 99–104.

Hardman R A (2006). 'Toxicologic review of quantum dots: toxicity depends on physicochemical and environmental factors'. *Environmental Health Perspec*tive, vol. 114: p. 165–172.

Hedderman TG, Keogh SM, Chambers G, and Byrne HJ (2004). 'Solubilization of SWNTs with organic dye molecules'. *Journal of Physics and Chemtry,* vol. 108: p. 18860–18865.

Heinrich K, Leslie D J and Jonas K (2015). 'Modulation of bacterial proliferation as a survival strategy'. *Advances in Applied Microbiology*, vol. 92: p. 127-171.

Holder A L, Goth-Goldstein R, Lucas D, Koshland C P (2012). 'Particle-induced artifacts in the MTT and LDH viability assays'. *Chemical Research in Toxicology*, vol. 25: p. 1885–1892.

Horváth L, Magrez A, Burghard M, Kern K, Forró L, and Schwaller B (2013). 'Evaluation of the toxicity of graphene derivatives on cells of the lung luminal surface'. *Carbon*, vol. 64: p. 45–60.

Huang X, Jain K, El-Sayed I and El-sayed M (2007). 'Gold nanoparticles: interesting optical properties and recent applications in cancer diagnostics and therapy'. *Nanomedicine*, vol. 2: no. 5, p. 681-693.

Huang X and El–Sayed M. A. (2010). 'Gold Nanoparticles: Optical Properties and Implementations in Cancer Diagnosis and Photothermal Therapy'. *Journal of Advanced Res*earch, vol. 1:no. 1, p. 13–28.

Huang J, Lima E, Akita T, Guzmán A, Qi C, Takei T, and Haruta M (2011). 'Propene epoxidation with O_2 and H_2: Identification of the most active goldclusters', *Journal of Catalysis*, vol. 278: p. 8–15.

Huang X, Jain K, El-Sayed I and El-sayed M (2007). 'Gold nanoparticles: interesting optical properties and recent applications in cancer diagnostics and therapy'. *Nanomedicine*, vol. 2: no.5, p. 681-693.

Huh A J and Kwon Y J (2011). 'Nanoantibiotics: a new paradigm for treating infectious diseases using nanomaterials in the antibiotics resistant era'. *Journal of Controlled Release,* vol.156: p. 128–145.

Jain, S, Hirst D G, O'Sullivan J M (2012). 'Gold nanoparticles as novel agents for cancer therapy'.*The British Journal of Radiology,* vol. 85: p. 101–113.

Jingyue Z, Bernd F (2015). 'Synthesis of gold nanoparticles via chemical reduction methods'. *IME Institute of Process Metallurgy and Metal Recycling, RWTH Aachen University, Aachen, Germany,* vol.1: p. 1-7.

Johal M S. Understanding nanomaterials. Boca Raton: CRC Press; 2011.

Jorgensen J H and FerraroM J (2009). 'Antimicrobial susceptibility testing: are view of general principles and contemporary practices'. *Clininical Infectious Dis*eases, vol. 49: p.1749–1755.

Kane R S and Stroock AD (2007). 'Nanobiotechnology: Protein-nanomaterial interactions'. *Biotechnology Progress,* vol. 23: p. 316–319.

Khan A K, Rashid R, Murtaza G and Zahra A (2014). 'Gold Nanoparticles: Synthesis and Applications in Drug Delivery'. *Tropical Journal of Pharmaceutical Research*, vol. 13: no. 7, p. 1169-1177.

Khlebtsov N G and Dykman LA. (2010). 'Optical properties and biomedical applications of plasmonic nanoparticles'. *Journal of Quantitative Spectroscopy and Radiation Transfusion*. vol. 111: p. 1-35.

Kim F, Song J H, and Yang P (2002). 'Photochemical Synthesis of Gold Nanorods'. *Journal of American Chemical Society,* vol. 124: p. 14316-14317.

Kim T (2008). 'Kinetics of Gold Nanoparticle Aggregation: Experiments and Modeling'. *Journal of Colloid Interface Sci*ence, vol. 318: no. 2, p. 238–243p.

Kim TH, Kim M, Park HS, Shin US, Gong MS, and Kim HW (2012). 'Size-dependent cellular toxicity of silver nanoparticles'. *Journal of Biomedical Materials Research part A.,* vol. 100: p. 1033–1043.

Konaté K, Mavoungou J F, and Lepengué A N (2012). 'Antibacterialactivityagainst β-lactamase producingMethicillinandAmpicillin-resistants Staphylococcus aureus: Fractional Inhibitory Concentration Index (FICI) determination', *Annals of Clinical Microbiology and Antimicrobials,* vol. 11: p.1-18.

Kong B, Seog J H, Graham L M, and Lee S B (2011). 'Experimental considerations on the cytotoxicity of nanoparticles'. *Nanomedicine (Lond),* vol. 6: no. 5, p. 929–941.

Konstantinos A (2010). 'Testing for tuberculosis'. *Australian Prescriber*, vol. 33: no.1, p. 12–18.

Kowalczyk B, Lagzi I, and Grzybowski B A (2011). 'Nanoseparations: Strategies for size and/or shape-selective purification of nanoparticles'. *Current Opinion in Colloid & Interface Science*. Vol. 16: p. 135–148.

Kuhn D M, Balkis M, and Chandra J (2003). 'Uses and limitations of the XTT assay in studies of Candida growth and metabolism', *Journal of Clinical Microbiol*ogy, vol. 41: p. 506–508.

Kulchavenya E (2009). 'Tuberculosis of urogenital system in Urology: National Manual. Lopatkin N (Ed) Geotar-Media'. *Moscow,* vol.1: p. 584-601.

Kulchavenya E, Filimonov P, and Shvetsova O (2007). 'An Atlas of a Urogenital tuberculosis and other extrapulmonary localizations (monograph)'. *Novosibirsk, Tirazh-Sibir*, vol.1: p.1-12.

Kumar C S (2012). 'Raman spectroscopy for nanomaterials characterization'. *Springer Verlag*, vol.1: p.1-14.

Kroll A, Pillukat M H, Hahn D, and Schnekenburger J (2012). 'Interference of engineered nanoparticles with in vitro toxicity assays'. *Archives of Toxicology,* vol. 86: p. 1123–1136.

Lancellotti M, Brocchi M, and da Silveira W D (2006). 'Bacteria-Induced apoptosis: An approach to bacterial pathogenesis'. *Brazilan Journal of Morphological Science,* vol. 23: no. 1, p. 75-86.

Lata K, Jaiswal A K, Naik L and Sharma R (2014). 'Gold Nanoparticles: Preparation, Characterization and Its Stability in Buffer'. *Nano Trends: A Journal of Nanotechnology and Its Applications,* vol. 17: no. 1, p. 1-10.

Lawn S D and Zumla A I (2011). 'Tuberculosis'. *Lancet*, vol. 378: no. 9785, p. 57–72.

Leid J G, Ditto A J, Knapp A, Shah P N, Wright B D, Blust R, Christensen L, Clemons C B, Wilber J P, Kang G W Y A G, PanznerM J, Cannon C L, Yun Y H, Youngs WJ, Seckinger N M, and Cope E K (2012). '*In vitro* antimicrobial studies of silver carbine complexes: activity of free and nanoparticle carbene formulations against clinical isolates of pathogenic bacteria'. *Journal of Antimicrobial Chemotheraphy*, vol. 67: p. 138–148.

Levy S B & Marshall B (2004). 'Antibacterial resistance worldwide: causes, challenges and responses'. *Nature*, vol 10: no. 12, p. S122-S129.

Li Y, Ma J and Ma Z (2013). 'Synthesis of gold nanostars with tunable morphology and their electrochemical application for hydrogen peroxide sensing'. *Electrochemical Activation,* vol. 108: p. 435– 440.

Li Z, Huang H, Tang S, Li Y, Yu X, Wang H, Li P, Sun Z, Zhang H, Liu C and Chu P (2015). 'Small gold nanorods laden macrophages for enhanced tumor coverage in photothermal therapy'. *Biomaterials,* vol. 74: p. 144-154.

Lin C, Tao K, Hua D, Ma Z, and Zhou S (2013). 'Size Effect of Gold Nanoparticles in Catalytic Reduction of p-Nitrophenol with NaBH4'. *Molecules*, vol. 18: p. 12609–12620.

Liang H, Xing Y, and Chen J (2012). 'Antimicrobialactivitiesofendophyticfungi isolated from Ophiopogon japonicus (Liliaceae)', *BMC Complementary and Alternative Medicine,* vol. 12: p. 1-238.

Lim J, Yeap S P, Che H X, and Low S C (2013). 'Characterization of magnetic nanoparticle by dynamic light scattering'. *Nanoscale Research Letter,* vol. 8: p. 1-10.

Lin P, Lin S, Wang P C and Sridhar R (2014). 'Techniques for physicochemical characterization of nanomaterials'. *Biotechnology Advances.* Vol. 32: no. 4,p. 711–726.

Lin X M, Sorensen C M and Klabunde K J (2000). 'Digestive ripening, Nanophase segregation and superlattice formation in gold nanocrystal colloids'. *Journal of Nano Research,* vol. 2: p. 157-164.

Liu Z, Wu Y, Guo Z, Liu Y, Shen Y, Zhou P, and Lu X (2014), Effects of Internalized Gold Nanoparticles with Respect to Cytotoxicity and Invasion Activity in Lung Cancer Cells. Viewed on 5 november 2015, from http://journals.plos.org/plosone/article?id=10.1371/journal.pone.0099175.

Mac Cormack TJ, Clark RJ, Dang M K M, Ma G and Kelly J A (2012). 'Inhibition of enzyme activity by nanomaterials: Potential mechanisms and implications for nanotoxicity testing'. *Nanotoxicology*, vol. 6: p. 514–525.

Magnusson M H, Deppert K, Malm J O, Bovin J O and Samuelson L(1999).'Gold nanoparticles: Production, reshaping, andthermal charging'. *Journal of Nano Research,* vol. 1: p. 243-251.

Misbahi A (2010). 'A review on gold nanoparticles radiosensitization effect in radiation therapy of Cancer'. *Reports of Practical Oncology and Radiother*apy, vol. 15: p. 176–180.

Misawa M and Takahashi J (2011). 'Generation of reactive oxygen species induced by gold nanoparticles under x-ray and UV Irradiation'. *Nanotechnology, Biology, and Medicine*, vol. 7, p. 604-614.

Moore T. L,Rodriguez-Lorenzo L,Hirsch V,Balog S,Urban D,Jud C,Rothen-Rutishauser B,Lattuad M and Petri-Fink A (2015). 'Nanoparticle colloidal stability in cell culture media and impact on cellular interactions'. *Chemistry Society Reviews, vol.*44, p. 6287-6305.

Monteiro M C, dela Cruz M, and Cantizani J (2012). 'A new approach to drug discovery: high-through put screening of microbial natural extracts against *Aspergillus fumigatus*using resazurin', *Journal of Biomolecular Screening,* vol. 17: p. 524–529.

Murphy C J, Sau T K, Gole A M, Orendorff C J, Gao J, Gou L, Hunyadi S E and Li T (2005).'Anisotropic MetalNanoparticles: Synthesis, Assembly, and OpticalApplications. *Journal of Physical Chemistry B.,* vol. 109: p. 13857–13870.

Mie G (1976). 'Contribution to the optics of turbid media, especially colloidal metal suspensions'. *Annals of Phys*ics, vol. 25: p. 377-445.

Nanocomposix (2012). 'Zeta Potential Analysis of Nanoparticles'. *NanoComposix*, vol. 11: p. 1-6.

Nel AE, Madler L, Velegol D, Xia T, Hoek EM, and Somasundaran P (2009). Understandingbiophysicochemical interactions at the nano-bio interface. *Nature Materials,* vol. 8: p. 543–557.

Niidome Y, Nishioka K, Kawasaki H and Yamada S (2003). 'Rapid synthesis of gold nanorods by the combination of chemical reduction and photoradiation processes; morphological changes depending on the growing processes'. *Chemical Communications,* p. 2376-2377.

Nijs A, Cartuyvels R, and Mewis A (2003).'Comparison and evaluation of sirs and Sirscan 2000 antimicrobial susceptibility systems in the clinical micro-biology laboratory'. *Journal of Clinical Microbiology,* vol. 41: p.3627–3630.

O'Brien J, Wilson I, Orton T and Pognan F (2002).'Investigation of the Alamar Blue (resazurin) fluorescent dye for the assessment of mammalian cell cytotoxicity'. *European journal of Biochemistry,* vol. 267: p. 5421-5426.

Ong K J, MacCormack T J, Clark R J, Ede J D, Ortega V A, Felix L C, Dang M K M, Ma G, Fenniri H, Veinot J G C, and Goss G G (2014). 'Widespread Nanoparticle-Assay Interference: Implications for Nanotoxicity Testing. *PLoS ONE,* vol. 9: no.3, p. 1-9.

Pan Y, Neuss S, Leifert A, Fischler M, Wen F,Simon U,Schmid G, Brandau W, and Jahnen-Dechent W (2007). 'Size-Dependent Cytotoxicity of Gold Nanoparticles'.*Cytotoxicity of Gold Nanoparticles,* vol. 3: no. 11, p. 1941 – 1949.

Pandey S, Oza G, Gupta A and Sharon M (2012).'Novel Biological Approach for Biosynthesis of Anisotropic Gold Nanoparticles using *Aloe barbedensis*: Role of pH and temperature'. *Annals of Research.* vol. 3, no. 5, p. 2330-2336.

Papasani M R, Wang G and Hill R A (2012). 'Gold nanoparticles: the importance of physiological principles to devise strategies for targeted drug delivery'. *Nanomedicine: Nanotechnology, Biology, and Medicine* .vol. 8, p. 804-814.

Patri A, Dobrovolskaia M, Stern S, McNeil S and Amiji M (2006). 'Nanotechnology for cancer therapy'. *CRC Press,* p. 105-138.

Pelgrift R Y and Friedman A J (2013). 'Nanotechnology as a therapeutic tool to combat microbial resistance'*. Advanced Drug Delivery Review,* vol 65: p. 1803-1815.

Pfaller M A, Sheehan J D, and Rex J H (2004). 'Determinationoffungicidalactivities against yeasts and molds: lessons learned from bactericidal testing and the need for standardization'. *Clinical Microbiology Rev*iews, vol. 17: p. 268–280.

Plascencia-Villa G, Bahena D, Rodríguez A R, Ponce A, and José-Yacamán M (2013). 'Advanced microscopy of star-shaped gold nanoparticles and their adsorption-uptake by macrophages'. *Metallomics,* vol. 5: no. 3, p. 242–250.

Placido R, Mancino G, Amendola A, Mariani F, VendettiS, and Piacentini M (1997). 'Apoptosis of human monocytes/macrophages in *Mycobacterium tuberculosis* infection'. *Journal of Pathology, vol. 181*: p. 31-38.

Powers K W, Brown S C, Krishna V B, Wasdo S C, Moudgil BM, and Roberts S M (2006). 'Research strategies for safety evaluation of nanomaterials. Part VI. Characterization of nanoscale particles fortoxicological evaluation'.*Toxicology Sci*ence, vol. 90: p. 296–303.

Prichard R (1994). 'Anthelmintic resistance'.*Veterinary Parasitology*, vol. 54: Issue 1, P. 259-268.

Rajeshkumar S, Malarkodi C, Gnanajobitha G, Paulkumar K, Vanaja M, Kannan C and Annadurai G (2013). 'Seaweed-mediated synthesis of gold nanoparticles using *Turbinaria conoides* and its characterization'. *Journal of Nanostructure in Chemistry,* vol. 3, p. 1-44.

Rao C N R and Biswas K (2009). 'Characterization of nanomaterials by physical methods'. *Annual Review of Analalytical Chemistry,* p. 435–462.

Ramakrishna G and Ghosh HN (2001). 'Emission from the charge transfer state ofxanthene dye-sensitized TiO2 nanoparticles: A new approach to determiningback electron transfer rate and verifying the marcus inverted regime'. *Journal of Physics and Chemistry,* vol. 105: p. 7000–7008.

Rau R (2005). 'Have traditional DMARDs had their day? Effectiveness of parenteral gold compared to biologicagents'. *Clinical Rheumatology,* vol. 24: p. 189-202.

Roberts I S (1996). 'The biochemistry and genetics of capsular polysaccharide production in bacteria'. *Annual Review of Microbiology*. vol. 50: p. 285–315.

Ruchez M, Moronne P, Gin S and Weiss A P (1998). 'Alivisatos: Semiconductor nanocrystals as fluorescentbiological labels'. *Science*, vol. 281: no. 5385, p. 2013-2016.

Russ J C (1984) Fundamentals of Energy Dispersive X-ray Analysis, Butterworths. London.

Santo C E, Tautde N, Nies D H and Grass G (2007) 'Contribution of copper ion resistance forsurvival of Escherichia coli on metallic copper surfaces'. *Applied Environmental Microbiology,* vol. 74: p. 977–986.

Scott J R and Barnett T C (2006) Surface proteins of gram-positive bacteria and how they get there. *Annual Review of Microbiology*, vol. 60: p. 397–423.

Shah M, Badwaik V, Kherde Y, Waghwani H K, Modi T, Aguilar Z P, Rodgers H, Hamilton W, Marutharaj T, Webb C, Lawrenz M B, and Dakshinamurthy R (2014). 'Gold nanoparticles: various methods of synthesis and antibacterial applications'. *Frontiers in Bioscience*, vol.19: p. 1320-1344.

Shahangian S, Ash K O, and Rollins D E (1984). 'An Enzymatic Method for the Analysis of Formate in Human Plasma'. *Journal of Analytical Toxicology*, vol. 8: no. 6, p. 273–276.

Shamaila S, Zafar N, Riaz S, Sharif R, Nazir J and Naseem S (2016). 'Gold Nanoparticles: An Efficient Antimicrobial Agentagainst Enteric Bacterial Human Pathogen'. *Nanomaterials*, vol. 6: no.71, p. 1-10.

Shekunov B Y, Chattopadhyay P, Tong H H, Chow A H (2007). Particle size analysis in pharmaceutics: principles, methods and applications. *Pharmaceutical Research,* vol. 24: p. 203–227.

Sherwani M S, Tufail S, Khan A A, and Owais M (2015), Gold Nanoparticle-Photosensitizer Conjugate Based Photodynamic Inactivation of Biofilm Producing Cells: Potential for Treatment of C. albicans Infection in BALB/c Mice.Viewed on 5 November 2015, from http://journals.plos.org/plosone/article?id=10.1371/journal.pone.0131684#pone.0131684.ref022.

Singh M, Bhui K, Singh R and Shukla Y (2013). 'Tea polyphenols enhance cisplatin chemosensitivity in cervical cancer cells via induction of apoptosis'. *Life Sciences*, vol. 93: p. 7-19.

Sosenkova L, Egorova E (2011). 'The effect of particle size on the toxic action of silver nanoparticles'. *Journal of Physics,* p. 12- 27

Sondi I and Salopek-Sondi B (2004). 'Silver nanoparticles asantimicrobial agent: a case study on *E. coli*as a model for Gram negative bacteria'. *Journal of Colloid Interface Sci*ence, vol. 275:p. 177–182.

Stiufiuc R, Iacovita C, Nicoara R, Stiufiuc G, Florea A, Achim M and Lucaciu C. M (2013). 'One-step Synthesis of PEGylated Gold Nanoparticles with Tunable Surface Charge', *Journal of Nanomaterials*. p. 1-7.

Sufrin C B and Ross J S (2008). 'Pharmaceutical industry marketing: Understanding its impact on women's health'. *Obstetrical & Gynecological Survey*, vol. 63: p. 585-596.

Sun S, Mendes P, Critchley K, Diegoli S, Hanwell M,Evans S D, Leggett G J, Preece J A and Richardson T H (2006). 'Fabrication of gold micro and nanostructures byphotolithography exposure of thiol stabilized goldnanoparticles'. *Nano Letters*, vol. 6: p. 345-350.

Sujit K G and Tarasankar (2007). 'Interparticle Coupling Effect on the Surface Plasmon Resornance of Gold Nanoparticles: From Theory to Application'.*Chemical Review*, vol. 107: no. 11, p. 4797-4862.

Sujitha M V and Kannan S (2013). 'Green synthesis of gold nanoparticles using Citrus fruits (Citrus limon, Citrus reticulata and Citrus sinensis) aqueous extract and its characterization'. *Spectrochimica Acta Part A: Molecular and Biomolecular Spectroscopy*, vol. 102: p. 15–23.

Szalek E, Kami—Ska A, Gozdzik-Spychalska J, Grzeskowiak E and Batura-Gabryel H (2011).' *Acta Poloniae Pharmaceutica - Drug Research*, vol. 68 no. 5, p. 777-783.

Todar K (2011) Bacterial mechanisms of antibiotic resistance.Todar's Online Textbook of Bacteriology, Madison. http://textbookofbacteriology.net/resantimicrobial_3.html

"Tuberculosis Fact sheet N°104". World Health Organization. November 2010. Retrieved 14 march 2015.

Turkevich J, Stevenson P C and Hillier J (1951). 'A study of the nucleation and growth process in the synthesis of colloidal gold'. *Discussion Faraday Society,* vol. 11: p. 55-75.

Umadevi M, Rani, T, Balkrishnan T, and Ramanibai R (2011). 'Antimicrobial activity of silver nanoparticles under an ultrasonic field'. *International Journal of Pharmaceutical Science and Nanotechnol*ogy, vol. 4: p. 1491–1496.

Verma H N, Singh p and Chavan R M (2014). 'Gold nanoparticle: synthesis and characterization'. *Veterinary World,* vol. 7: no. 2, p. 72-77.

Vicky V M, Rodney S, Ajay S and Hardik R (2010). 'Introduction to Metallic nanoparticles'. *Journal of Pharmaceutics and Bioallied Science*, vol. 2: no. 4, p. 282-289.

Wang, Z L. Characterization of nanophase materials. Wiley-VCH Verlag: GmbH; 2001. Transmission electron microscopy and spectroscopy of nanoparticles; p. 37-80.

Wiegel J (1981). 'Distinction between the Gram Reaction and the Gram Type of Bacteria'. *International Journal of Bacteriology*, vol. 31: no. 1, p. 1-88.

Williams D B and Carter C B (2009). 'Transmission electron microscopy'. *Springer*, vol. 1: p. 3-22.

Xue C, Xue Y, Dai L, Urbas A and Li Q (2013). 'Size- and Shape-Dependent Fluorescence Quenching of Gold Nanoparticles on Perylene Dye', *Advances in Optical Materials,* p.1-7.

Yugang S U N, Changhua A N (2011). 'Shaped gold and silver nanoparticles'. *Frontiers of Materials Science*, vol. 5: p. 1–24.

Zawrah M and El-Moez S I A (2011). 'Antimicrobial Activities of Gold Nanoparticles against Major Foodborne Pathogens'. *Life science journal,* vol. 8: no. 4, p. 37-44.

Zhang X, Shen W and Gurunathan S (2016). 'Biologically synthesized Gold Nanoparticles Ameliorate cold and heat stress-induced oxidative stress in *Escheristia coli'. Molecules,* vol. 21: no. 6, p. 1-18.

Zhi-Chuang X, Cheng-Min S, Cong-Wen X, Tian-Zhong Y, Huai-Ruo Z, Jian-Qi L and Hong-Jun G (2007). 'Wetchemical synthesis of gold nanoparticles using silver seeds: a shape control from nanorods to hollow spherical nanoparticles'. *Nanotechnology,* vol. 18: p.115-608.

Zhou Y, Kong Y, Kundu S, Cirillo J, and D and Liang H (2012). 'Antibacterial activities of gold and silver nanoparticles against *Escherichia coli* and *bacillus Calmette-Guérin'*. *Journal of Nanobiotechnology,* vol. 10: p.1-19.

Appendix

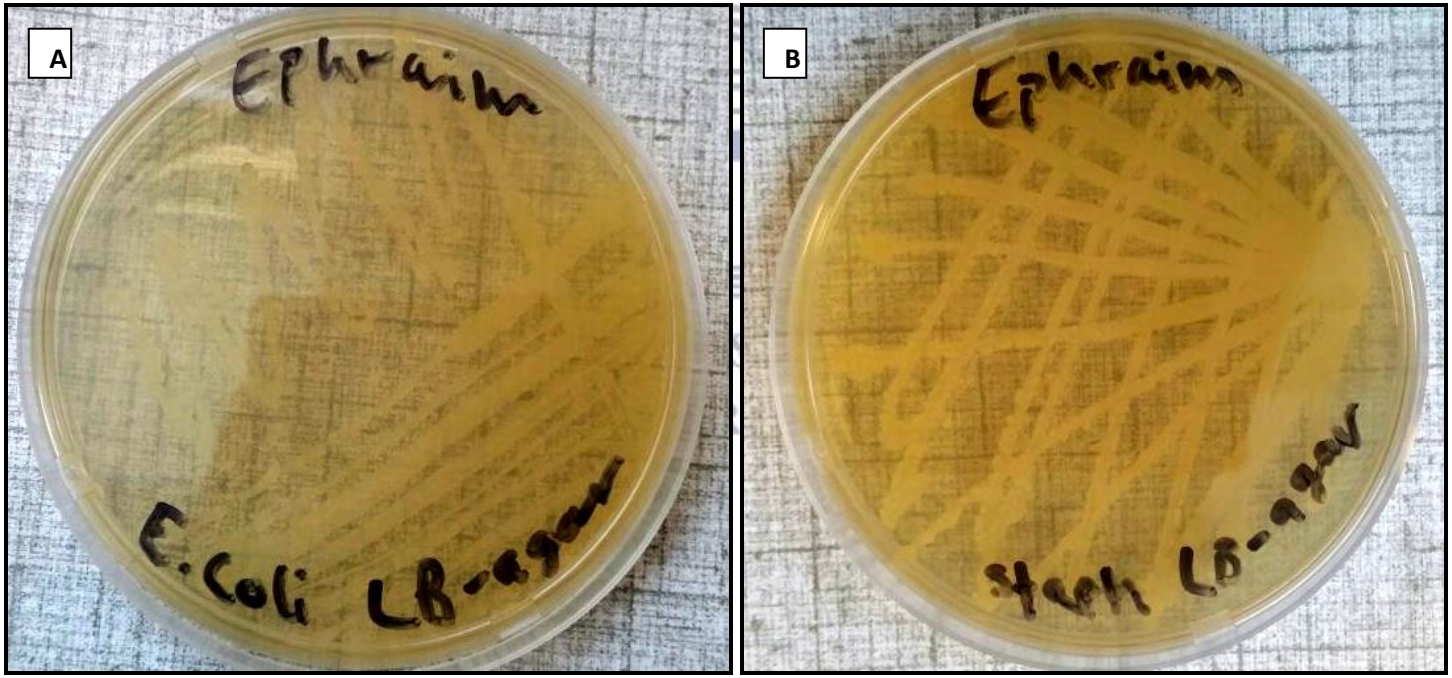

Figure 1: 0.5 McFarlen standards of A) *E. coli* and B) *S. Aureus* grown on LB agar plates

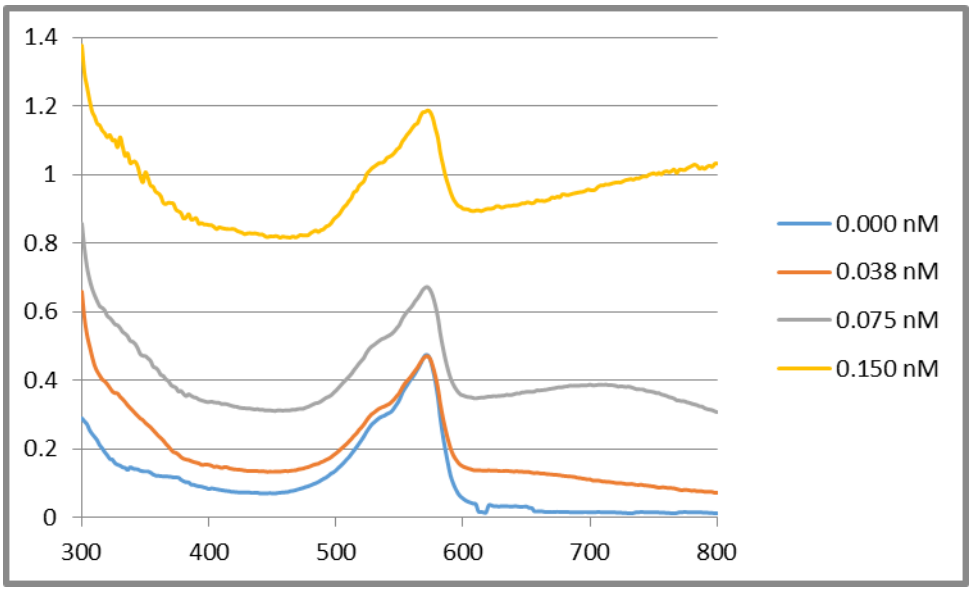

Figure 2: The effect of the concentration of AuNP 1 on the absorbance of Alamar blue

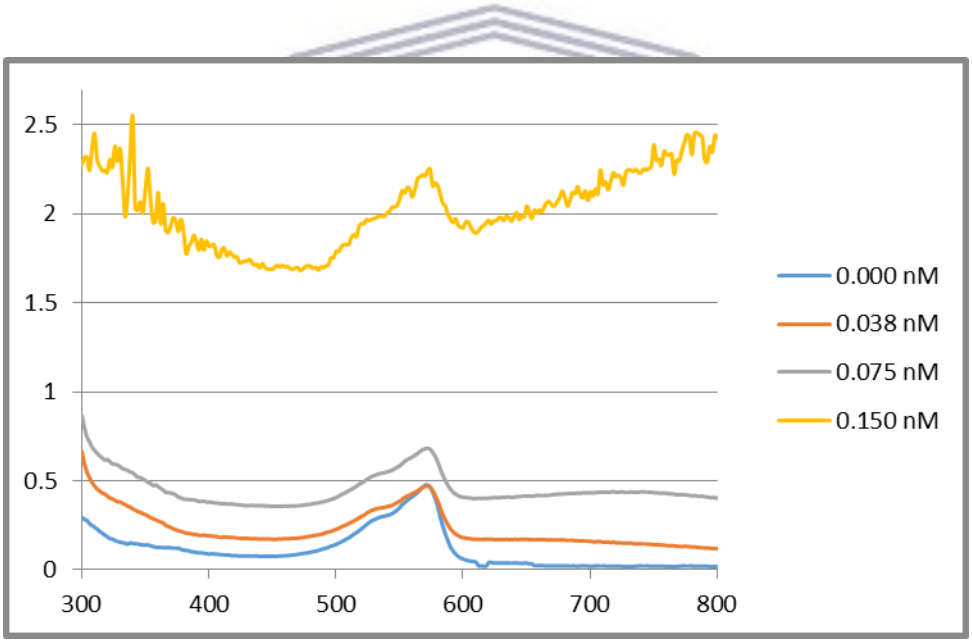

Figure 3: The effect of the concentration of AuNP 2 on the absorbance of Alamar blue

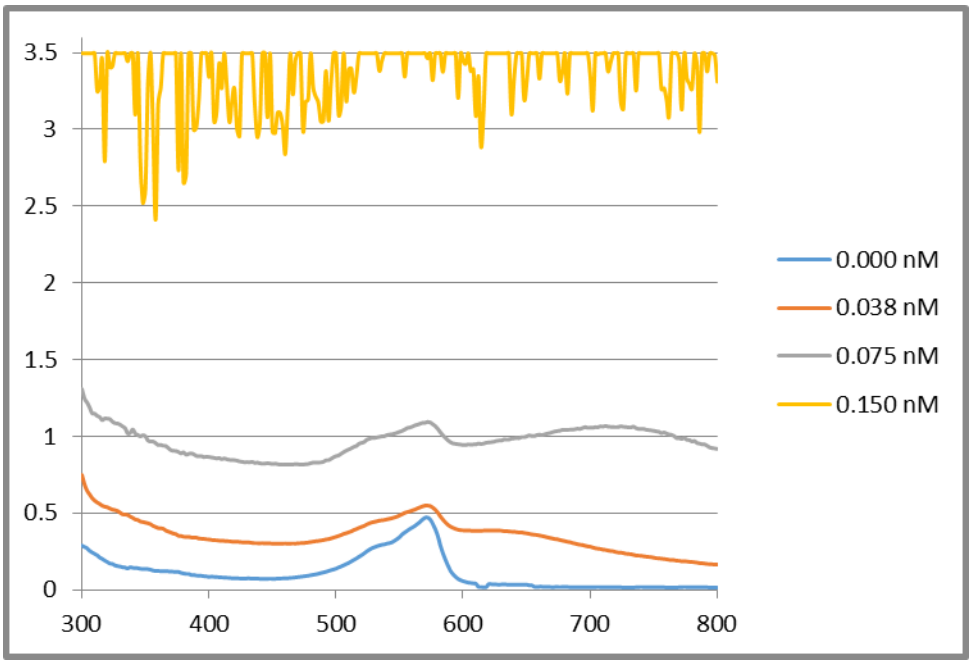

Figure 4: The effect of the concentration of AuNP 3 on the absorbance of Alamar blue.

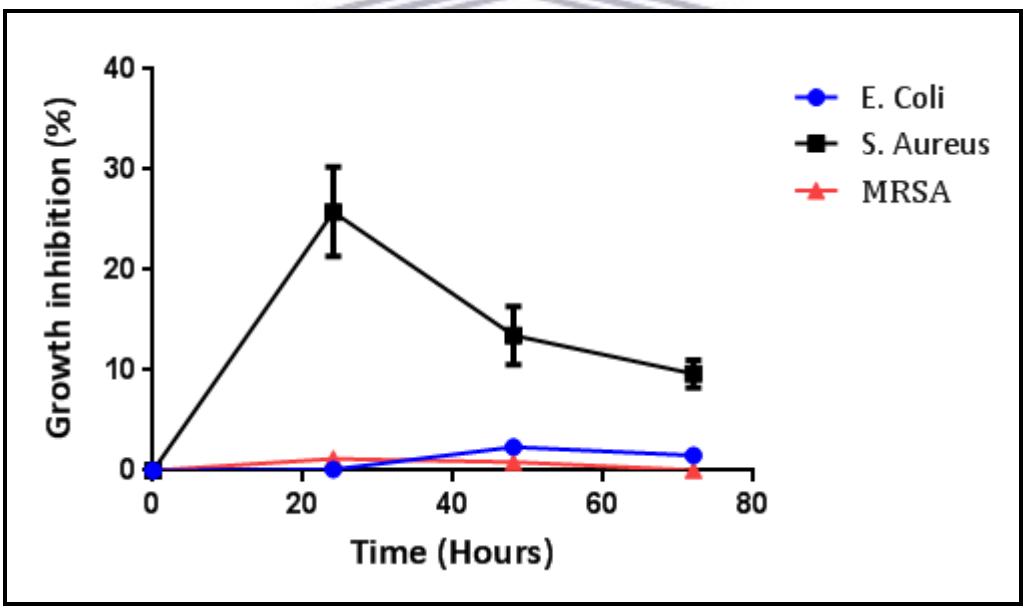

Figure 5: The effect of 50 ng/ml of Ampicillin on E. Coli, S. Aureus and MRSA after 72 hours of incubation at 37°C.